Institut für Hydrologie
Albert-Ludwigs-Universität Freiburg i. Br.

Veit Stadelbacher

Water balance modeling of a meso-scale mountainous catchment in Cyprus - process analysis and climate change impact

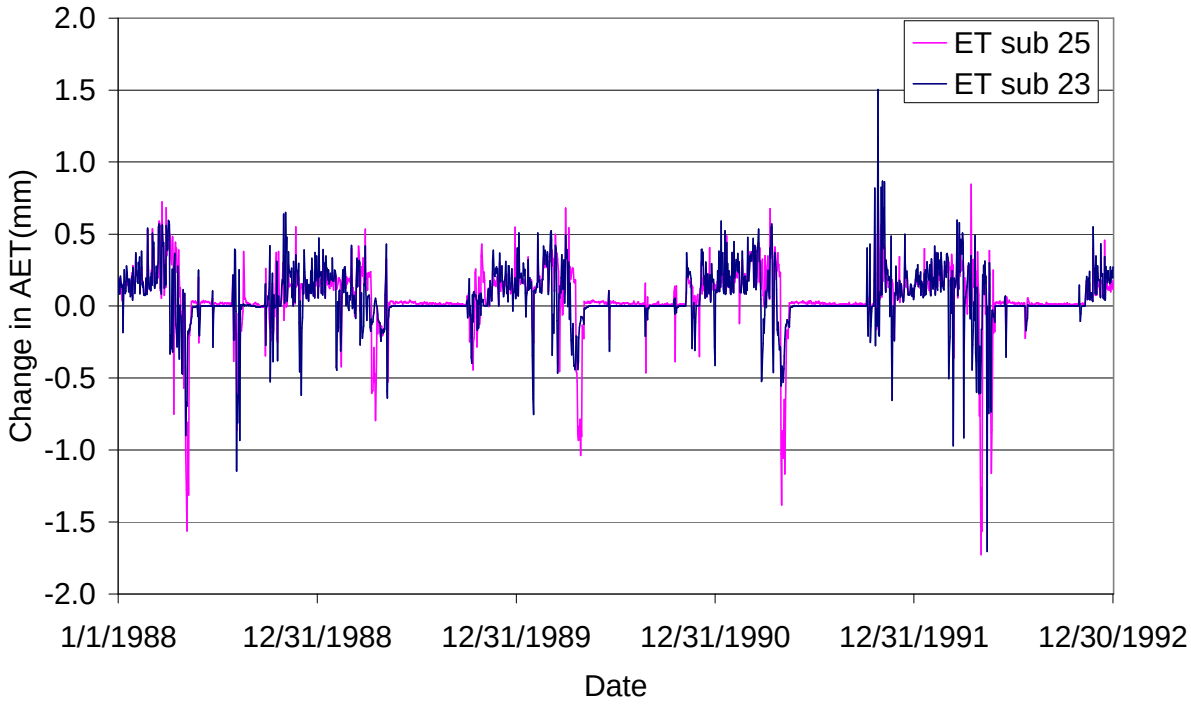

Diplomarbeit unter Leitung von Prof. Dr. Chr. Leibundgut
Freiburg im Breisgau, Oktober 2007

Institut für Hydrologie
Albert-Ludwigs-Universität Freiburg i. Br.

Veit Stadelbacher

Water balance modeling of a meso-scale mountainous catchment in Cyprus- process analysis and climate change impact

Referent: Prof. Dr. Chr. Leibundgut
Koreferent: Dr. C. Külls

Freiburg im Breisgau, Oktober 2007

Acknowledgements

With the difficulties and successes in the progress of writing this diploma thesis, the last nine months had many ups and downs. Without the help I received it would not be what it is now.

First of all, I would like to thank Dr. Christoph Külls for the support, advice and ideas he offered me during these nine months.

Matti Gerspacher and Tobias Schütz for proof-reading and the helpful discussions.

Jürgen Strub and Volker Abraham for preventing the worst case one can experience when working with computers.

My family for the continuous allowance.

All the others not named who helped me to bring this to an end, and, last but not least, Anna.

I. Table of Content

II. Table of Figures

III. List of Tables

IV. List of Abbreviations

Actual Evapotranspiration	AET	mm/y
Atmosphere-Ocean General Circulation Models	AOGCM	
Bundesanstalt für Geowissenschaften und Rohstoffe	BGR	
Curve Number	CN	
Digital Elevation Model	DEM	mm
Evapotranspiration	ET	
Greenhouse Gases	GHG	
Geological Survey Department of Cyprus	GSD	
Hydrological Response Unit	HRU	
Intergovernmental Panel on Climate Change	IPCC	
meters above sea level	m a.s.l.	
Precipitation	PCP	mm
Potential Evapotranspiration	PET	mm/y
Soil Conservation Service	SCS	
United Nations Development Program	UNDP	
United States Department of Agriculture	USDA	
Soil and Water Assessment Tool	SWAT	

V. Extended Summary

The objective of this study is to simulate the water balance and all of its compounds for the Kouris catchment in Cyprus. As a further step, based on the water balance modeling, the simulation of the impact of climate change on the water balance is carried out. Therefore, the Soil and Water Assessment Tool (*SWAT*) is used.

The Kouris catchment is located at the southern flank of the Troodos massive. It has a mountainous relief, elevating from 150 m a.s.l. to 1860 m a.s.l..
For the water balance of the whole island, the Troodos is of high importance. As well as the Kouris, the Limnatis and the Kryos, which drain the catchment, most of the rivers of Cyprus originate from it and deliver water to the plains and coastal areas.
From a geological point of view, the Kouris catchment is dominated by the Troodos terrane in the northern half and the circum-Troodos sedimentary succession in the southern halt, linked by the Arakapas fault zone in the middle.
The pedology is dominated by Leptosols and Regosols.
The land use is dominated by scrubland, pine forests and deciduous trees, mostly in the form of vineyards and not irrigated orchard trees. Wetlands only occur in the northern half, proving the connection of surface- and groundwater.

SWAT is physically based and requires specific information about weather, soil properties, topography, vegetation, and land management practices occurring in the watershed. Climatic data is statistically analyzed and implemented into the *SWAT* weather generator.
SWAT provides a database for land use and soils. The soil database is extended with the six soiltypes determined for the Kouris catchment during the GRC project. Therefore, the tool “Soil Water Characteristics” developed by Keith E. Saxton is used to calculate soil properties.
For the land use, the predefined *SWAT* land use classes are applied.

SWAT provides a sensitivity analysis tool. Together with the information of previous simlulations of the uncalibrated model, lateral flow, surface runoff and snowmelt are

determined to be the important processes for runoff generation. The model is calibrated stepwise taking into account the theoretical documentation of *SWAT*.
Comparison of annual volumes of measured and simulated discharge and the Nash&Sutcliffe coefficient act as quality criteria. The Nash&Sutcliffe coefficient of 0.78 for the Kouris and 0.63 for the Limnatis prove the quality of the calibration. This is validated in using another time period. For the Kouris, the Nash&Sutcliffe coefficient improved to 0.84, for the Limnatis it declined to 0.46.

The calibrated model is used to simulate the impact of climate change on the water balance. The climatic data is adjusted according to the future projections of climate change stated by the IPCC (2001a). The applied scenarios comprise the changes in air temperature and precipitation for two time periods centered on the 2050s and the 2080s. Additionally, the effect of the increase of CO_2 on plants is taken into account.
For the 2050s, the increased Evapotranspiration, caused by the raise in air temperature, weights more than the increased precipitation. In the mean, the remaining water cycle compounds decrease, above all the Snowfall.
For the 2080s, the increased precipitation weights more than the increased evapotranspiration. With the exception of snowfall, all compounds increase.

In either case, there is a decrease during the summer months and, if there is an increase, then during the winter months. This means one has to manage with less water available when mostly needed. Therefore, further efforts to improve water and demand management as well as the use of storage and recharge enhancement techniques is recommended.

VI. Zusammenfassung

Ziel dieser Arbeit ist die Simulation der Wasserbilanz mit ihren Komponenten für das Kouris Einzugsgebiet in Zypern. Auf Basis der Wasserhaushalts-Simulationen ist der Einfluss der Klimaveränderung auf die Wasserbilanz simuliert worden. Für die Simulationen diente das Modell SWAT (Soil and Water Assessment Tool).

Das Kouris Einzugsgebiet befindet sich an der Südseite des Troodos Massivs. Es ersteckt sich von 150 m ü.M. bis auf 1869 m u.M. Das Troodos Gebirge ist für den Wasserhaushalt der Insel von großer Bedeutung. Wie auch der Kouris, der Limnatis und der Kryos, welche das Einzugsgebiet entwässern, entspringen die meisten Flüsse Zyperns diesem Gebirge und transportieren Wasser in die Ebenen und Küstengebiete.

Vom geologischen Standpunkt aus wird das Kouris Einzugsgebiet dominiert von Gesteinen des Troodos terrane in der nördlichen Hälfte sowie der Circum-Troodos Sedimentfolge in der südlichen Hälfte. Diese werden „verbunden“ durch die Arakapas Verwerfung.

Leptosole und Regosole sind die vorherrschenden Bodentypen.

Die Landnutzung wird von Buschland, Pinien- und Laubwäldern, hauptsächlich in der Form von Weinbergen und unbewässerten Obstgärten. Feuchtgebiete finden sich ausschließlich in der nördlichen Hälfte. Dies zeigt die dortige Verbindung von Oberflächen- und Grundwasser.

SWAT ist ein physikalisch basiertes Modell und benötigt Klimadaten, Eigenschaften der Böden, Topographie, Vegetation und Landnutzung des zu untersuchenden Gebietes.

Die Klimadaten werden statistisch analysiert und in den SWAT Wettergenerator implementiert.

Das *SWAT* Modell beinhaltet Datenbanken für Landnutzung und Böden. Für das GRC Projekt wurden die Bodentypen Zyperns aufgenommen. Die Bodendatenbank ist um die sechs Bodentypen, die im Kouris- Einzugsgebiet vorkommen, erweitert worden. Für die Landnutzung wurden die Klassen der SWAT Datenbank verwendet.

SWAT beinhaltet ein Tool zur Sensitivitätsanalyse. Zusammen mit den Informationen, die aus vorangegangenen Läufen des unkalibrierten Modells stammen, wurden die für die Abflussbildung bedeutsamen Prozesse bestimmt. Diese sind Zwischenabfluss, Oberflächenabfluss und Schneeschmelze. Das Modell wurde dann schrittweise kalibriert, unter Verwendung der Theoretischen Dokumentation von *SWAT.*

Als Gütemasse dienten Vergleiche der Jahressummen von simuliertem und gemessenem Abflusses sowie der Nash&Sutcliffe-Koeffizient.

Für die Qualität der Modellierung sprechen die Nash&Sutcliffe-Koeffizienten von 0.78 für den Kouris und 0.64 für den Limnatis. Mit der Simulation einer anderen Zeitreihe wurden diese Ergebnisse validiert. Für den Kouris stieg der Nash&Sutcliffe-Koeffizient auf 0.84, während er für den Limnatis auf 0.46 zurückging.

Das kalibrierte Modell ist weiter verwendet worden um den Einfluss der Klimaveränderung auf den Wasserhaushalt zu simulieren. Die Klimadaten wurden nach den Einschätzungen der IPCC (2001a) angepasst. Die verwendeten Szenarien beinhalten die Veränderung der Lufttemperatur sowie des Niederschlags für zwei Zeitperioden: die 2050er und 2080er Jahre. Zusätzlich wurde der der Effekt des steigenden CO_2-Gehalts auf die Pflanzen berücksichtigt.

Für die Perioden um 2050 wiegt die durch den Anstieg der Lufttemperatur verstärkte Evapotranspiration mehr als der erhöhte Niederschlag. Die übrigen Wasserhaushaltskomponenten nehmen im Mittel ab, vor allem Schneefall geht stark zurück.

Für die Periode um 2080 überwiegt der gestiegene Niederschlag die gestiegene Evapotranspiration. Mit Ausnahme des Schneefalls, nehmen im Mittel alle Wasserhaushaltskomponenten zu.

In jedem Falle nehmen die Wasserhaushaltskomponenten in den Sommermonaten ab. Wenn sie zunehmen, dann in den Wintermonaten. Dies bedeutet, dass mit weniger Wasser gewirtschaftet werden muss, wenn am meisten davon benötigt wird. Daher müssen weitere Anstrengungen im Bereich water management unternommen werden. Die Anwendung sowie Verbesserung von Techniken zur Anreicherung der Grundwasserneubildung wird empfohlen.

Keywords: Water balance modeling; SWAT; Climate change; semiarid; Cyprus, mountainous

1 Introduction

This study contains results of the simulation of the water balance for the Kouris catchment in Cyprus. The “Soil and Water Assessment Tool” *(SWAT)* is able to model water balance, nutrient transport and many other applications and thus seems to be a good choice.

For simulating the water balance, necessary data is processed and implemented into *SWAT*, which works as an extension in ArcView. This includes climatic data, soil properties, land use data, hydrological data and geological data. The results are discussed within the context of these data, both of the calibration and the validation.

The impact of climate change on the water balance is the second part of this work. With the ongoing depletion of groundwater resources in Cyprus, the change of the water balance caused by the climate change becomes of a special interest. Therefore, the future projections of climate change by the IPCC (2001b) are applied to *SWAT.*

1.1 Objectives

The high importance of the Troodos for the water balance of Cyprus is beyond doubt. Most rivers of Cyprus originate in the Troodos due to the high amounts of precipitation, supplying the plains and coastal areas.

The aim of this work is to understand processes of runoff generation and to simulate the water cycle within the Kouris catchment, located at the southern flank of the Troodos massive, the water tower of Cyprus.

Water resources have been depleted to a large extent during the last 60 years. The IPCC (2001b) calculated changes in mean daily air temperature and precipitation for the 2050s and 2080s for the Mediterranean. Therefore, several AOGCMs (atmosphere-ocean general circulation models) have been compared. Thus, as a further step beyond water balance modeling, the impact of climate change on the water balance is determined for the Kouris catchment.

1.2 State of the Art

In this study a regional thematic and a methodological review of previous work has been carried out in order to characterize the state of the art.

Hydrogeology

One of the earliest studies about the geology of Cyprus is “Géologie de l´ile de Chypre” by A. GAUDRY (1862, in UDLUFT, 2001). In terms of hydrogeology first publications date from the 1940´s. D. J. BURDON published “Characteristics of the water-bearing rocks of Cyprus” in 1953 (UDLUFT, 2001). HENSON et al. (1949) and RAEBURN (1945) made hydrogeological classifications differentiating three categories of rocks (cited in UDLUFT, 2001). Category 1 includes non-porous crystalline masses, mainly the rock of the Troodos and the Hilarion limestone. Category 2 consists of non-fissured and non porous rocks of the Mammonia Formation, the Pillow Lavas and parts of other formations. Category 3 includes porous material of the Mesaoria and coastal plains. BURDON states the meaning of the Troodos as an area providing groundwater.

Following a request from the Government of Cyprus a team from the U.N. suggested an international development program for the ´Survey for Groundwater and Mineral resources´ that started in 1962 and was finished in 1970 (UNDP, in UDLUFT, 2001). The final report recommends further geological and geophysical surveys for both mining and water development and included a Hydrogeological Map of Cyprus in the scale 1:250000. The meaning of the Troodos massive for water supply for the circum-Troodos sediments was clearly underestimated, considering the whole central part of Cyprus as nearly impermeable.

In 1984, AFRODISIS suggested to drill in the Troodos igneous rocks for exploitable amounts of water (UDLUFT, 2001). He pointed out that, without the Troodos, “Cyprus would almost be a desert” and that the Troodos is “of vital importance” being the “water tower of the island”.

The Federal Institute for Geosciences and Natural Resources (BGR) performed a numerical groundwater modeling and a groundwater quality and isotope survey in cooperation with the Geological Survey Department (GSD) in 1984/85.

From 1997 to 2000 the GREM (Groundwater Resources in the eastern Mediterranean) project was accomplished by the University of Würzburg supported by the U.N (INCO-DC project ERBIC18-CT97-0143). It intended to study the rate of groundwater recharge in several mediterranean countries. For the Kouris catchment the recharge rate was determined to 69 mm/y (URL 7).

From 2001 to 2004 the GRC project was carried out to re-evaluate the groundwater resources of Cyprus. It included the survey of changes in the conditions of Cyprus´ aquifers and a groundwater modeling of selected aquifers.

ZAGANA et al. (2006) described “Methods of Groundwater Recharge Estimation in Eastern Mediterranean”, including northwest Greece, Cyprus and Jordan. For Cyprus the mean groundwater recharge was determined to 70 mm/y.

The Arc View *SWAT* model can perform a wide range of applications including the simulation of the impact of climate change on water cycle compounds. Therefore the *SWAT* model was chosen for this work.

SWAT

SWAT is used for many applications, such as modeling of pesticide, nitrogen, phosphorus or sediment loads, impact of land use or climatic change or modeling of water cycle components. The current *SWAT* model derives two models: From the ´Simulator for Water Resources in Rural Basins´ (SWRRB), designed to simulate “management impacts on water and sediment movement” (GASSMAN et al., 2007), and the ´Routing Outputs to Outlets´ (ROTO) model, designed to “support an assessment of the downstream impact of water management” (GASSMAN et al., 2007). Yet, *SWAT* was applied mostly in the U.S.

As one of the first major applications, *SWA*T was used within the Hydrologic Unit Model of the U.S. (HUMUS) modeling system. It was used to “simulate hydrologic

and/or pollutant loss impacts of agricultural and municipal water use, tillage and cropping system trends, and other scenarios" (GASSMAN et al., 2007).

In the U.S., *SWAT* is increasingly used to calculate total maximum daily pollutant to meet the requirements of the U.S. Clean Water Act.

In projects supported by the European Commission agencies, *SWAT* was used to quantify the impacts of climate change within the Climate Hydrochemistry and Economics of Surface-water Systems.
GASSMAN et al. (2007) grouped articles of *SWAT* and modified *SWAT* applications into eight subcategories. As Table 1.1 lists, *SWAT* is mostly applied for hydrologic assessments and for pollutant assessment.

Table 1.1 Overview of major applications categories of *SWAT* studies reported in literature (GASSMAN et al., 2007)

Primary application category	Hydrologic Only	Hydrologic & Pollutant Loss	Pollutant Loss Only
Calibration and/or sensitivity analysis	14	20	2
Climate change impacts	21	7	-
GIS interface descriptions	3	3	2
Hydrologic assessments	40	-	-
Variation in configuration or data input effects	18	14	-
Comparisons with other models/techniques	5	7	-
Interfaces with other models	13	16	6
Pollutant assessments	-	52	5

Due to the possibilities *SWAT* offers in modeling issues, a considerable number of studies on the effect of variation in configuration and data input have been carried out too. The modeling of climate change impacts with *SWAT* is of growing relevance.

2 Study Area: The Kouris Catchment

The Kouris catchment comprises an area of about 310 km² located on the southern flank of the Troodos massive. It extends about 25 km in length and 13 km in width, based on the DEM prepared within the GRC project and the watershed delineation made with *SWAT*. Figure 2.1 displays the topographic map of Cyprus and the Kouris catchment.

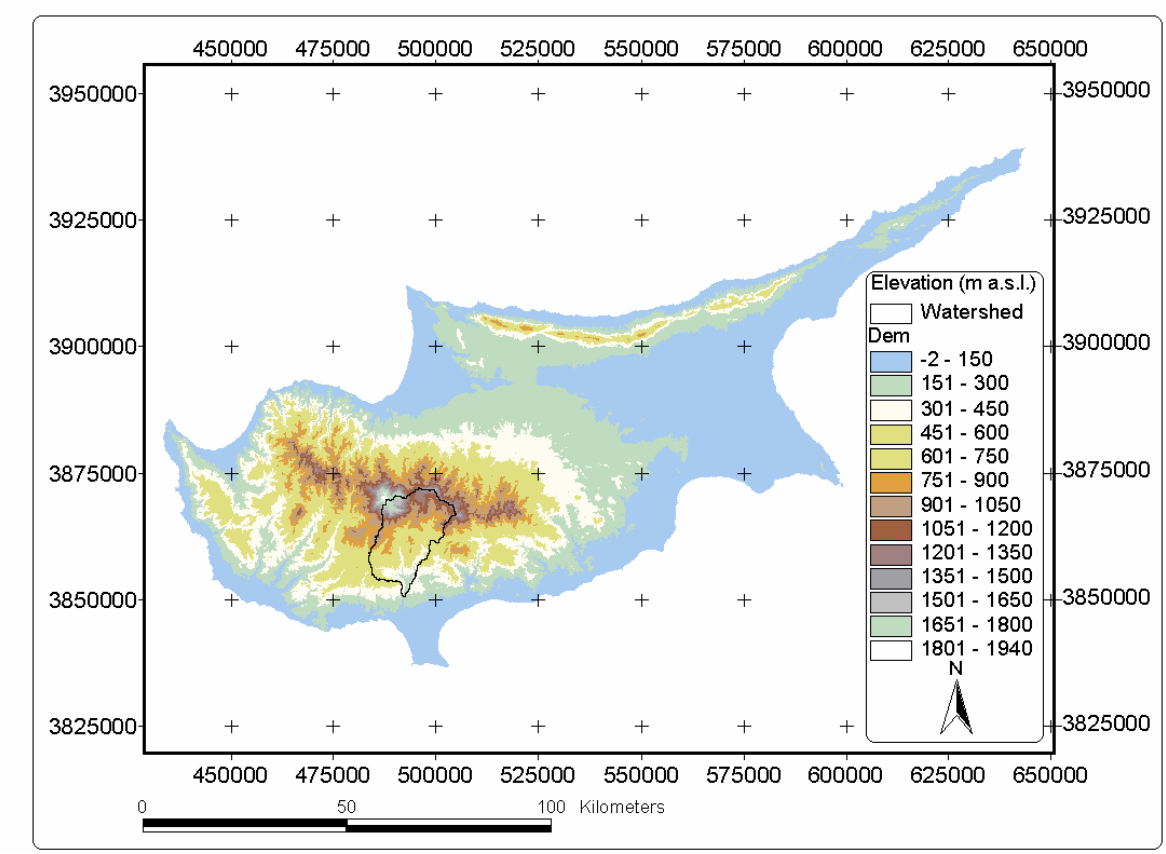

Figure 2.1 Topographic map of Cyprus and the Kouris catchment

The elevation rises from 150 m a.s.l. at the Kouris dam to 1860 m a.s.l. in the north-west of the watershed.

Most of the region is mountainous; the relief is dominated by the river valleys of the rivers Kouris, Limnatis, Kryos and their tributary channels, draining the catchment. Like most rivers in Cyprus, they have their source in the Troodos.

Table 2.1 gives a summary of the parameters calculated with the DEM.

Table 2.1 DEM derived terrain parameters

Total area	307 km^2
Maximum elevation (m a.s.l.)	1884 m
Mean elevation (m a.s.l.)	806 m
Minimum elevation (m a.s.l.)	160 m
Mean slope	15°
Maximum slope	47°

Figure 2.2 displays the DEM derived slope angle (°) . The river valleys of the Kouris, Kryos and Limnatis and their tributary channels are recognizable.

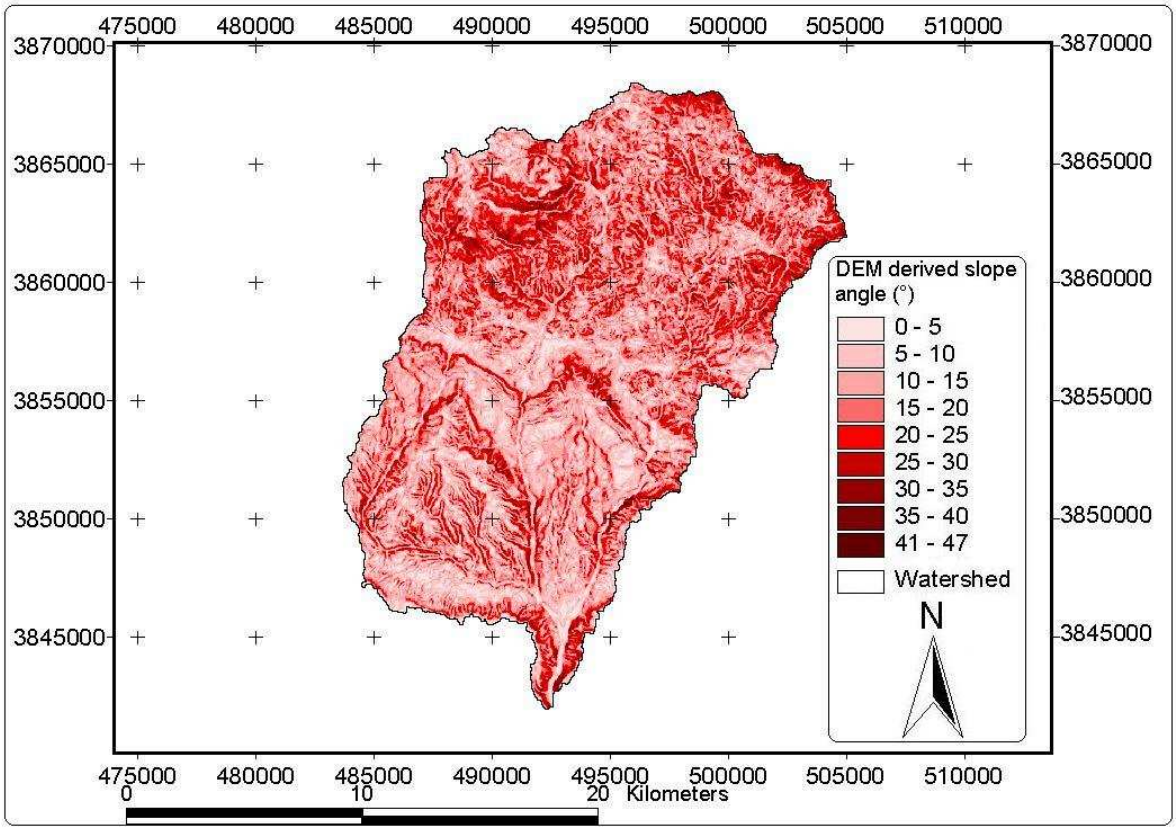

Figure 2.2 DEM derived slope angle within the Kouris catchment (°)

2.1 Climate

Due to its geographical location in the Mediterranean, the climate of Cyprus is generally dominated by a mediterranean climate with mild winters, long hot and dry summers and short autumn and spring seasons.

2.1.1 Precipitation

Precipitation in the Kouris catchment ranges from 580 mm/y (virtual station) at the lowest elevations to 900 mm/y in the uppermost parts of the catchment. This results in a mean annual precipitation of 725 mm/y for the whole catchment during the analyzed time series (1987-1997). Precipitation varies in a wide range both from year to year, e.g. 1279 mm for 1994 and 473 mm in 1995, and interannually, e.g. for 1991 July and August together 15 mm but 622 mm in December for weather gage ´Pano Amiantos´. About 85% of the annual precipitation distributes from November to March with heavy precipitation events at regular intervals.

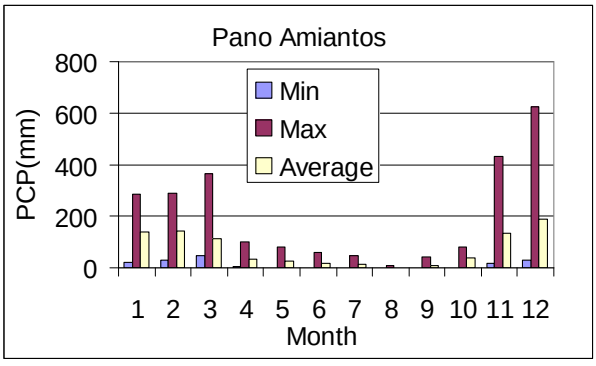

Figure 2.3. Minimum, maximum and average monthly precipitations for weather gage ´Pano Amiantos´ during time series.

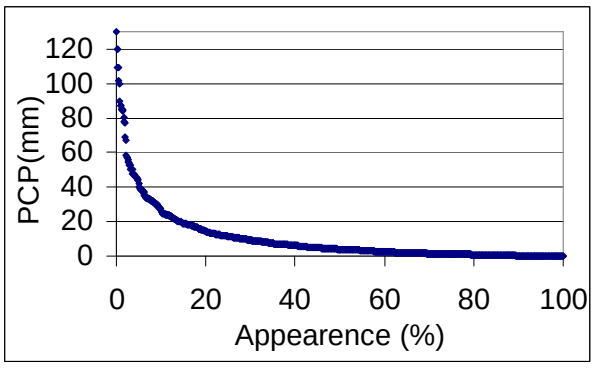

Figure 2.4 Distribution of appearance of precipitation events during time series

2.1.2 Air Temperature

As well as for weather gage “Pano Amiantos” (Figure 2.5), the monthly means of air temperature are always above zero ℃ for all weather gages relevant for the catchment.

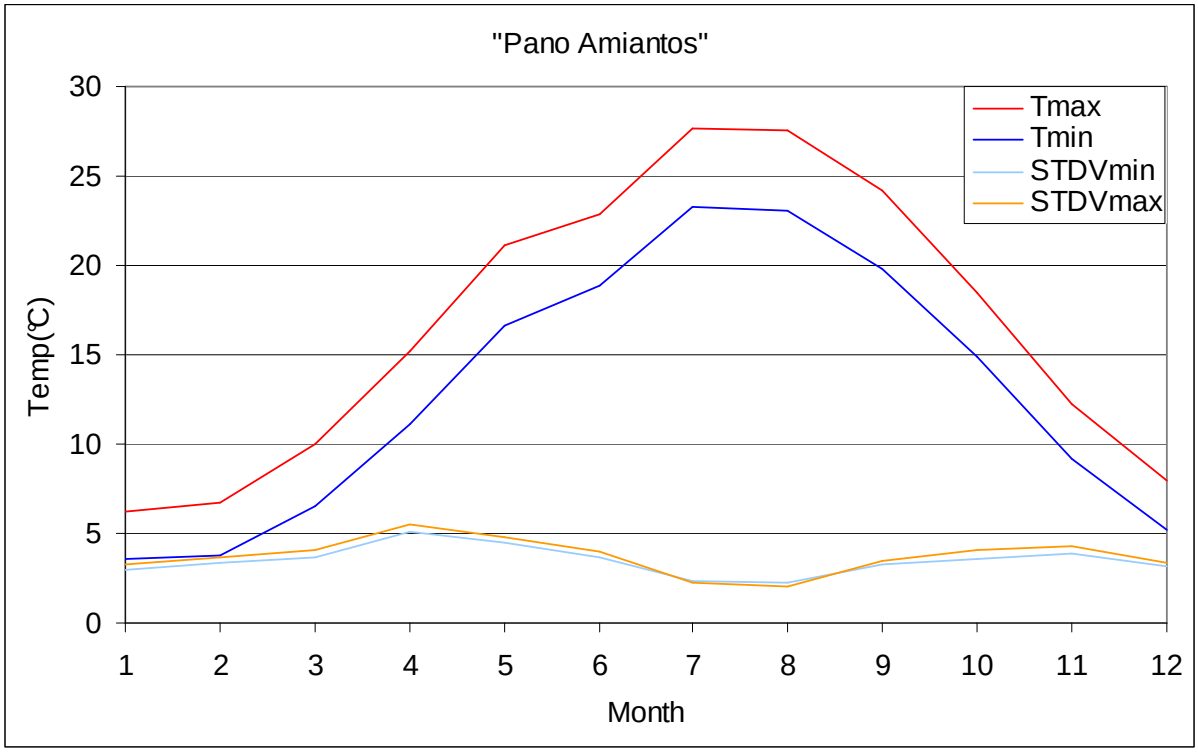

Figure 2.5 Average minimum and maximum air temperature and their standard deviations for weather gage Pano Amiantos (1988-1996)

However, for the weather gage ´Pano Amiantos` at 1360 m a.s.l., 30 days within the 10 years of record showed air temperatures below zero, the minimum at -6.5℃. Thus, snowfall and snowmelt occur. This is important for the recharge, being more effective than recharge from precipitation, but is not considered being a dominant process for runoff dynamic.

2.2 Soils

During the GRC project the soil groups for Cyprus were designated. The following six soil groups occur in the Kouris catchment:

- eutric-lithic-LEPTOSOLS and eutric-skeletic-REGOSOLS
- eutric-CAMBISOLS and eutric-anthropic-REGOSOLS
- lithic-LEPTOSOLS and epipetric-CALCISOLS
- calcaric-fluvic-CAMBISOLS and vertic-CAMBISOLS
- calcaric-rendzic-LEPTOSOLS and calcaric-leptic-CAMBISOLS
- skeletic-calcaric-REGOSOLS and calcaric-lithic-LEPTOSOLS

Table 2.2 sums the percentage composition of soils occurring within the Kouris catchment. With a total contribution of about 58% solely by Regosols and Leptosols, the dominance of these soil types is evident.

Table 2.2 Soils within the Kouris catchment and their percentage composition

Soil Name	AREA (%)
eutric-lithic-LEPTOSOLS and eutric-skeletic-REGOSOLS	35.73
skeletic-calcaric-REGOSOLS and calcaric-lithic-LEPTOSOLS	22.32
eutric-CAMBISOLS and eutric-anthropic-REGOSOLS	21.89
calcaric-rendzic-LEPTOSOLS and calcaric-leptic-CAMBISOLS	19.72
lithic-LEPTOSOLS and epipetric-CALCISOLS	0.27
calcaric-fluvic-CAMBISOLS and vertic-CAMBISOLS	0.08

The dominating soil types within the Kouris catchment are the Leptosols and Regosols (Figure 2.6). The northern half of the catchment is solely covered by these two soil types. Of further importance are the Cambisols, which cover together with Leptosols and Regosols most of the southern half. The Calcisols play hardly a role.

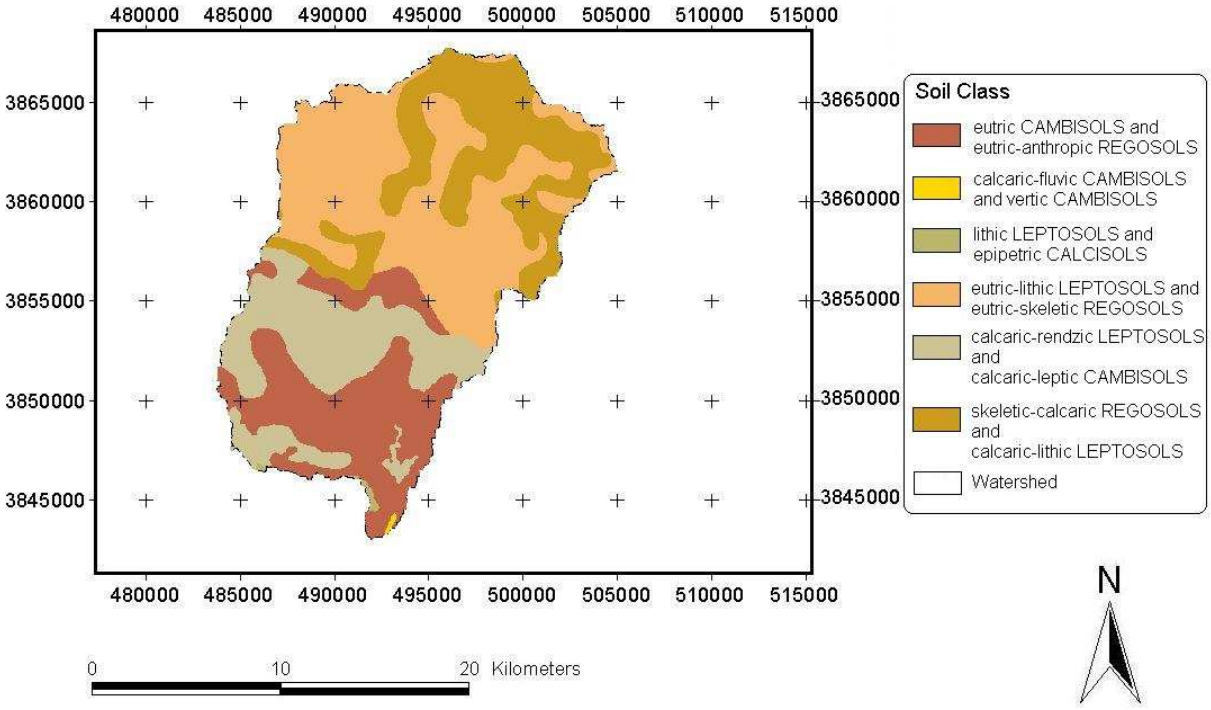

Figure 2.6 Soil map of the Kouris catchment

The following brief description of the dominant soiltypes orients by “Lecture Notes On The Major Soils Of The World” (DRIESSEN et al. 2002):

2.2.1 Leptosols

Leptosols are generally very shallow soils over hard rock. When Leptosols show a higher depth, the are usually extremely gravelly and/or stony. Leptosols are azonal with an incomplete solum and/or without clearly expressed morphological features. As the most extensive Reference Soil Group on earth, Leptosols extend over approximately 1655 million hectares, and are particularly widespread in mountainous

regions on hard rocks or where erosion has kept pace with soil formation or removed the top of the soil profile.

A Leptosol is a genetically young soil; soil formation is normally limited to a thin A-horizon over an incipient B-horizon or directly over the unaltered parental material. The use of Leptosols is limited since they are unattractive for arable cropping or tree crop production; they are best kept under forest. From a hydrological point of view Leptosols are free-draining soils with few exceptions: stagnic properties can occur on slight slopes or in pockets but are rather uncommon.

2.2.2 Regosols

Regosols are a taxonomic rest group containing all soils that could not be accommodated in any of the other Reference Soil Groups. Thereby they are not defined in terms of their soil properties but in terms of properties that they do not have. In practice, Regosols are soils in unconsolidated mineral material excluding coarse textured materials.

They are common at all elevations and in all climates without permafrost, particularly in arid areas, in the dry tropics and mountain regions.

Most Regosols have a low coherence of the matrix what makes them vulnerable for erosion. Low water holding capacity and high permeability makes them sensitive droughts.

The land use and management varies widely: some Regosols are used for irrigated farming, but mostly as pasture. In mountain regions they are best left under forests.

2.2.3 Cambisols

The Cambisols are soils at an initial state of pedogenesis. Most of them are soils with beginning horizon differentiation in a transitional stage of development. Parental material is usually medium to fine-textured material, mostly colluvial, alluvial or fluvial. Most Cambisols contain at least some weatherable minerals in the silt and sand

fractions, occur in regions with a precipitation surplus but in terrain positions that permit surface runoff. Cambisols have a good structural stability, a high porosity, good water holding capacity and good internal drainage. By and large, Cambisols are well suited for agricultural land and are intensively used. The Eutric Cambisols of the Temperate Zone are among the most productive soils on earth. Vertic and calcaric Cambisols in (irrigated) alluvial plains in the dry zone are intensively used for production of food and oil crops.

2.3 Geology

From a lithological point of view the Kouris catchment can be subdivided in three different units: The Troodos terrane (Troodos ophiolite), the circum Troodos sedimentary succession and the Arakapas sequence.

As Figure 2.7 displays, the lithologies of the Troodos terrane with the Diabase and Harzburgites and the Troodos sedimentary succession with the Pakhna and the Lefkara formation clearly dominate the catchment. Nevertheless, the lithologies of the Arakapas sequence are very important. Due to the high permeabilities of the fractured rocks, it influences the water balance and thereby the land use.

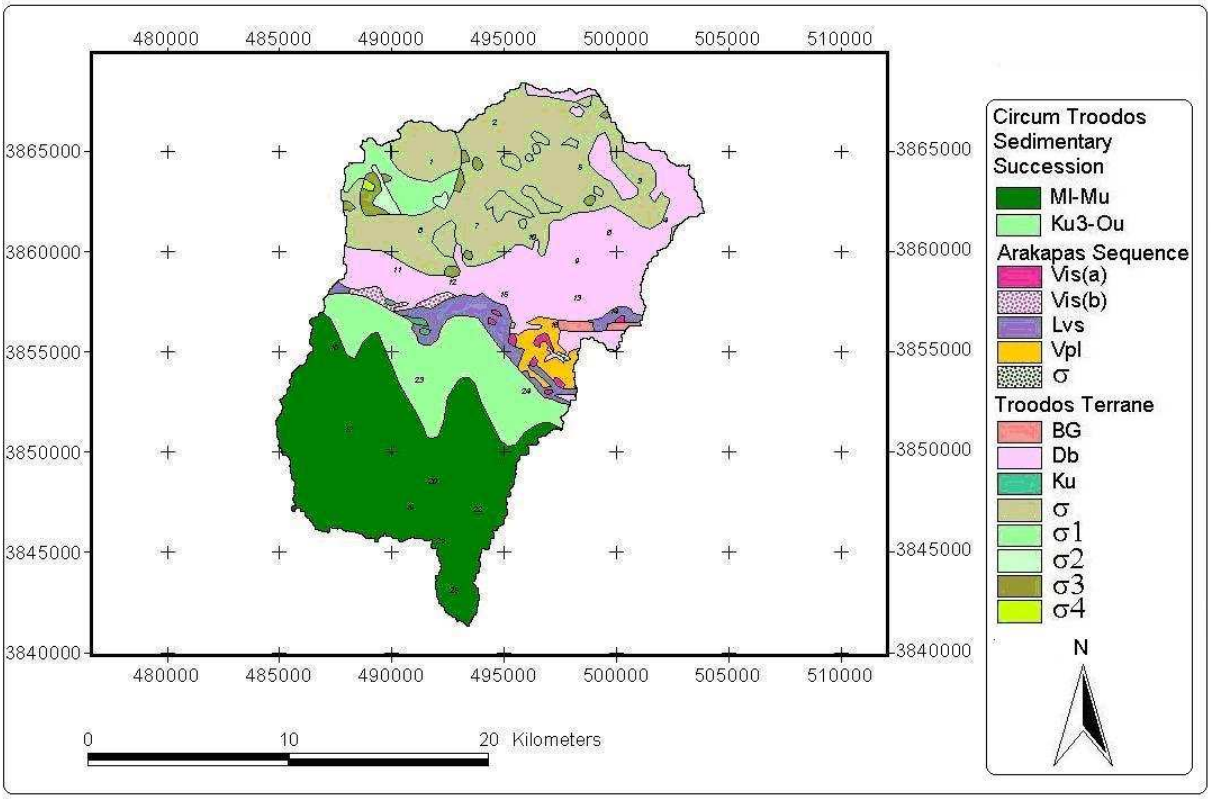

Figure 2.7 Geological map of the Kouris catchment

Table 2.3 summarizes the geological circumstances and describes the lithological units.

Table 2.3 Lithology of the Kouris catchment

Lithology		**Formation**
Circum Troodos Sedimentary Succession		
MI-Mu	chalks, marls, marly chalks, chalky marls and calcarenites	Pakhna
Ku3-Ou	chalks, marls, marly chalks, chalky marls with cherts in places as bands or nodules	Lefkara
Arakapas Sequence		
Vis(a)	fine grained interlava volcanogenic sediments: a) sandstones , silts and grits interbedded with laminated iron and manganese-rich mudstones	
Vis(b)	b) coarse polymict breccias with lava, dyke and isotropic gabbro clasts	
Lvs	olivine- and/or pyroxene.phyric, aphyric pillow lavas with some hyloclastites, sheet lava flows and dykes, altered to zeolite facies	
Vpl	vitrophyric pillow lavas, generally olivine-phyric and/or orthopyroxene-phyric	
σ	Serpentinite in subvertical shear zones, 50-500 m wide	
Troodos Terrane		**Rock Type**
Db	diabase dykes upto 3m wide, aphyric and clinpyroxene- and plagioclase-phyric altered to greenschist facies	Sheeted Dykes (Diabase)
BG	diabase dykes (>50%) with pillow lava screens, altered to greenschist facies	Basal Group
Ku	hydrothermal and deep-water sediments; umbers, manganoan shales, pink radiolarian shales and mudstones	
δ	isotropic gabbros, uralite gabbros, olivine gabbros and layerewd melagabbros	Gabbro
γ	tronhjemites, granophyres, diorites, quartz-diorites, and micro grano-diorites	Plagiogranite
σ	pervasively serpentinized , tectonized harzburgites with minor dunites and iherzolites	Serpentinite
σ1	tectonized harzburgites with minor dunites and herzolites	Harzburgite
σ2	dunites with subordinate clinopyroxene-dunite	Dunite
σ3	wehrlites and plagioclase-bearing wehlites, massive or layered	Wehrlite
σ4	websterites, clinopyroxyenite, orthopyroxenite and plagioclase-bearing pyroxenites	Pyroxenite

2.4 Hydrology

The Kouris catchment is drained by three rivers: the Kryos, the Limnatis and the Kouris. Both Kouris and Limnatis are not perennial, from July to September the discharge is at least close to zero.

The distribution of wetlands reflects the connection of surface water to groundwater. In parts, this is due to the Arakapas fault zone and the spatial distribution of precipitation. The Arakapas fault zone subdivides the catchment into two halfs, “forming a drain for the groundwater due to low elevation and high permeabilities of the faulted fractured lithologies” (UDLUFT et al., 2003). Isotope investigations indicated that a part of the groundwater flows through the fault zone to give indirect recharge to the lithologies of the Circum Troodos Sedimentary Succession. In the upper half of the basin, streams are effluent due to a connection to groundwater. The lower half of the catchment has both less precipitation and nearly all field areas; therefore higher groundwater abstractions are conducted to feed the water demands for irrigation purposes.

2.5 Land use

The land use for Cyprus was classified during the GRC project using a Landsat 5 scene. Table 2.4 shows the nine different classes and their percentages in the catchment:

Table 2.4 Land use classes in the Kouris catchment

Nr.	Hydrological land-use class	Area(%)
1	Deciduous Trees	23.38
2	Scrubland	28.99
3	Pine Forest	27.84
4	Settlement	1.36
5	Field	6.92
6	Moist-areas	5.89
7	Waters	0.21
8	Sealed Areas	0.00
9	Bareland	5.40

With only 1.36% of the land surface covered by settlements, the Kouris catchment is a region with low population density. This reflects in the fact that sealed areas are

effectively meaningless in all aspects. Scrubland, pine forests and deciduous trees are the dominating land covers in the Kouris catchment with more than 75% of the total area. Deciduous trees are mostly in the form of vineyards and not irrigated orchard trees (UDLUFT et al., 2003). Interesting is the spatial distribution of moist areas. As Figure 2.8 depicts, moist areas only exist in the northern half of the catchment.

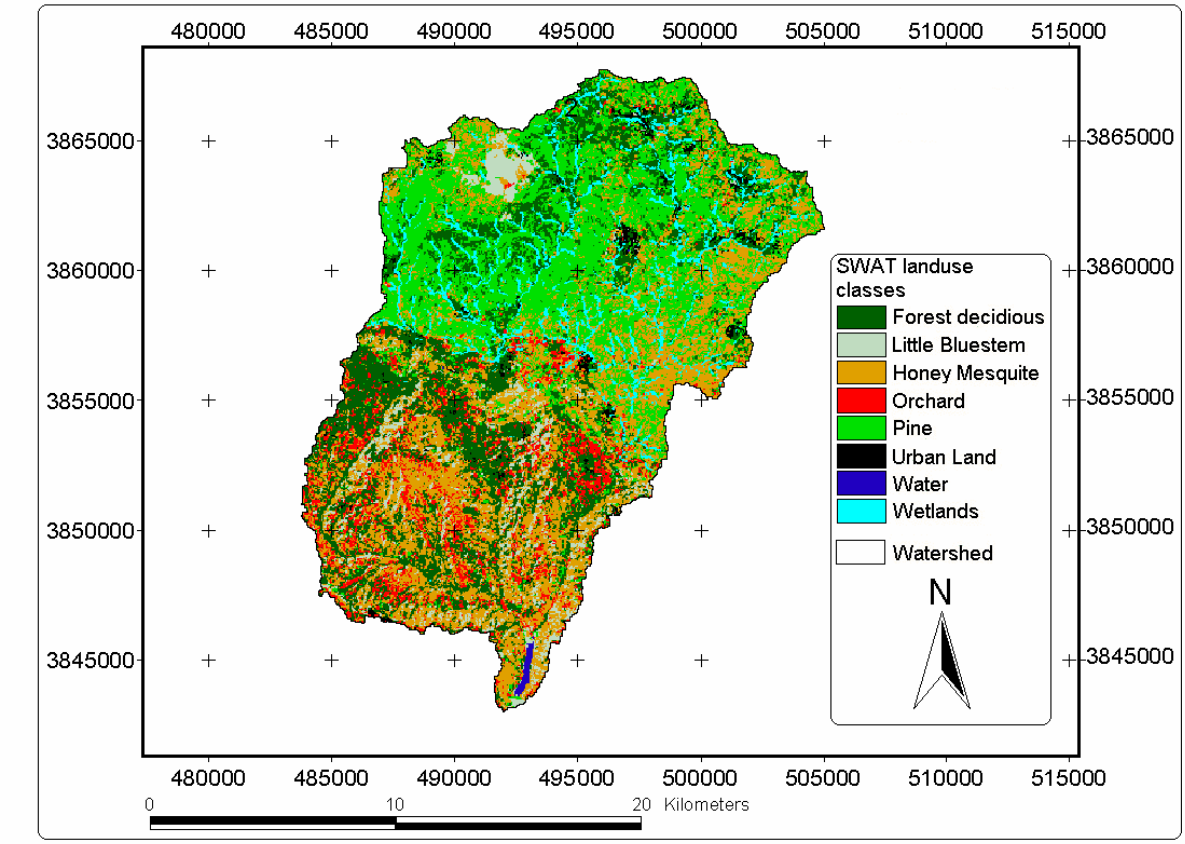

Figure 2.8 Distribution of land use within the Kouris catchment

2.6 Summary

The Kouris catchment is located at the southern flank of the Troodos massive. The region is mountainous with slope angle close to 50°. The climate is mediterranean with mild winters, long hot and dry summers and short spring and autumn seasons. Precipitation decreases from north to south along the altitude gradient, ranging from 580 to 900 mm/y. From a geological point of view, the Kouris catchment can be subdivided into 3 different regions: the Troodos terrane, the circum Troodos sedimentary succession and the Arakapas sequence.

The shallow Leptosols and Regosols are the dominating soils with more than 50% of the area in the percentage composition. Distribution of lithologies, soils and the climatic influence reflect in the distribution of land use, especially the wetlands.

3 Methods

3.1 Model Description

AVSWAT is an *ArcView* extension which acts as a graphical user interface for the *SWAT* (Soil and Water Assessment Tool) model, developed by Dr. Jeff Arnold for the *USDA* Agricultural Research Service (*ARS*). "*SWAT* is a river basin, or watershed, scale model developed to predict the impact of land management practices on water, sediment, and agricultural chemical yields in large, complex watersheds with varying soils, land use, and management conditions over long periods of time" (DI LUZIO et al., 2002). It is organized in several linked tools which are grouped in the following eight modules:

- Watershed Delineation
- HRU Definition
- Definition of the Weather Stations
- AVSWAT Databases
- Input Parameterization, Editing and Scenario Management
- Model Execution
- Read and Map-Chart Results
- Calibration tool

"*SWAT* was developed to predict the impact of land management practices on water, sediment and agricultural chemical yields in large complex watersheds (…) over long periods of time" (NEITSCH et al., 2005). Therefore the model is physically based and requires specific information about weather, soil properties, topography, vegetation, and land management practices occurring in the watershed. "The physical processes associated with water movement, sediment movement, crop growth, nutrient cycling, etc. are directly modeled by *SWAT* using this input data" (NEITSCH et al., 2005).

SWAT is a continuous time model, i.e. a long-term yield model. The model is not designed to simulate detailed, single-event flood routing.

For modeling purposes, a watershed may be partitioned into several subbasins. “The use of subbasins in a simulation is particularly beneficial when different areas of the watershed are dominated by land uses or soils dissimilar enough in properties to impact hydrology” (NEITSCH et al., 2005).

The water balance is the base for all other processes in the watershed. Therefore, for an accurate prediction of the movement of pesticides, sediments or nutrients, regardless of the issue, the hydrologic cycle as simulated by the model must conform to the processes in the catchment. The simulation of the hydrology of a watershed can be separated into two major divisions: the land phase of the hydrologic cycle and the water or routing phase of the hydrologic cycle.

“The land phase of the hydrologic cycle controls the amount of water, sediment, nutrient and pesticide loadings to the main channel in each subbasin. The second division is the water or routing phase of the hydrologic cycle which can be defined as the movement of water, sediments, etc. through the channel network of the watershed to the outlet”(NEITSCH et al., 2005).

Prior to simulation, the user has to set up the input data so input files can be generated. *SWAT* provides databases for soils, weather stations, landcover/plant growth, fertilizer, pesticides, tillage and urban areas. Because *SWAT* was developed in the U.S., the databases contain data, e.g. soil types, that relate to the U.S.. For applications in other countries the databases have to be upgraded, or at least modified.
The following is a summary of the theoretical documentation of *SWAT*, reduced to the important modules and equations.

3.2 The land phase

The simulated processes for the hydrologic cycle are precipitation, evapotranspiration, surface runoff, lateral subsurface flow, groundwater flow and river flow. The base for the simulation is the following equation:

$$SW_t = SW_0 + \sum_{i=1}^{t} \left(R_{day} - Q_{surf} - E_a - w_{seep} - Q_{gw} \right) \qquad \text{Equation 3.1}$$

with

SW_t = the final soil water content (mm H_2O)

SW_0 =the initial soil water content on day *i* (mm H_2O)

t = the time (days)

R_{day} = the amount of precipitation on day *i* (mm H_2O)

Q_{surf} = the amount of surface runoff on day *i* (mm H_2O)

E_a = the amount of evapotranspiration on day *i* (mm H_2O)

w_{seep} = the amount of water entering the vadose zone from the soil profile on day *i* (mm H_2O)

Q_{gw} = the amount of return flow on day *i* (mm H_2O)

To reflect differences in runoff generation, the watershed is subdivided in subbasins. Runoff is predicted separately for each hydrological response unit (HRU) and routed to obtain the total runoff for the entire watershed.

3.2.1 Input – The Weather generator

SWAT requires daily values of precipitation, temperature, solar radiation, wind speed and relative humidity. The user can read the inputs from a file or generate the values

using the *SWAT* implemented weather generator model, the WXGEN weather generator model.

3.2.2 Soil Water

Water that enters the soil profile can percolate through the bottom of the profile and become aquifer recharge, if it is not removed earlier by plant uptake, evaporation or through lateral flow that contributes to the stream flow. Plant uptake usually removes the majority of water in the soil zone.
Percolation is calculated for each layer in the soil profile. Water can percolate if the water content exceeds field capacity and the layer below is not saturated. The amount is calculated as

$$SW_{ly,excess} = SW_{ly} - FC_{ly} \quad if \; SW_{ly} > FC_{ly} \qquad \text{Equation 3.2}$$

$$SW_{ly,excess} = 0 \quad if \; SW_{ly} < FC_{ly} \qquad \text{Equation 3.3}$$

with
$SW_{ly,excess}$= drainable water(mm)
SW_{ly} = water content (mm)
FC_{ly} = water content at Field capacity (mm)

Field capacity is calculated:

$$FC_{ly} = WP_{ly} + AWC_{ly} \qquad \text{Equation 3.4}$$

with

WP_{ly} = water content at permanent wilting point, calculated with clay content and bulk density
AWC_{ly} = the plant available water content, defined by the user (mm)

both parameters expressed as fractions of the total soil volume.

The amount of water leaving one layer and entering the one below is calculated using a storage routing methodology:

$$w_{perc} = SW_{ly,\,excess}\left(1-\exp\left[\frac{-dt}{TT_{perc}}\right]\right) \qquad \text{Equation 3.5}$$

with

w_{perc} = amount of water percolating to the underlying soil layer(mm)
dt = the length of time step
TT_{perc} = the travel time for percolation (hrs), calculated with field capacity, water mass at saturation and the saturated hydraulic conductivity

3.2.3 Lateral Flow

Lateral flow appears when soils have impermeable or semi-permeable layers at a shallow depth. Rainfall then percolates vertically until it reaches such a layer and form a saturated zone of water, a perched aquifer. *SWAT* uses a kinematic storage model for subsurface flow, based on mass continuity equation with the entire hillslope segment as the control volume.

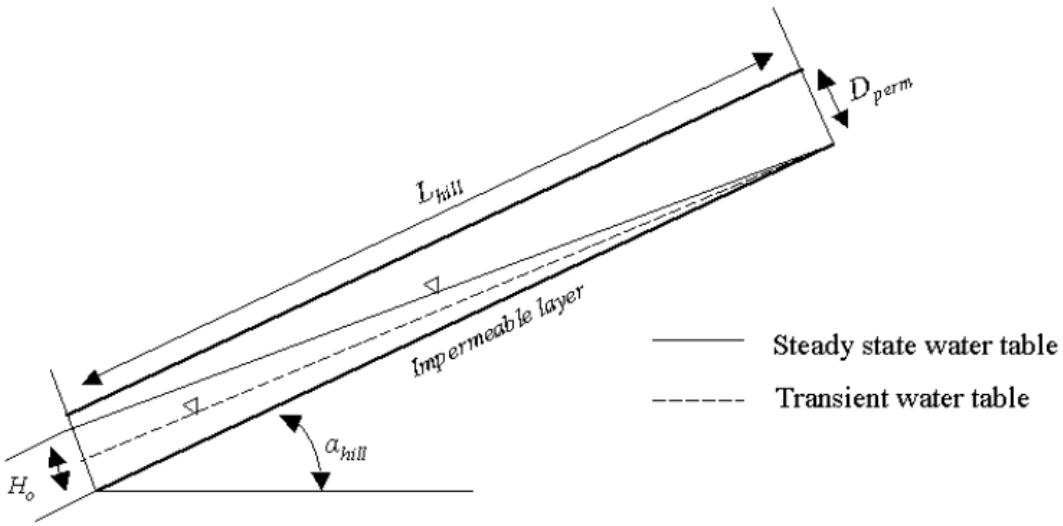

Figure 3.1 Behaviour of the water table as assumed in the kinematic storage model for lateral flow (Neitsch et al., 2005)

The drainable water volume stored in the saturated zone of the hillslope segment per unit area is

$$SW_{ly,\,excess} = \frac{1000 * H_0 * \phi_d * L_{hill}}{2} \qquad \text{Equation 3.6}$$

with

$SW_{ly,excess}$ = the drainable water volume stored in the saturated zone of the hillslope segment per unit area (mm)

H_0 = saturated thickness normal to the hillslope at the outlet expressed as a fraction of the total thickness (mm/mm)

ϕ_d = drainable porosity of the soil (mm/mm)

The net discharge at the outlet of the hillslope, Q_{lat} (mm), is given by

$$Q_{lat} = 24 * H_0 * V_{lat} \qquad \text{Equation 3.7}$$

The velocity of flow at the outlet (mm/h) is defined as

$$v_{lat} = K_{sat} * sin(\alpha_{hill}) \qquad \text{Equation 3.8}$$

with

K_{sat} = saturated hydraulic conductivity ($mm*h^{-1}$)

For *SWAT,* the slope is the increase in elevation per unit distance (*slp*) which is equivalent to $\tan(\alpha_{hill})$. With $\tan(\alpha_{hill}) \approx \sin(\alpha_{hill})$, and equations Equation 3.6 and Equation 3.7 , the net discharge is

$$Q_{lat} = 0,024 * \left(\frac{2 * SW_{ly,\,excess} + K_{sat} * slp}{\phi_d * L_{hill}} \right) \qquad \text{Equation 3.9}$$

When the time of concentration is more than 1 day, only a portion of the lateral flow reaches the streamflow on the day it is generated. Therefore the amount of lateral flow released to the main channel is

$$Q_{lat} = \left(Q'_{lat} + Q_{latstor,\,i-1}\right) * \left(1 - \exp\left[\frac{-1}{TT_{lag}}\right]\right) \qquad \text{Equation 3.10}$$

with

Q'_{lat} = generated amount of lateral flow in the subbasin on a given day (mm)
$Q_{latstor,i-1}$ = lateral flow stored or lagged from the previous day(mm)
TT_{lag} = lateral flow travel time (days)

3.2.4 Groundwater

For each subbasin *SWAT* simulates two aquifers. The shallow aquifer is unconfined and contributes to the streamflow. The deep aquifer is confined and is assumed to contribute to a streamflow outside the watershed. Water percolates through the soil layers, flows through the vadose zone and becomes recharge. The recharge to both aquifers is calculated with an exponential decay weighting function to account for the time delay in aquifer recharge once the water exits the soil profile:

$$w_{rchrg,\,i} = \left(1 - \exp\left[\frac{-1}{\delta_{gw}}\right]\right) * w_{seep} + \exp\left[\frac{-1}{\delta_{gw}}\right] * w_{rchrg,\,i-1} \qquad \text{Equation 3.11}$$

with

$w_{rchrg,i}$ = amount of recharge entering the aquifer on day i(mm)
δ_{gw} = delay time of the overlaying geologic formation(days)
w_{seep} = total amount of water exiting the bottom of the soil profile on day i(mm)
$w_{rchrg,i-1}$ = amount of recharge entering the aquifer on day i-1(mm)

The total amount of water exiting the bottom of the soil profile w_{seep} is

$$w_{seep} = w_{perc,ly=n} + w_{crk,btm} \quad \text{Equation 3.12}$$

with

$w_{perc,ly=n}$= amount of water percolating out of the lowest layer n on day i (mm)
$w_{crk,btm}$ = amount of bypass flow on day i (mm)

SWAT partitions the recharge volume. A fraction of the total recharge is diverted from the shallow aquifer to the deep aquifer to simulate percolation.

$$w_{deep} = \beta_{deep} * w_{rchrg} \quad \text{Equation 3.13}$$

with

w_{deep} = amount of water moving to the deep aquifer (mm)
β_{deep} = aquifer percolation coefficient

For the shallow aquifer the recharge is then

$$w_{rchrg,sh} = w_{rchg} - w_{deep} \quad \text{Equation 3.14}$$

Baseflow contributes to the streamflow by the shallow aquifer if the amount stored in the aquifer exceeds a threshold value ($aq_{shthr,q}$) specified by the user. The amount of groundwater flow into the main channel is

$$Q_{gw,i} = Q_{gw,i-1} * \exp\left[-\alpha_{gw} * \Delta t\right] + w_{rchrg,sh} * \left(1 - \exp\left[-\alpha_{gw} * \Delta t\right]\right) \quad \text{Equation 3.15}$$
$$\text{if} \quad aq_{sh} > aq_{shthr,q}$$

If this condition is not given then the amount of groundwater flow into the main channel is

$$Q_{gw,i} = 0 \quad \text{if} \quad aq_{sh} < aq_{shthr,q} \qquad \text{Equation 3.16}$$

where

$Q_{gw,i}$ = groundwater flow into the main channel on day i (mm)
α_{gw} = baseflow recession constant
Δt = time step (days)
aq_{sh} = amount of water stored in the shallow aquifer(mm)

If no recharge occurs, the second term becomes zero and the contribution descends exponentially.
The model calculates bypass-flow for Vertisols, soils with a high fraction of clay characterized by a propensity to shrink when dried and swell when moistened. A perched aquifer is created if the soil profile is saturated and percolation to underlying layers is inhibited. A detailed description can be found in the theoretical documentation.

3.2.5 Evapotranspiration

SWAT is able to calculate the potential ET using three methods: the Penman-Monteith method, the Priestley-Taylor method or the Hargreaves method. If data from different methods is available, reading in from a file is possible. A detailed description of these methods is to be found in the theoretical documentation.

3.2.6 Canopy Storage

The maximum amount of water that can be stored in the canopy for each day is a function of the leaf area index:

$$can_{day} = can_{mx} * \frac{LAI}{LAI_{mx}} \qquad \text{Equation 3.17}$$

with

can_{day} = maximum amount of water that can be stored in the canopy on a given day (mm)
can_{mx} = maximum amount of water that can be stored at full development of the canopy (mm)
LAI = actual leaf area index
LAI_{mx} = maximum leaf area index for the plant

For each event the canopy storage is filled before any water is can reach the ground.

When calculating actual evaporation, *SWAT* removes the water stored in the canopy. If potential evaporation E_0 is less than the stored water R_{INT} then

$$E_a = E_{can} = E_0 \qquad \text{Equation 3.18}$$

and

$$R_{INT(f)} = R_{INT(i)} - E_{can} \qquad \text{Equation 3.19}$$

Where

E_a = amount of actual evaporation occurring in the watershed on a given day (mm)
E_{can} = amount of evaporation from free water in the canopy on day i (mm)
E_0 = potential evaporation on a given day (mm)
$R_{INT(i)}$ = initial amount stored in the canopy (mm)
$R_{INT(f)}$ = final amount stored in the canopy (mm)

If potential evaporation exceeds the amount of free water in the canopy, then

$$E_{can} = R_{INT(i)}$$

and

$$R_{INT(f)} = 0$$

The remaining evaporative water demand is partitioned between vegetation and snow/soil.

3.2.7 Surface Runoff

SWAT generates surface runoff if rainfall exceeds infiltration rates and surface depressions are filled. The user can choose between two methods for estimating surface runoff: the SCS curve number method and the Green & Ampt infiltration method.

The SCS curve number equation is an empirical model to predict surface runoff under varying land use and soil types. This method calculates surface runoff with the amount of precipitation *P* and the potential maximum retention after runoff begins *S. S* depends on the curve number. The major factors that determine the curve numbers (CN) are the hydrological soil group, cover type, treatment, hydrologic condition, and antecedent runoff condition (MAIDMENT, 1995). However, rainfall intensity is not regarded.

The equation is:

$$Q_{surf} = \frac{\left(R_{day} - I_a\right)}{\left(R_{day} - I_a + S\right)} \qquad \text{Equation 3.20}$$

with

Q_{surf} = accumulated surface runoff (mm)

R_{day} = rainfall depth for the day (mm)

I_a = initial losses (mm)

S = retention parameter (mm)

Surface Runoff occurs if rainfall exceeds the initial losses, commonly approximated as 0,2*S.

Typical curve numbers for moisture condition II (average moisture) are listed in the theoretical documentation for various land covers and soil types.

Fore large subbasins *SWAT* can calculate a surface runoff lag. Thereby only a portion of the surface runoff reaches the main channel on the day it is generated. When surface runoff is generated, the amount released to the main channel Q_{surf} is:

$$Q_{surf} = \left(Q'_{surf} + Q_{stor,i-1}\right) * \left(1 - \exp\left[\frac{-surlag}{t_{conc}}\right]\right) \qquad \text{Equation 3.21}$$

with

Q'_{surf} = amount of surface runoff generated in the subbasin on a given day (mm)

$Q_{stor,i-1}$ = surface runoff stored from the previous day (mm)

t_{conc} = time of concentration for the subbasin (hrs)

surlag = surface runoff lag coefficient

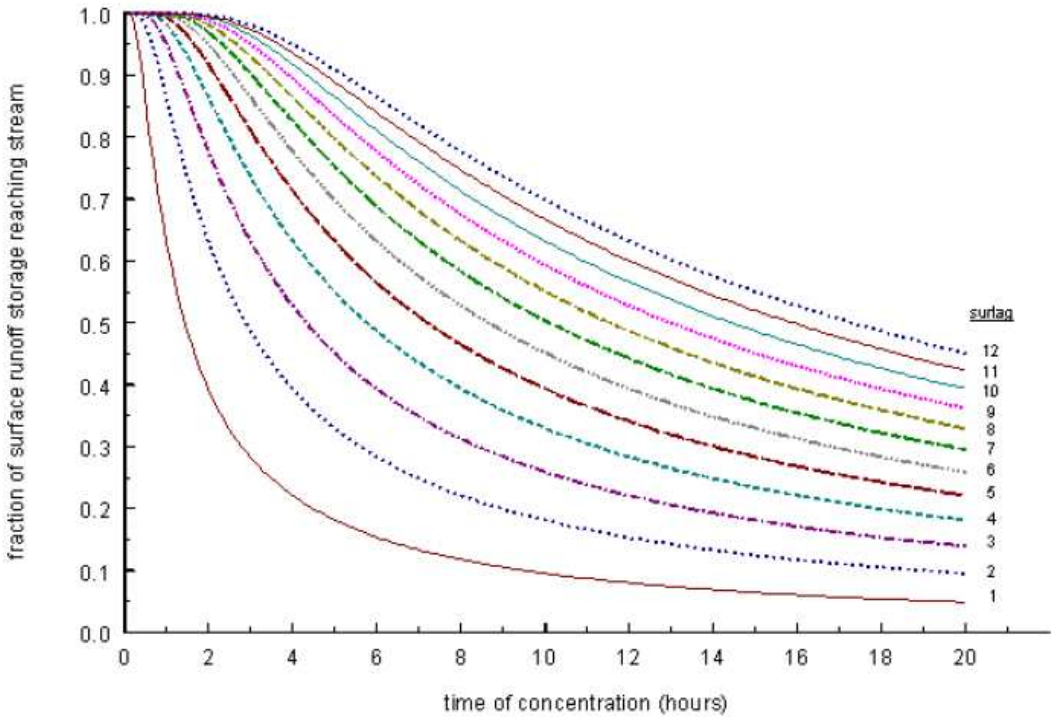

Figure 3.2 Influence of *surlag* and time of concentration on fraction of surface runoff (NEITSCH et al. 2005)

Disadvantage of the curve number method is that rainfall intensity is not taken into account.

Since *SWAT* did not run simulations with the Green&Ampt infiltration method for surface runoff estimations, this method is not further described.

3.2.8 Transmission Losses

Transmission losses reduce the runoff volume during the downward flow of water in the channel. Runoff volume after transmission losses is predicted as

$$vol_{Qsurf} = 0 \quad \text{if } \mathrm{vol}_{\mathrm{Qsurf,i}} \leq \mathrm{vol}_{\mathrm{thr}} \qquad \text{Equation 3.22}$$

$$vol_{Qsurf} = a_x + b_x * vol_{Qsurf,\,i} \quad \text{if} \quad \mathrm{vol}_{\mathrm{Qsurf,i}} > \mathrm{vol}_{\mathrm{thr}} \qquad \text{Equation 3.23}$$

with

Vol_{Qsurf} = volume of runoff after transmission losses (m³)
a_x = regression intercept for a channel of length L and width W (m³)
b_x = regression slope for a channel of length L and width W
$Vol_{Qsurf,i}$ = volume of runoff prior to transmission losses (m³)
Vol_{thr} = threshold volume for a channel of length L and width w (m³)

The threshold volume is

$$vol_{thr} = -\frac{a_x}{b_x} \qquad \text{Equation 3.24}$$

The corresponding equation of the peak runoff rate is

$$q_{peak,\,f} = \frac{1}{3600 * dur_{flw}} * \left[a_x - (1 - b_x) * vol_{Qsurf,\,i} \right] + b_x * q_{peak,\,i} \qquad \text{Equation 3.25}$$

where

$Q_{peak,f}$ = peak rate after transmission losses (m3/s)
dur_{flw} = duration of flow (hrs)
$Q_{peak,I}$ = peak rate before accounting for transmission losses (m³/s)

The duration of flow is

$$dur_{flw} = \frac{Q_{surf} * Area}{3,6 * q_{peak}} \qquad \text{Equation 3.26}$$

with

Area = area of the subbasin (km²)
Q_{peak} = peak runoff rate (m³/s)

3.3 The routing phase

SWAT determines the amount of water, sediments, nutrients and pesticides reaching the stream network. *SWAT* uses Manning's equation to define the rate and velocity of flow. Water is routed through the channel network using the variable storage routing method or the Muskingum river routing method. Both the variable storage and Muskingum routing methods are variations of the kinematic wave model.
As water flows downstream, *SWAT* calculates losses and supplements. Water may be lost due to evaporation and transmission through the bed of the channel. Another

potential loss is removal of water from the channel for agricultural or human use. Flow may be supplemented by direct rainfall on the channel and/or by addition of water from point source discharges.

3.4 Summary

SWAT is a complex hydrological model using a multitude of parameters for water balance modeling. At first, climatic data is processed by the weather generator, which delivers precipitation as input. Depending on land use, climatic data and soil properties, the input decreases by surface runoff or evaporation. The remaining amount becomes soilwater, which is then partitioned into lateral flow and recharge. Recharge is again partitioned between the deep and the shallow aquifer. Water in the deep aquifer cannot participate in the water cycle. The amount of water in the shallow aquifer is diminished by baseflow or re-evaporation. The discharge is composed of the contributions of lateral flow, baseflow, surface runoff, and rainfall into the channel as plus compounds, and transmission losses and evaporation as minus compounds.
The theoretical documentation of *SWAT* provides a detailed description of all modules.

4 Modeling Results

4.1 Parameterization

4.1.1 Land Cover/Plant Growth Database

Swat includes a “Land Cover/Plant Growth” Database providing 99 different land cover classes, divided in perennial (e.g. Little Bluestem), warm season annual (e.g. Corn), cool season annual (e.g. Winter Wheat), warm season annual legume (e.g. Soybeans), cool season annual legume (e.g. Field Peas) and trees (e.g. Pines).
The database thereby contains information needed by SWAT to simulate the growth of a particular land cover. Growth affects the water and the nutrient cycle. All parameters define plant growth under ideal conditions and quantify the impact of some stresses on plant growth.
Plant growth is controlled by the plants attributes summarized in the plant growth database and by the operations listed in the management file.

Assignment of the land use classes

The following table shows the land use classes assigned during GRC project and the class assigned in *SWAT*.

Table 4.1 Land use Classes (GRC Project and *SWAT*)

Land use class (GRC)	Land use class (*SWAT*)
Deciduous trees	Deciduous trees
Scrubland	Honey Mesquite
Pine Forest	Pine
Settlement	Urban land – low density
Field	Orchard
Moist-Areas	Wetland
Waters	Water
Sealed Areas	Sealed area
Bare Land	Little bluestem

For the classes deciduous trees, pine forest, settlement, moist areas, water and sealed areas already existed adequate classes in *SWAT*. For scrublands the *SWAT*-class honey mesquite is used, for bare land the *SWAT* class little bluestem. All parameters remained at their default values for the particular land use class.

Honey Mesquite

The honey mesquite (Prosopis Glandulosa) belongs to the Fabaceae (Pea family). It can be a shrub or a tree. Its size ranges from 4 to 6 m, and can normally be found on plains or dry ranges (Plant Guide, USDA, 2002). The Honey Mesquite occurs over climatically diverse regions. It grows well on all soil types and thrives well in high temperatures above 38℃. The frost and salt toleran ce of the honey mesquite is regarded moderate (URL 1).

Figure 4.1ab Honey Mesquite (Prosopis Glandulosa) (URL3), Little Bluestem (Schizachyrium scoparium) (URL2)

Little Bluestem

Little bluestem (Schizachyrium scoparium) is a medium height grass. “As a warm season grass it begins growth in late spring and continues through the hot summer period until the first killing frost (…). It will grow on a wide variety of soils but is very well adapted to well-drained, medium to dry, infertile soils. The plant has excellent

drought and fair shade tolerance, and fair to poor flood tolerance" (Plant Fact Sheet, USDA, 2002).

4.1.2 Soil Database

The integrated *SWAT* soil database provides parameters for common soil types of the U.S.. Therefore, the mediterranean soil types which occur in Cyprus are not available in the existing database. Thus, these Mediterranean soils had to be added to the existing *SWAT* soil database. *SWAT* uses 17 parameters to characterize different soil types. The parameters are:

- **NLAYERS**: number of layers in the soil
- **HYDGRP**: soil hydrological group according to the U.S. Natural Resource Conservation Service (NRSC) based on infiltration characteristics
- **SOL_ZMX**: maximum rooting depth for a soil (mm)
- **ANION_EXCL**[optional]: fraction of porosity from which anions are excluded
- **SOL_CRK**[optional]: potential or maximum crack volume of the soil profile expressed as a fraction of the total volume (m^3/m^3)
- **SOL_Z**: depth from surface to bottom of the layer (mm)
- **SOL_BD**: bulk density (g/cm^3)
- **SOL_AWC**: soil available water capacity (mmH2O/mm soil)
- **SOL_K**: saturated hydraulic conductivity (mm/hr)
- **SOL_CBD**: organic carbon content (% soil weight)
- **CLAY**: clay content (% soil weight)
- **SILT**: silt content (% soil weight)
- **SAND**: sand content (% soil weight)
- **ROCK**: rock fragment content (% total weight)
- **SOL_ALB**: moist soil albedo
- **USLE_K**: USLE equation erodibility factor
- **SOL_EC**: electric conductivity (µS/cm)

Parameterization

Hydraulic Conductivity (Sol_K)

Within the GRC project, twenty different soil types or groups and 48 geological units have been defined for Cyprus. The Kouris catchment contains six different soil types, eighteen different geological units and a total of 37 soil-geology combinations. For the different lithologies are documented the field capacity (FC) and two different K_f-values: one represents the soil (k_f1), whereas the other stands for the subsoil – the boundary layer to the conterminous lithology- (k_f2), (GRC Task 6/7, 2003). The geometrical mean is used to calculate kf1 and kf2 for each of the six soil types. The equation is:

$$\bar{x}_{\mathrm{geom}} = \sqrt[n]{\prod_{i=1}^{n} x_i} = \sqrt[n]{x_1 \cdot x_2 \cdot \ldots \cdot x_n} \qquad \text{Equation 4.1}$$

Organic Carbon Content (SOL_CBD)

Contents of organic carbon (OC) are estimated according to the “World Soil Resources Report 94: Lecture Notes on the Major Soils of the World” (DRIESSEN et al., 2001) and “Soil Taxonomy - A Basic System of Soil Classification for Making and Interpreting Soil Surveys” (Soil Survey Staff, 1999). For the soil group “LP.li-CL.ptp” (lithic LEPTOSOLS and epipetric CALCISOLS), for instance, the content of organic carbon is set to 1.5%, since “most Calcisols contain only 1 or 2 percent organic matter” (DRIESSEN et.al. 2001). Soil organic matter generally contains approximately 56% OC. The following equation is used to estimate the total organic matter content of the soils from OC measurements (URL 4):

$$\%\ \text{Organic Matter} = \%\ \text{Organic Carbon} \times 1.78 \qquad \text{Equation 4.2}$$

Rock Fragment Content

Rock fragment content is estimated similar to the content of organic carbon. The attribute ´skeletic´ is specified by DRIESSEN et al. (2001) as “having, to a depth of 100 cm from the soil surface, between 40 and 90 percent (by weight) gravel or other coarse fragments”. Thus, for “RG.ca.sk-LP.li.ca” (skeletic-calcaric-REGOSOLS and calcaric-lithic-LEPTOSOLS) the rock fragment content is set to 60 percent for all layers.

Clay Content

The clay content is estimated using the tool “Soil Water Characteristics”, included in the SPAW model (Soil-Plant-Atmosphere-Water), developed by Keith E. Saxton. This program is used to estimate the hydrologic water holding and transmission characteristics of a soil profile layer. The estimating equations were developed by correlations of 1722 samples provided by the USDA/NRCS National Soil Survey Laboratory.
With this hydraulic properties calculator it is possible to revise different assumed combinations of clay and sand contents for the given K_f value.
Scheffer and Schachtschabel (2002) specifiy for a vertic Cambisol a clay content >45% between the A- and C-horizon for vertic Cambisols. According to “Bodenkundliche Kartieranleitung”, the Ah-horizon has less than 45% clay content. For the soil group “CM.fv.ca-CM.vr” (calcaric-fluvic-CAMBISOLS and vertic-CAMBISOLS) the clay content is set to 22% for the uppermost layer and to 45% for the remaining layers. This leads to K_f-values of 12.2 mm/hr and 4mm/hr. The K_f-values are thereby changed arbitrarily to take into account the soil documentation.

Sand Content

The sand content is determined similar to the clay content by choosing the “best fit” for the known K_f-value.

Silt Content

The silt content results from the calculations of sand and clay content as the residual value to 100%.

Bulk Density (SOL_BD)

Bulk density is calculated by “Soil Water Characteristics” as a function of the contents of clay, sand, silt, gravel and organic matter. The values range from 1.24 g/cm³ (CM.fv.ca-CM.vr) to 1.67g/cm³ (LP.li-CL.ptp). Scheffer and Schachtschabel (2002) specify values for bulk density for sand in the range of 1.16-1.7 g/cm³ for silt 1.17-1.63 g/cm³ and for clay 0.93-1.72 g/cm³.

Available Water Capacity (SOL_AWC)

Soil available water capacity is calculated by “Soil Water Characteristics”. It is a function of the contents of clay, sand, silt, gravel and organic matter.

Hydrologic Group (HYDGRP)

The U.S. Natural Resource Conservation Service (NRCS) classifies soils into four hydrologic groups (A, B C, or D) based on infiltration characteristics of the soils. A hydrologic group is a group of soils, which similar runoff potential under similar storm and cover conditions. Parameters that influence runoff potential are those that have an impact on the minimum rate of infiltration for a bare soil after prolonged wetting. These parameters are depth to a seasonally high water table, saturated hydraulic conductivity, and depth to a very slowly permeable layer. Due to the lack of data, parameters are set to class B for all soil groups added to the database. Class B includes “soils having moderate infiltration rates when thoroughly wetted, chiefly

moderately deep to deep, moderately well to well drained, with moderately fine to moderately coarse textures" (NEITSCH et al., 2005).

The guidelines used by the USDA Soil Survey to categorize soils into Hydrologic Groups are summarized in Table 4.2.

Table 4.2 Hydrologic Group Rating Criteria (NEITSCH et al., 2005, modified)

Criteria	Hydrologic Soil Groups			
	A	**B**	**C**	**D**
Final constant infiltration rate (mm/hr)	7.6 - 11.4	3.8 - 7.6	1.3 - 3.8	0 - 1.3
Mean permeability: surface layer (mm/hr)	> 254.0	84.0 - 254.0	8.4 - 84.0	< 8.4
Mean permeability: most restrictive layer below the surface layer to a depth of 1.0 m (mm/hr)	> 254.0	84.0 - 254.0	8.4 - 84.0	< 8.4
Shrink-swell potential: most restrictive layer	Low	Low	Moderate	High-Very High
Depth to bedrock or cemented pan (mm)	> 1016	> 508	> 508	< 508

Rooting Depth (SOL_ZMX)

For all soil groups containing lithic Leptosols the maximum rooting depth is set to 500 mm. This is due to the high rock fragment content and the shallow depth. For all other soil groups a maximum rooting depth of 1000 mm is applied.

Soil Albedo (SOL_ALB)

The moist soil albedo expresses the amount of solar radiation reflected by the soil to the amount incident upon it, expressed as a fraction. Since no data is available, the albedo is set to 0.05 for all soil groups as the average of the soil moist albedo of the provided soils within the *SWAT* database.

USLE Factor (USLE_K)

The USLE (Universal Soil Loss Equation) factor describes the differences in erodibility of soils, caused by the soil properties. The given range is 0.0-0.65 ((0.013 metric ton m^2 hr)/ (m^3-metric ton cm)). Due to the lack of data the factor is set to 0.3.

Electric Conductivity (SOL_EC)

The soil electrical conductivity is currently not active.

Number of Layers (NLAYERS)

The number of assigned layers firstly depends on the soil type being modeled. Second, is it recommended to use at least 3 layers for soilwater calculations to get proper results for the soilwater gradient.

Anion Exclusion (ANION_EXCL)[optional]

“Most soil minerals are negatively charged at normal pH and the net interaction with anions such as nitrate is a repulsion from particle surfaces. This repulsion is termed negative adsorption or anion exclusion” (NEITSCH et al., 2005). Because of the preferential attraction of cations, anions are excluded from the area directly adjacent to mineral surfaces because of the preferential attraction of cations. This process has a direct influence on the transport of anions in the soil because it excludes anions from the part of the water volume flowing close to the charged particle surfaces. Therefore the pathway is shorter.
The ANION_EXCEL value is the fraction of porosity (void space) from which anions are excluded. It is set to 0.5 by default.

Crack Volume Potential (SOL_CRK) [optional]

SOL_CRK is the potential or maximum crack volume of the soil profile expressed as a fraction of the total soil volume. It is used for accurate prediction of surface runoff and infiltration in areas dominated by Vertisols.
Vertisols are “clayey soils that have deep, wide cracks for some time during the year and have slickensides within 100 cm of the mineral soil surface” (SOIL SURVEY STAFF, 1999). They shrink when dry and swell when moistened
The maximum clay content of soils in the Kouris catchment is 28% for “eutric Cambisols and eutric-anthropic Regosols” (CM.eu-RG.ah.eu). Therefore, this parameter is irrelevant.

Depth (SOL_Z)

The depth for each layer ranges from 100mm for the upper layers up to 350mm for the lowest layers, depending on the soiltype.

4.1.3 The Weather Generator

SWAT requires daily values of precipitation, temperature, solar radiation, wind speed and relative humidity. The user can read the inputs from a file or generate the values using *SWAT* weather generator model.

“The weather generator input file contains the statistical data needed to generate representative daily climate data for the subbasins. Climatic data will be generated in two instances: when the user specifies that simulated weather will be used or when measured data is missing” (NEITSCH et al., 2005).

The required parameters are:

- **TMPMX(mon)**: average or mean daily maximum air temperature (°C) for each month
- **TMPMN(mon)**: average or mean daily minimum air temperature (°C) for each month
- **TMPSTDMX(mon)**: Standard deviation for daily maximum air temperature (°C) for each month
- **TMPSTDMN(mon)**: Standard deviation for daily minimum air temperature (°C) for each month
- **PCPMM(mon)**: average or mean total monthly precipitation (mm H_2O)
- **PCPSTD(mon)**: standard deviation for daily precipitation in month (mm H_2O)
- **PCPSKW(mon):** Skew coefficient for daily precipitation in month
- **PR_W(1,mon):** probability of a wet day following a dry day
- **PR_W(2,mon)**: probability of a wet day following a wet day
- **PCPD(mon)**: average number of days of precipitation in month
- **RAINHHMX(mon)**: maximum 0,5-hour rainfall in the entire period of record for month (mm H_2O)
- **SOLARAV(mon):** average solar radiation for month (MJ/m²/d)
- **DEWPT(mon**): average daily dew point temperature in month (°C)
- **WNDAV(mon)**: average daily wind speed in month (m/s)

Calculations

Temperature and Precipitation

With one exception, all needed parameters describing precipitation and temperature are calculated according to the I/O documentation for the weather generator using EXCEL spreadsheets.
For the standard deviation of daily precipitation for each month the I/O documentation gives the following equation:

$$\sigma_{\text{mon}} = \sqrt{\frac{\sum_{d=1}^{N} \left(R_{day,\,mon} - R_{mon} \right)^2}{N - 1}} \qquad \text{Equation 4.3}$$

with

σ_{mon} = the standard deviation for daily precipitation in month *mon* (mm H_2O)
$R_{day,mon}$ = the amount of precipitation for record *d* in month *mon* (mm H_2O)
R_{mon} = the average precipitation for the month (mm H_2O)
N = is the total number of daily precipitation records for month *mon*

In general, the standard deviation is known as the root mean square deviation of values from their arithmetic mean. The arithmetic mean of a list of numbers is generally thought to be the sum of all the members of the list divided by the number of items in the list. Therefore the given equation - with R_{mon} as the average *monthly* precipitation - does not correspond to the common idea of the standard deviation.
SWAT provides a dataset for the weather generator for weather gages in the United States. The listed standard deviation for daily precipitation for each month implies that these were calculated with the common idea of the standard deviation.
The *SWAT* web site provides a pre-processing tool (*URL 5*) to calculate several of the needed parameters for the weather generator, including the standard deviation of daily

precipitation for each month. The calculation seems to have used the mean as the sum of all the members of the list divided by the number of items in the list, too.
Thus, the common idea of the standard deviation is used to calculate it, although it might be sensible for some other reason to use the preserved equation.

Solar Radiation

The average daily solar radiation is calculated by summing the daily values for the months and dividing by the number of days summed.
Solar radiation for every day is calculated in EXCEL according to MAIDMENT (1993).
The extraterrestrial solar radiation (mm/d) is calculated with

$$S_0 = 15.392 \cdot d_r \cdot (\omega_s \cdot \sin(\phi) \cdot \sin(\delta) + \cos(\phi) \cdot \cos(\delta) \cdot \sin(\omega_s)) \qquad \text{Equation 4.4}$$

with ω_s is the sunset hour angle in radians as

$$\omega_s = \arccos(-\tan\phi \cdot \tan\delta) \qquad \text{Equation 4.5}$$

Φ is the latitude and δ is the solar declination given by

$$\delta = 0{,}4093 \sin(\frac{2\pi}{365} J - 1{,}405) \qquad \text{Equation 4.6}$$

with J as the Julian day number.
d_r is the relative distance between sun and earth:

$$d_r = 1 + 0{,}033 \cos(\frac{2\pi}{365} J) \qquad \text{Equation 4.7}$$

The extraterrestrial solar radiation is then calculated by setting against the maximum daylight hours N,

$$N = 24/pi * \omega_s \qquad \text{Equation 4.8}$$

a cloud cover of 2/10 and an assumed albedo of 0,2.

Dewpoint temperature

This value is calculated by summing the dew point temperature T_{DP} for every day in the month for all years of record and dividing by the number of days summed.
The dewpoint for every day is calculated with mean air temperature (T_a) and relative humidity (R_h): The saturated vapor pressure is

$$VP_{\max} = 6{,}1078 \cdot 10^{\frac{7{,}53 \cdot T_a}{237{,}3 + T_a}} \qquad \text{Equation 4.9}$$

and the actual vapor pressure is

$$VP = VP_{\max} \cdot \left(\frac{R_h}{100} \right) \qquad \text{Equation 4.10}$$

According to HÄCKEL (1999), the dewpoint temperature is than

$$T_{DP} = \frac{234{,}18 * \log VP - 184{,}2}{8{,}204 - \log VP} \qquad \text{Equation 4.11}$$

All daily values are summed up for each month, the arithmetic mean leads to the average daily dewpoint for each month.

Windspeed

The average daily wind speed is assumed to be 1m/s. During the calibration it is set to 1.5 m/s.

Virtual weather gage

The weather gages within the Kouris catchment are not evenly distributed. A virtual station was created for the southernmost part in order to make allowance to the

decrease in precipitation from north (high altitude) to south (low altitude). Therefore, the inverse distance weighting (IDW) method is applied (WIEGAND, 2002). IDW is an interpolation technique in which interpolated estimates are made based on values at nearby locations weighted only by distance from the interpolation location.

4.1.4 Conclusions

Parameterization of *SWAT* is both complex and time-consuming due to the multitude of parameters. For the weather generator, climatic data has to be statistically analyzed. The soil database has to be extended with the required soiltypes, the land use has to be assigned and modified if necessary. This a potential source of error. For the quality of the parameterization in this study only the results can serve, uncertainty cannot be stated, in particular for the calculations of soil properties with SPAW.

4.2 Calibration

SWAT is a complex hydrologic model and uses a multitude of parameters. The calibration can be done manually or by using an auto calibration tool. *SWAT* offers techniques such as sensitivity analysis, especially helpful when dealing with a considerable number of parameters.

The first step is the watershed delineation. Then, the land use and soitypes are assigned, and *SWAT* calculates the hydrological response units (HRU). HRUs are distributed according to the dominant land use und soil type or as multiple HRUs., which is the applied method. After the implementation of climatic data for the weather generator, a few simulations were conducted using default parameters.

For a detailed analysis an output-mask is created in EXCEL providing plots of all water cycle components and the measured discharge at gauging stations Nō. 1967 654 70 (Limnatis, Kouris Dam) and Nō.1964 646 90 (Kouris, Kouris Dam) for the 5 years calibration period (1988-1992).
The Nash&Sutcliffe efficiency coefficient and the annual sums of measured and simulated discharge are taken into account for efficiency analysis. Therefore the *SWAT* output data has only to be pasted into the output-mask to get quick information about the effects of parameter changes.

For a more detailed examination, a sensitivity analysis is accomplished providing insights on which parameters contribute most to the output variance due to input variability.

4.2.1 Sensitivity Analysis

The sensitivity analysis is performed and results in 27 parameters that may have a potential influence on river flow (Table 4.3).

Table 4.3 Parameters used in the sensitivity analysis

Parameter	*Definition*	*Process*
canmx	Max canopy storage (mm)	*Runoff*
ALPHA_BF	Baseflow recession constant (days)	*GW*
Sol_z	Soil depth for layer n (mm)	*Soil*
SOL_AWC	Soil available water content	*Soil*
CN2	Curve Numbers	*Runoff*
ESCO	Soil evaporation compensation factor	*Evap*
CH_K2	Effective hydraulic conductivity of the channels (mm/hr)	*Channel*
SMFMX	Max snow melt rate (mm/℃/day)	*Snow*
ch_n	Manning coefficient for channel	*Channel*
SMTMP	Snow melt base temperature (℃)	*Snow*
SFTMP	Snow fall temperature (℃)	*Snow*
TIMP	Snow pack temperature lag factor	*Snow*
SMFMN	Min. snow melt rater (mm/℃/day)	*Snow*
Slope	Average slope steepness (m/m)	*Runoff*
BLAI	Leaf area index for crop	*Evap*
SOL_K	Soil conductivity (mm/hr)	*Soil*
Surlag	Surface runoff lag coefficient	*Runoff*
EPCO	Plant evaporation compensation factor	*Evap*
BIOMIX	Biological mixing efficiency	*Soil*
Sol_alb	Moist soil albedo	*Evap*
RCHRG_DP	Groundwater recharge to deep aquifer	*GW*
GW_DELAY	Groundwater delay (days)	*GW*
TLAPS	Temperature laps rate (℃/km)	*Snow*
SLSSUBSN	Average slope length (m/m)	*Runoff*
REVAPMN	Threshold depth of water in the shallow aquifer for “revap” to occur (mm)	*GW*
GW_REVAP	Groundwater “revap” coefficient	*GW*
GWQMN	Threshold depth of water in the shallow aquifer required for return flow to occur (mm)	*GW*

The analysis is carried out using simulations for the period between 1988 and 1992. Figure 4.2 summarizes the sensitivity ranking

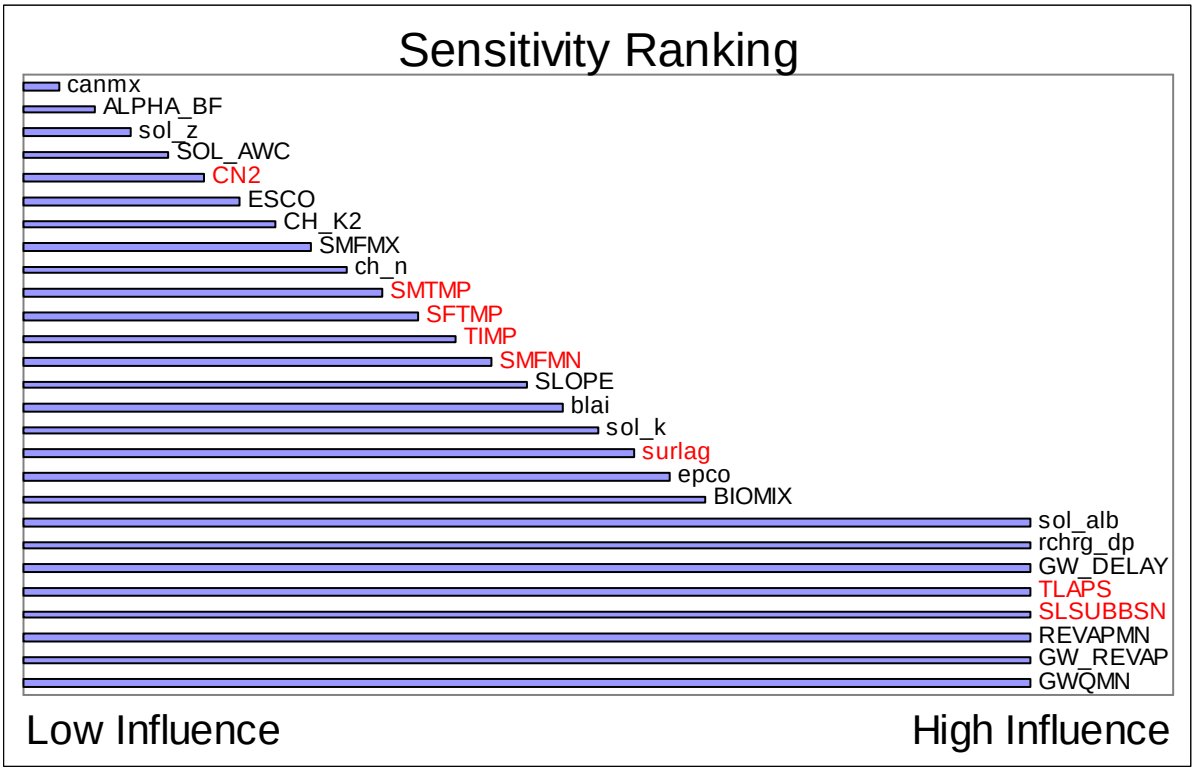

Figure 4.2 Parameters of the sensitivity ranking, parameters of special interest are red

The most sensitive factors are *GWQMN*, *rchrg_dp* and *GW_DELAY* effecting groundwater, *SLSUBBSN* and *TLAPS* effecting lateral flow and *sol_alb*, *REVAPMN* and *GW_REVAP* effecting both evaporation and groundwater. Surprisingly, the Curve Number parameter *CN_2* is within the last fifth, although surface runoff contributes large quantities to the streamflow.

During the first few model runs, *SWAT* calculated too much surface runoff, resulting in huge peak discharges, and too much snowmelt, resulting in simulated peaks that did not occur in the measured data. The sensitivity analysis leads to 8 parameters, being highly sensitive. Thereof, only *SLSUBBSN* and *TLAPS* affect the simulated discharge on the event scale. The importance of the remaining six parameters is rather related to water balance on an annual scale.

Therefore, the next step is a stepwise analysis of these processes within *SWAT* according to the theoretical documentation.

In order to reduce simulation time, it turned out to be useful to set up an extra calibration project during the calibration process. This project includes only the Kouris

catchment without the Limnatis and Kryos. Therefore the numbers of subbasins varies: 12 for the calibration project and 25 for the whole catchment. Results are readily comparable because in both cases the calibration refers to the hydrograph of the Kouris gauging station.
The following is a description of the calibration steps of the particular processes, in order of there assumed relevance for streamflow discharge.

4.2.2 Lateral Flow

Lateral flow appears when soils have impermeable or semi-permeable layers at shallow depths. Rainfall percolates vertically until it reaches such layers and form a saturated zone of water, a perched aquifer. *SWAT* uses a kinematic storage model for subsurface flow, based on mass continuity equation with the entire hillslope segment as the control volume.
According to Equation 3.9, the amount of lateral flow depends on the soilwater excess, the saturated conductivity, the increase in elevation per unit distance (*slp*), the drainable porosity of the soil layer and the hillslope length. If lateral flow is calculated, *SWAT* has an incorporated storage feature to lag portions of the lateral flow in large subbasins, represented by the parameter *TLAPS*. As a result of the sensitivity analysis, the lateral flow lag time and the average slope length (*SLSUBBSN*) are chosen to be modified.
The average slope length seems to depend on the average slope steepness. For slope steepness < 0.25 (m/m) the slope length is 15.244 m, for a slope steepness > 0.25 (m/m), however, it is 0.05 m by default. Subbasin 15, 16, 17, 19, 22, 23 and 24 have a slope steepness < 0.25. For all other subbasins *SWAT* calculated an average slope length of 0.05 m. Thus, three quarters of the 25 subbasins effectively have no slope length at all.
These subbasins produce an immediate response on the input which is one reason for the large amounts of runoff. The average slope length is then set at 15 m for all subbasins. For a further mitigation of the simulated discharge, calibration leads the adaptation of the lag time for lateral flow from zero to ten days.

Figure 4.3ab show the effects of the adjusted lag time and slope length for the time between 11/1/1991 and 04/30/1992. The total streamflow volumes are almost equal with a modeled volume of 54.10 * 10^6 m³ before the changes compared to a volume of 53.16 * 10^6*m³ after the changes. However, the streamflow hydrograph is smoothed, and the output reaction decelerated.

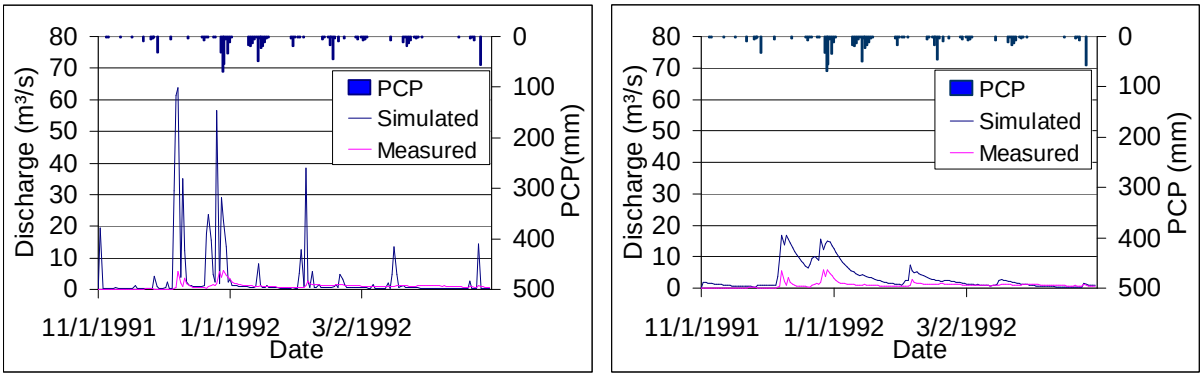

Figure 4.3ab Discharge before and after adjusting Lateral Flow

While absolute amounts of discharge increase from 356% to 360% of measured discharge, the Nash Sutcliffe efficiency improves from -21.5 to -2.8.

Spatial Distribution

In general the amount of lateral flow is high, ranging in the mean from 49-167 mm/y (Figure 4.4). The highest amounts are found in subbasins 3, 4, 5, 20 and 25 with more than 150 mm/y. Subbasins 15 and 16 have with a mean of 49 and 54 mm/y the smallest amounts of lateral flow. Direct underneath subbasins 15 and 16 is subbasin 24 with 80 mm/y lateral flow on average, subbasin 14 in the east has 137 mm/y lateral flow on average.

Because all subbasins with small amounts of lateral flow are located within the same soilgroup, namely the eutric-lithic-LEPTOSOLS and the eutric-skeletic-REGOSOLS first reflections indicate that soil properties cause the low volumes of lateral flow.

The field capacity, as it directly affects soil water excess, is of particular interest. Due to the small amounts of lateral flow, this soil is expected to show high field capacities. In contrast to this, it proved to have surprisingly low field capacities which predestine it

to produce high amounts of soil water excess. Hence, although there is theoretically more water available, the lateral flow is less.

When taking a closer look to water cycle compounds, it turns out that, within the subbasins with small amounts of lateral flow, recharge is higher than in the surrounding subbasins. In subbasin 24 lateral flow averages 80 mm/y and recharge is 143 mm/y while in subbasin 15 lateral flow is 54 mm/y and the recharge is 192 mm/y.

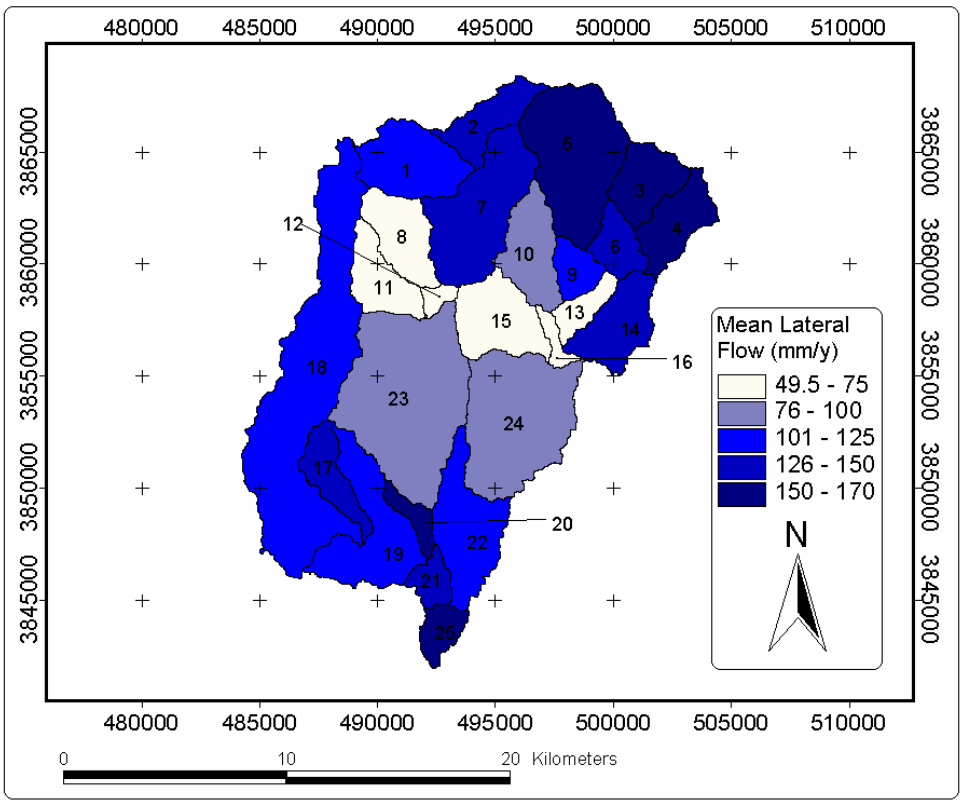

Figure 4.4 Mean annual Lateral flow during calibration period (1988-1992).

To sum up, lateral flow is the most dominant runoff process within the Kouris catchment. About 17% of the mean annual precipitation reaches the streamflow via lateral flow. Together with surface runoff, lateral flow comprises quickflow, the rapid runoff after rainfall.

4.2.3 Surface Runoff

Surface runoff occurs if rainfall intensity exceeds the infiltration capacity (infiltration excess runoff), or if saturated soils prevent infiltration longer periods of rainfall (saturation excess runoff).

The SCS curve number method for surface runoff estimation calculates with daily amounts of precipitation, and with the curve number for a given land use type. Table 4.4 lists the *SWAT* default curve numbers for the particular land use for moisture condition II, and hydrological soil group A.

Table 4.4 *SWAT* land use class and their default curve numbers

SWAT Land use class	Curve Number
Forest Decidious	41
Honey Mesquite	65
Pine	62
Residential Area – low density	31
Orchard	45
Wetlands - mixed	49
Waters	92
Sealed Areas	90
Little Bluestem	31

Although the hydrological soil groups are set to A for all soils, representing low runoff potential and a high infiltration rate, even when thoroughly wetted, *SWAT* calculates large amounts of surface runoff due to intense rain events with more than 100 mm/d.

Figure 4.5 shows the amounts of surface runoff and precipitation during the event between 1/8/1989 and 1/9/1989 (calibration project, Kouris catchment only). Subbasins 3, 4 and 5 yield large quantities of surface runoff in the range of 65 - 71 mm to the streamflow, amounting about 50% of the precipitation volume.

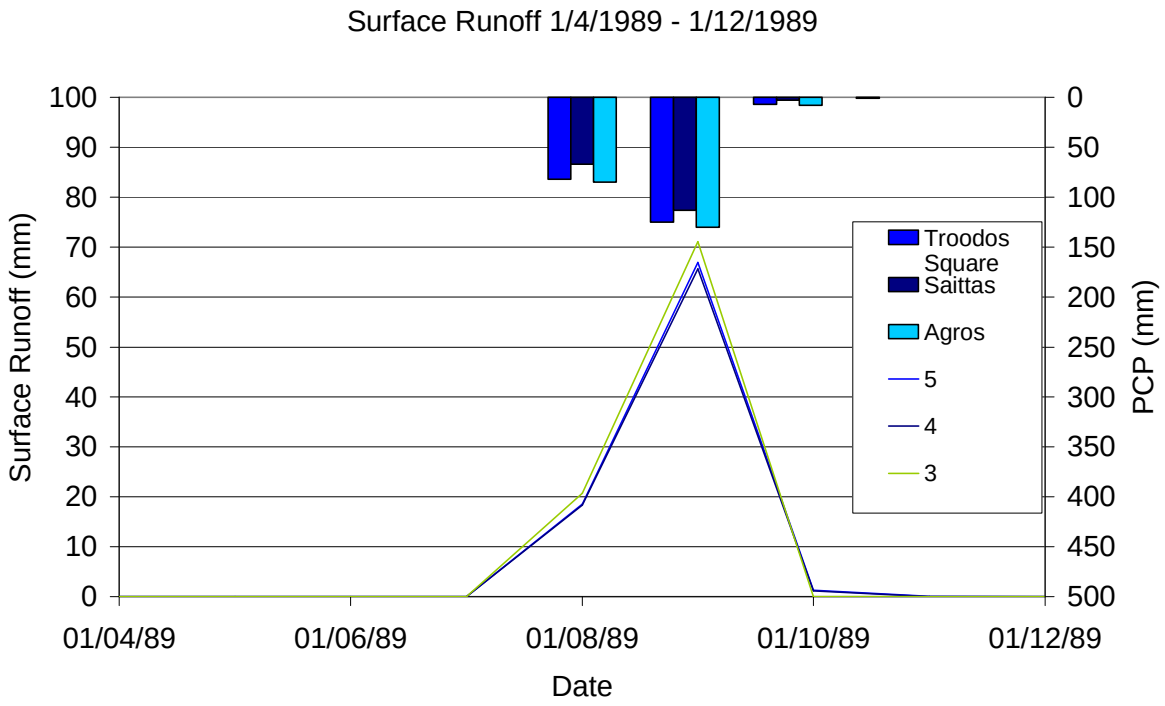

Figure 4.5 Surface Runoff (mm) and precipitation (mm) for event 1/8/1989-1/9/1989.

Therefore the curve numbers have to be adjusted to get proper results. The final curve numbers are listed in Table 4.5.

Table 4.5 *SWAT* land use class and final curve numbers

SWAT Land use class	**Curve Number**
Forest Decidious	30
Honey Mesquite	40
Pine	32
Residential Area – low density	45
Orchard	45
Wetlands - mixed	49
Waters	92
Sealed Areas	74
Little Bluestem	31

Although the values do not reflect the natural set-up of the system, there are several reasons to do so. Colluvial plains for instance can store large quantities of water,

therefore preventing surface runoff to emerge. However, because the soil shape file used for *SWAT* does not include colluvial plains, it had to be implemented by adapting the curve numbers. Similar to the lateral flow, *SWAT* incorporates a surface runoff storage feature to lag a portion of the surface runoff release to the main channel resulting in a smoother streamflow hydrograph.

While lateral flow is important for runoff generation for every precipitation event, surface runoff is only important for intense rainfall events. Figure 4.6 ab displays the hydrographs for the event from 1/8/1989 to 1/9/1989 with 67 mm resp. 113 mm precipitation.

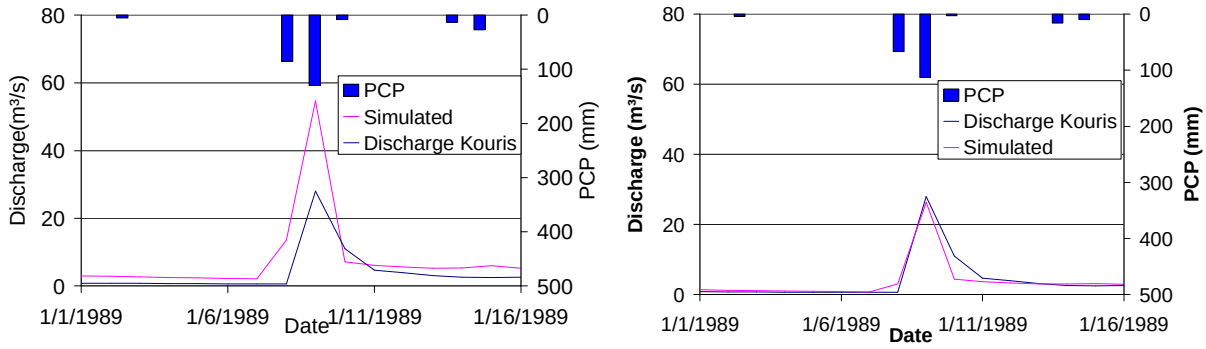

Figure 4.6 ab Hydrographs before and after CN adjustment

With the default Curve Numbers the simulated discharge exceeds the measured by 92%.

With the adjusted Curve Numbers the peaks are almost equal with a simulated discharge of 26.36 m³/s compared to a measured discharge of 28 m³/s measured.

Because the SCS Curve Number method estimates surface runoff using daily precipitation and the land use-dependent Curve Numbers, the occurrence of surface runoff highly depends on the spatial distribution of daily precipitation and of the land use. The land use distribution and the particular Curve Numbers lead to a rather equal surface runoff potential for all subbasins.

Spatial Distribution

Figure 4.7 displays the spatial distribution of the mean annual surface runoff. Although subbasin 1 gains the highest amount of precipitation (900mm/y), it is not the one with the highest amount of surface runoff (15 mm/y). In the north-eastern subbasins, amounts of surface runoff are the highest with a range of 22-29 mm/y on average, gaining an annual mean of 825 mm/y of precipitation.

For the class representing 11-15 mm, occurring in sub-basins 1, 2, and 7, precipitation is higher than 800 mm/y. for the remaining subbasins, precipitation is less than 600 mm/y, the calculated surface runoff is less than 10 mm/y.

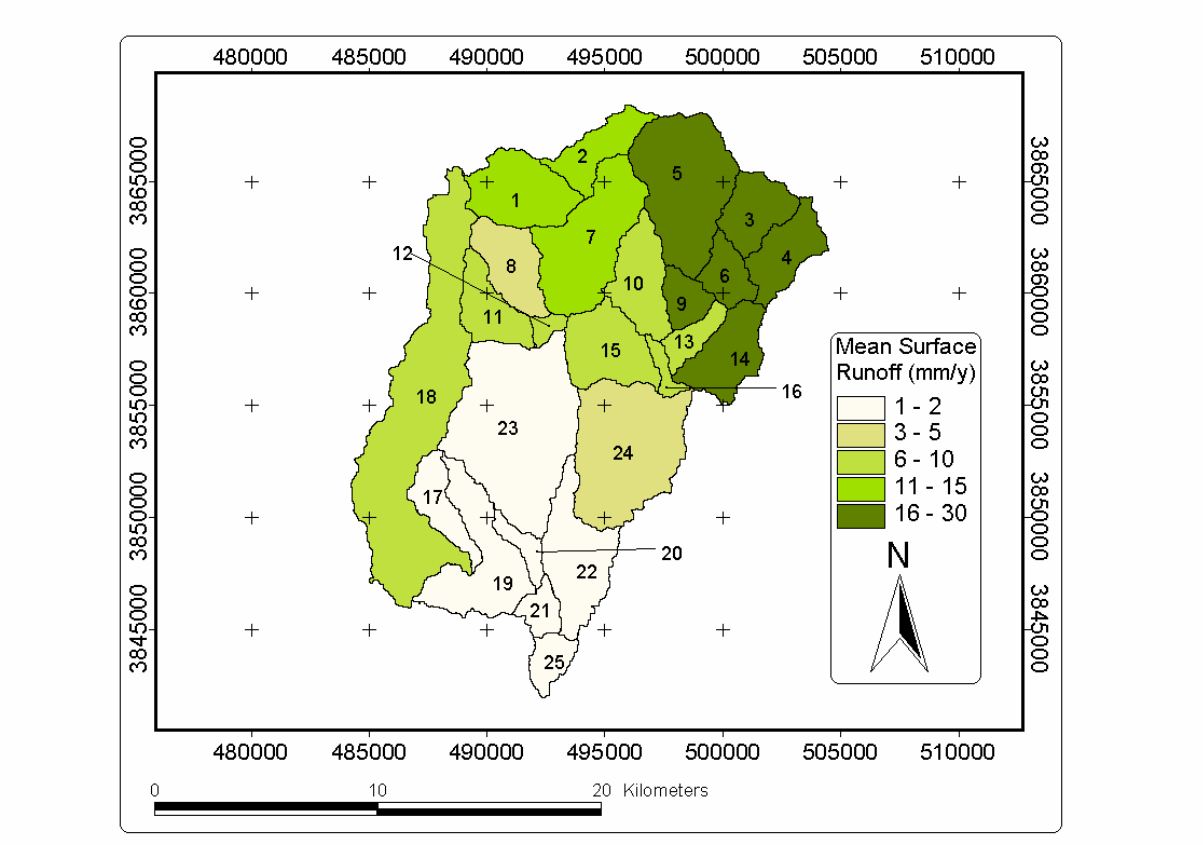

Figure 4.7 Mean annual surface runoff (mm/y) during calibration period

Therefore, surface runoff depends at first on the amount of daily precipitation, but is not limited to it.

Figure 4.8 demonstrates the occurrence of surface runoff in dependency on precipitation. With the applied parameter set, a threshold of 40 mm/d precipitation must be exceeded to generate surface runoff.

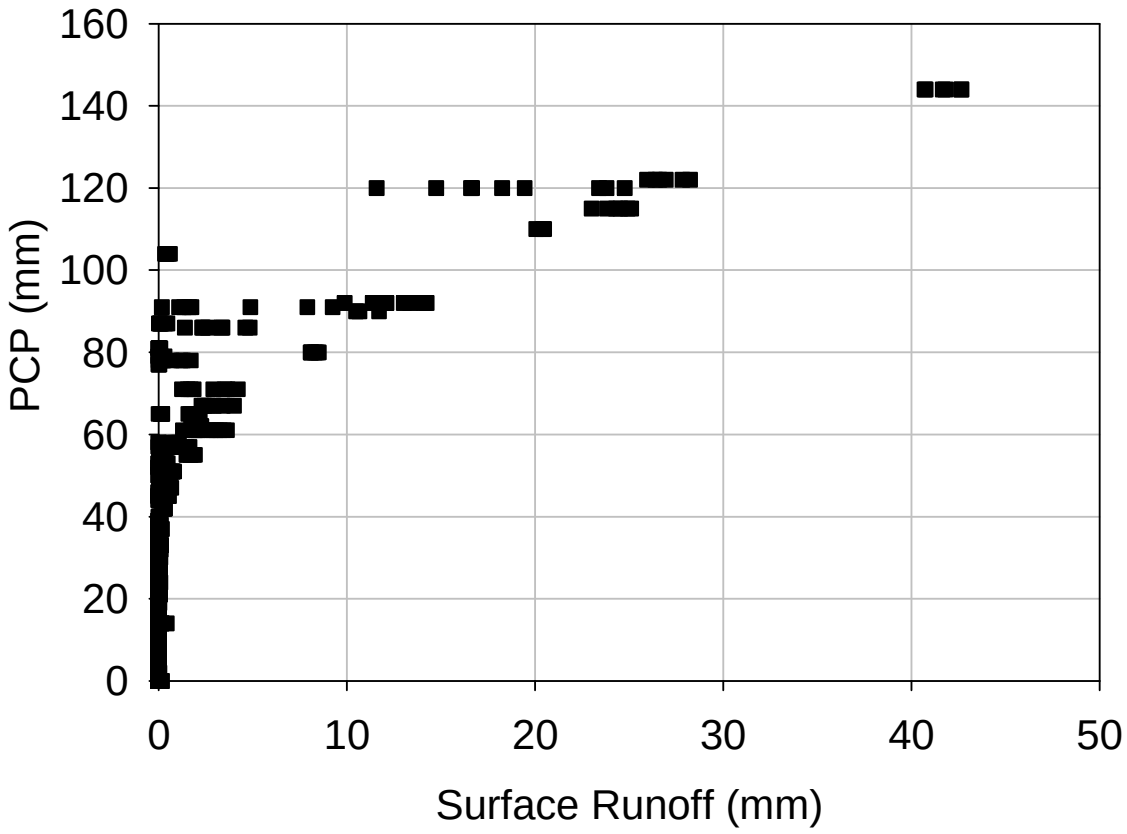

Figure 4.8 Precipitation-dependency of surface runoff, daily values for all subbasins during calibration period

Whether saturation excess runoff or infiltration excess runoff is the dominant process for surface runoff generation, can not be distinguished,.

4.2.4 Snowmelt

SWAT calculates snowfall respectively snowmelt in the upper part of the Kouris catchment. Although the mean monthly air temperature is always above 0℃ for all weather gages, days with air temperature below zero occur, e.g. 30 days for station ´Pano Amiantos´ during the 10 year time series.

SWAT has six parameters affecting snowfall and snowmelt (see Table 4.3). The first simulations produced too much runoff caused by snowmelt. Therefore, in order to get less snowfall, the snowfall temperature is reduced from 1.0℃ to 0.5 ℃. To smoothen the discharge peaks related to snowmelt, the snowfall melting rates are reduced from 4.5 mm/(℃*d) to 1.5 mm/(℃*d). All other parameter s remained the default values.

Spatial Distribution

Snowfall resp. snowmelt only occurs in the northern third of the Kouris catchment (Figure 4.9). This is as expected; the mean air temperature decreases together with the altitude from the mountainous north to the south.

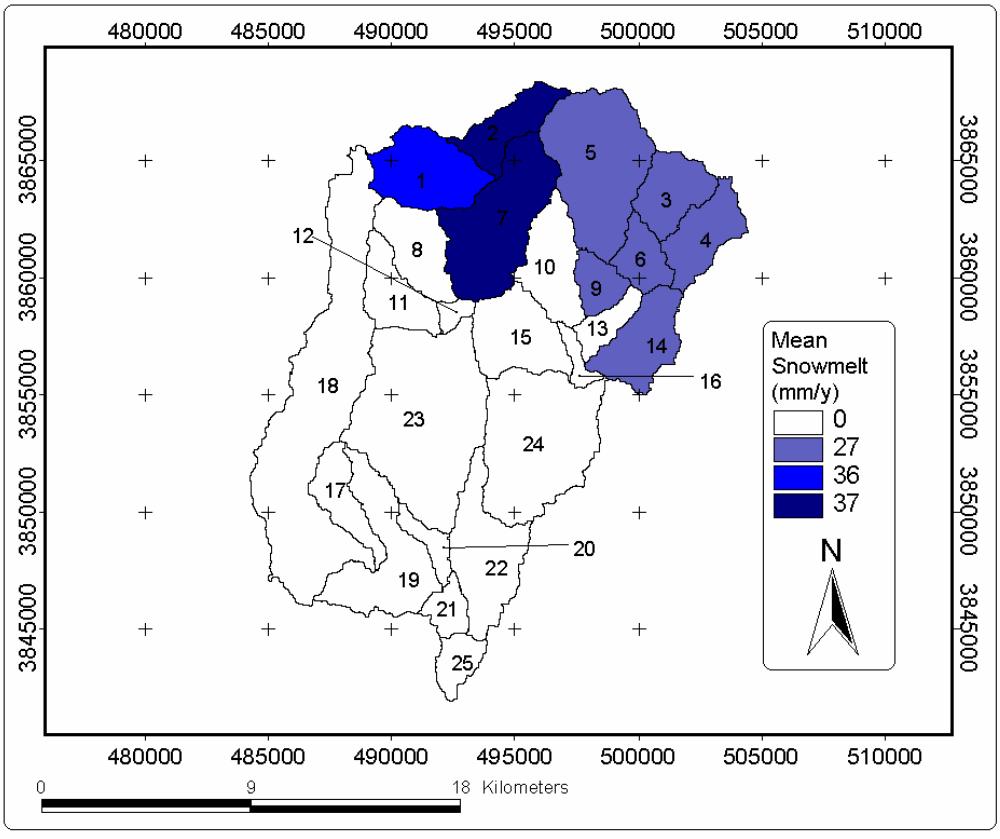

Figure 4.9 Mean annual snowmelt (mm/y) during calibration period

4.2.5 Groundwater Recharge

Water that enters the soil profile percolates through different layers. Water that moves past the last layer becomes recharge. *SWAT* partitions between recharge for the shallow and the deep aquifer. While water in the shallow aquifer can be re-evaporated or contribute to the streamflow as baseflow or lateral flow, water in the deep aquifer is out of the system. For modeling issues, the user has to determine how *SWAT* partitions between the shallow and the deep aquifer (*RCHRG_DP)* and, for the temporal element, the delay time for aquifer recharge (*GW_DELAY*). According to the sensitivity ranking both parameters are considered to be sensitive parameters. The best results are achieved with a fraction of 30% percolating to the deep aquifer and a delay time of 31 days.

Spatial Distribution

As expected, the spatial distribution is declining from north to south along the altitude gradient.

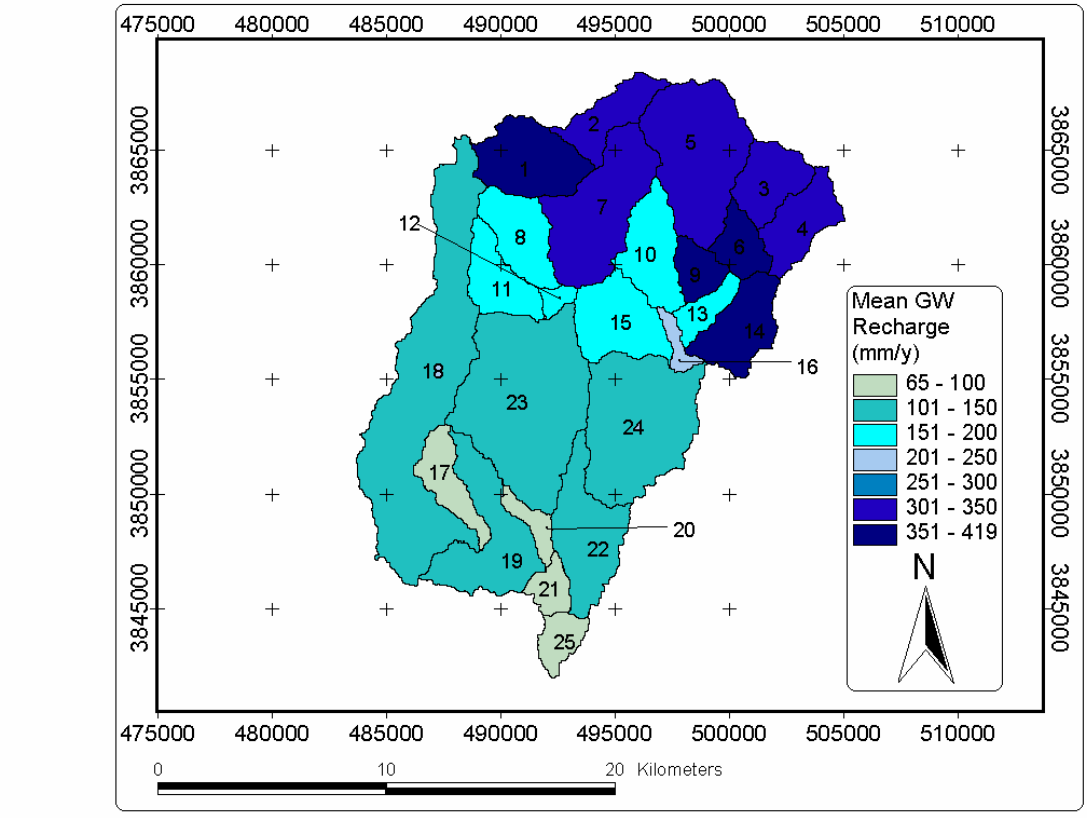

Figure 4.10 Mean annual recharge (mm/y) during calibration period

On one hand, the northern part receives more precipitation. On the other hand and, it gains recharge from snowmelt, which is more effective than from precipitation. The distribution of snowmelt matches the subbasins with the highest amounts of recharge. Another important aspect is the influence of soil properties, resp. the field capacity. Subbasins 17, 18 and 19-25 show the smallest recharge rates in the range of 65 – 150 mm/y, and are dominated by the soil group with the highest field capacity.

The mean groundwater recharge for the whole Kouris catchment is 216 mm/y, which corresponds to the calculation of 224 mm/y for the Limnatis catchment within the GRC project

4.2.6 Baseflow

The threshold water level in the shallow aquifer for baseflow to occur (*GWQMN*) is 200 mm, the baseflow recession constant (*ALPHA_BF*) is 0.18 days. Return flow from groundwater only occurs in the upper third of the Kouris catchment.

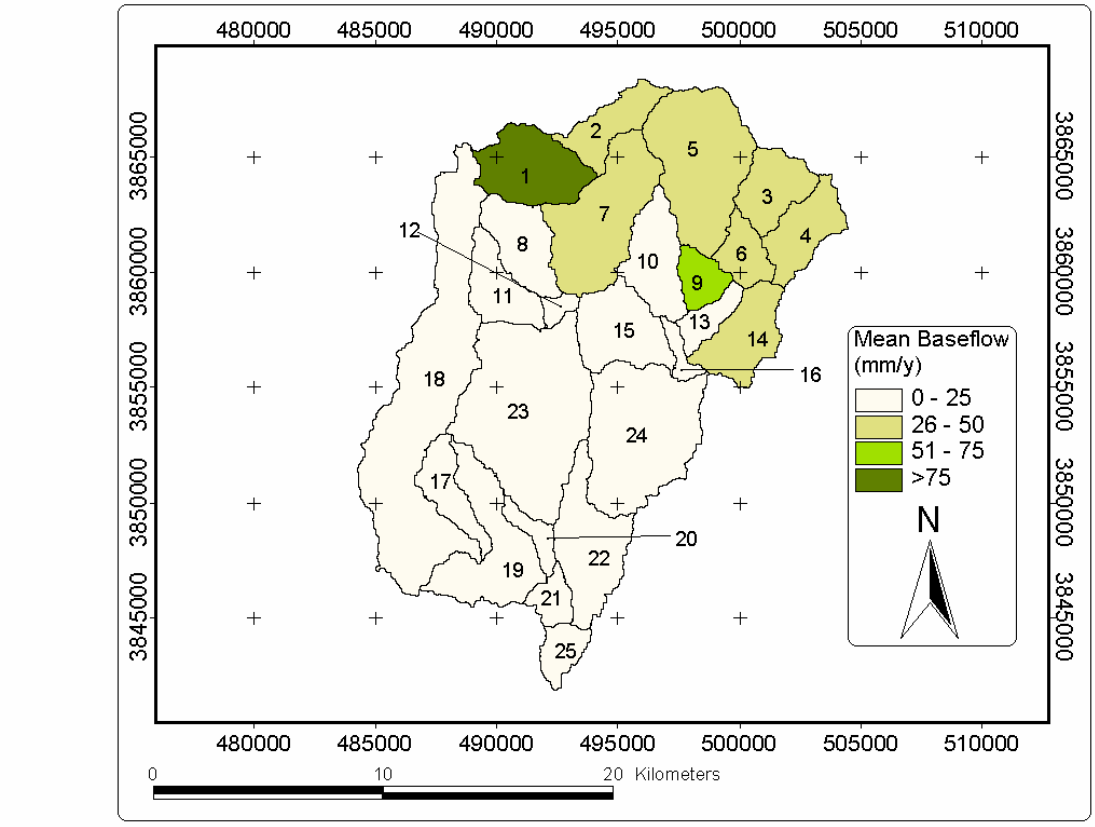

Figure 4.11 Mean annual baseflow (mm/y) during calibration period

SWAT calculates the amount in the range of 25 – 76 mm/y during calibration period.

This corresponds with the geological context. In the north of the Arakapas Fault Zone groundwater recharge is high, the distribution of moist areas demonstrates the connection of surface- and groundwater.

Snowmelt is important for groundwater recharge. Groundwater recharge replenishes the shallow aquifer. Baseflow occurs in those subbasins, where recharge exceeds 250 mm/y. Only the upper third of the Kouris catchment contributes baseflow to the streamflow discharge.
Figure 4.12 shows the baseflow hydrographs (1988-1992). During the months July to September, *SWAT* calculates no baseflow for the entire catchment.

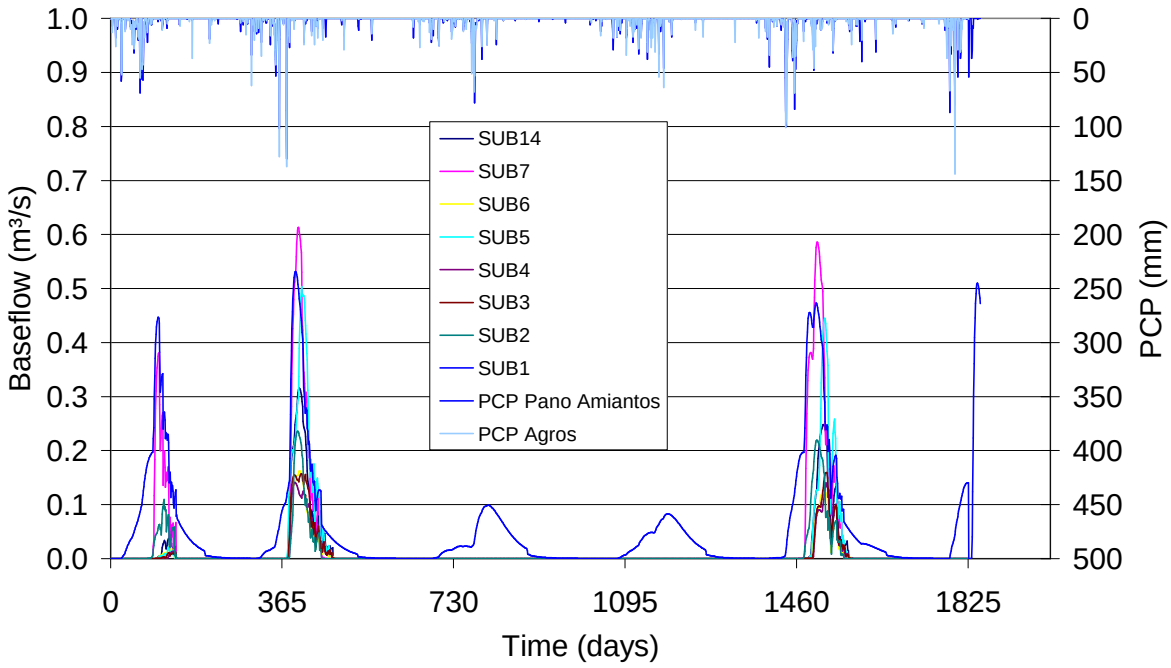

Figure 4.12 Baseflow hydrographs for subbasins with baseflow

This corresponds well with the measured discharge, as is it reduces at least close to zero during these months.

4.2.7 Evapotranspiration

Evapotranspiration calculated according to Penman-Monteith requires windspeed and radiation as inputs. The remaining parameters are predefined in the *SWAT* land use database. Solar radiation is calculated as described in chapter 4.1.3. The average daily windspeed initially amounts 1 m/s. Initially, the mean actual Evapotranspiration ranges from 150-250 mm/y. In order to increase AET, average daily windspeed is set to 1.5 m/s during calibration.

Spatial Distribution

With this, *SWAT* calculates Potential Evapotranspiration in the range of 1150 to 1480 mm/y with a mean of 1340 mm/y. A gradient in PET-rates from north to south with a minimum in the north-east is discernable (Figure 4.13).

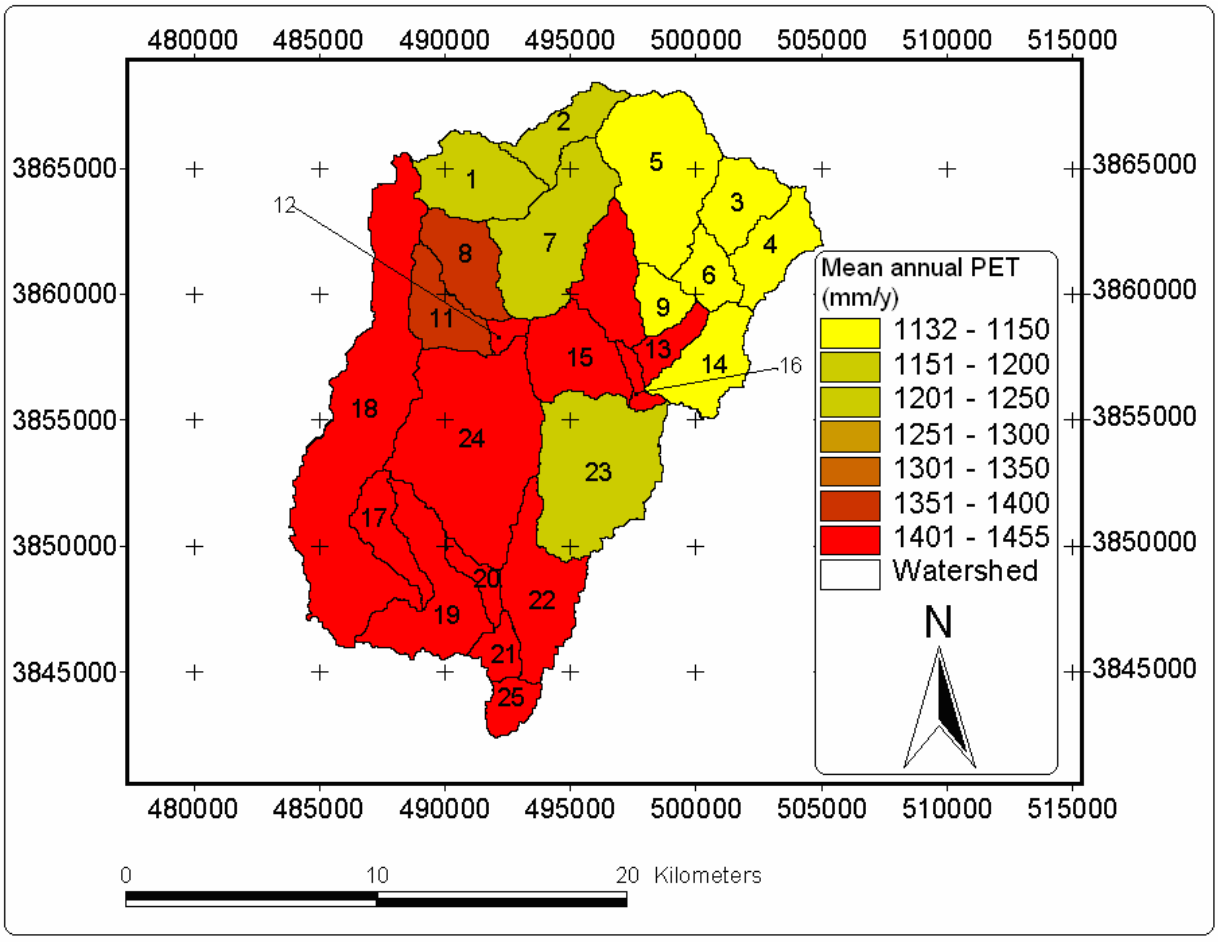

Figure 4.13 Mean annual potential Evapotranspiration (mm/y) during calibration period

The upper part of the Limnatis catchment has the lowest PET with less than 1150 mm/y, the upper Kouris catchment shows slightly higher PET rates around 1200 mm/y. This is due to the air temperature, ascending from north to south along the altitude gradient.

The Actual Evapotranspiration ranges from 297-371 mm/y, the mean is 321 mm/y. The spatial distribution shows a rather contrary gradient, where the northern half has – with one exception – higher ET-rates than the southern part. A possible reason for this could be the distribution of wetlands.

Except for subbasin 18 and 25, all subbasins in the southern half have mean actual evapotranspiration rates below 310 mm/y. Subbasin 18 is partially covered by wetlands, subbasin 25 includes most part of the Kouris Dam resulting in higher AET rates.

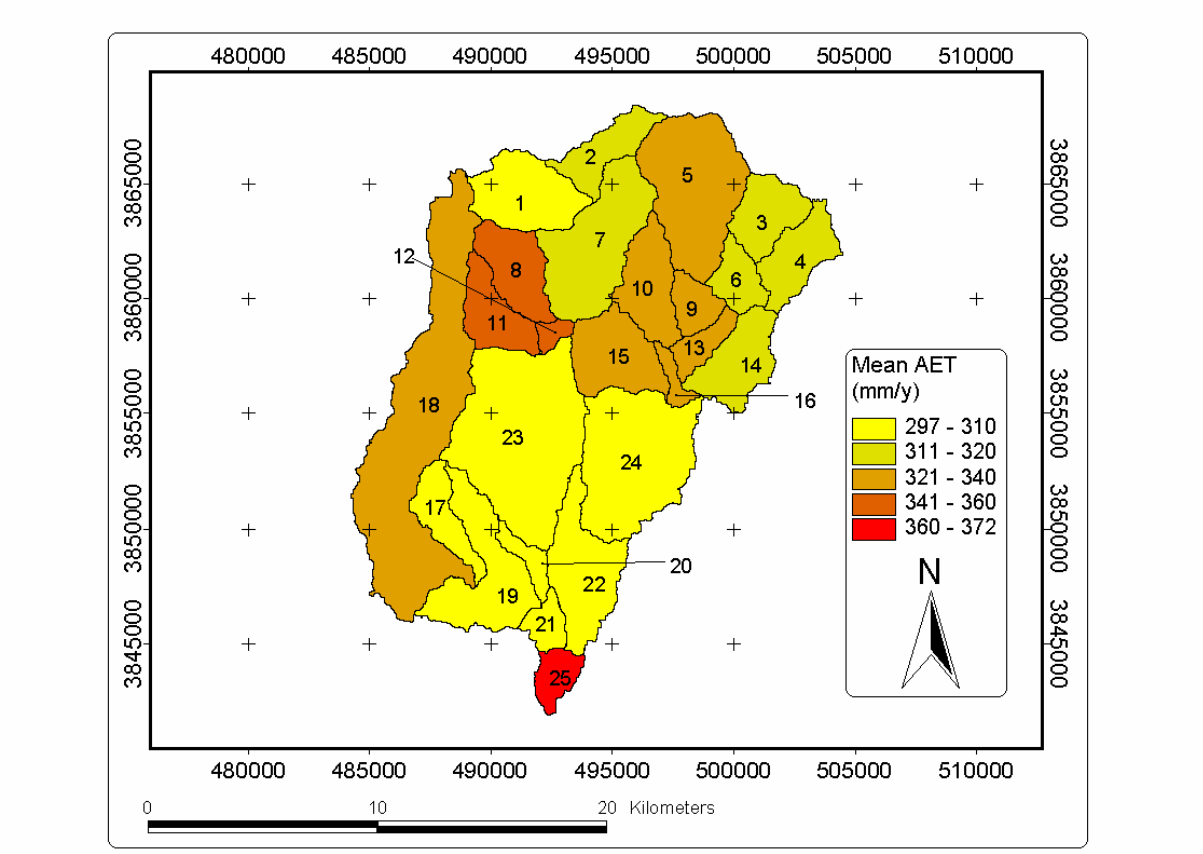

Figure 4.14 Mean annual actual Evapotranspiration (mm/y) during calibration period

BORONINA et al. (2005) estimated actual Evapotranspiration from an alluvial aquifer of the Kouris catchment using continuous streamflow records. They assumed that variations of streamflow “were caused by transpiration of water by trees in the river

valley and direct evaporation from the water table of the alluvial aquifer", and that "the influence of other factors on streamflow is negligible". Their calculations resulted in 2,4 ± 0,5 Mm^3 actual evapotranspiration from the alluvial aquifer for April-September 2001, or in other words 1100 -1690 mm for 6 months. This is in strong contrast to the results achieved with *SWAT*.

SWAT can simulate re-evaporation or secondary evapotranspiration of water from the shallow aquifer. *SWAT* cannot calculate this separately, but the influence is reflected in the distribution of AET. The threshold water level in the shallow aquifer for revap to occur (*REVAPMN*) and the revap coefficient (β_{rev}) are defined in order that re-evaporation will occur with a minimum amount of 10 mm in the shallow aquifer and contribute an additional fraction of 20% of the PET at most to the AET.
For the Limnatis, secondary Evapotranspiration from shallow groundwater discharge zones and irrigation has been determined within the GRC project (Figure 4.15). The calculations resulted in a mean of 133 mm/y for the Limnatis catchment, although only applied to raster cells with irrigation, moist areas and settlements.

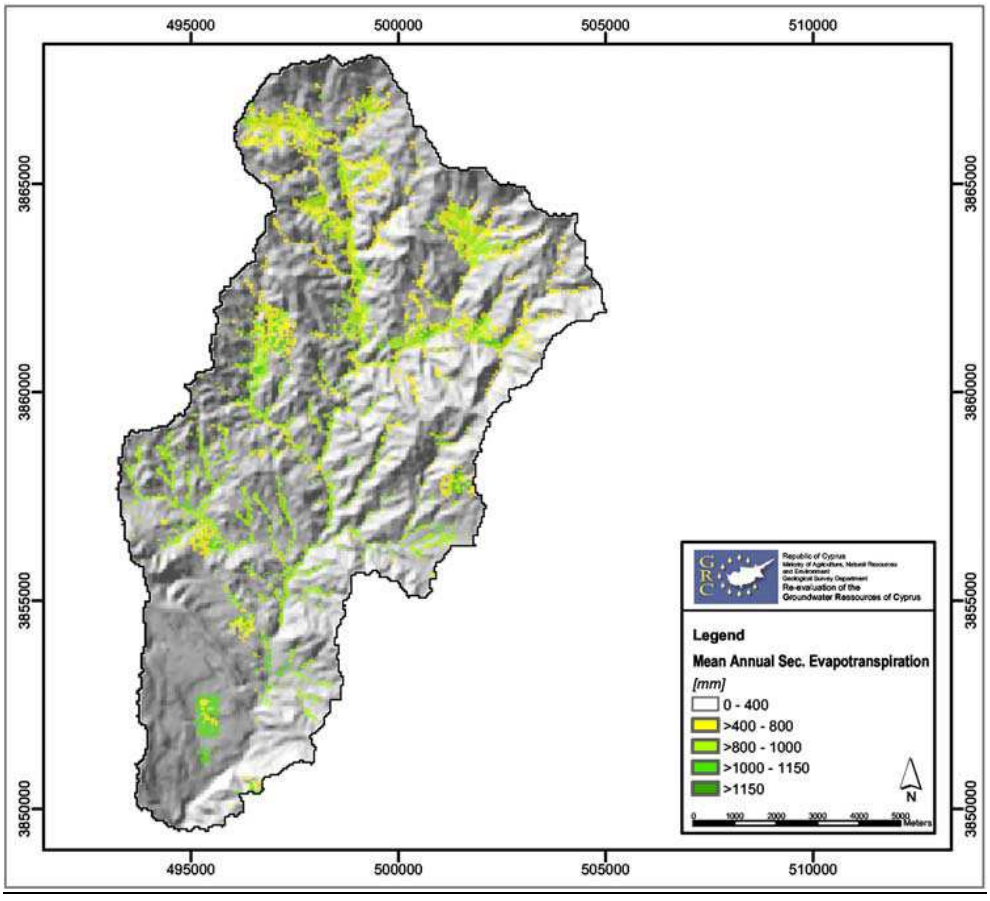

Figure 4.15 Mean annual sec. Evapotranspiration for the Limnatis catchment (UDLUFT et al., 2003)

4.2.8 Conclusions

Lateral flow and surface runoff are the dominant processes for runoff generation within the Kouris catchment.

Most peak discharges issue from surface runoff. The adjustment of the curve numbers does certainly not reflect the natural behavior of the particular land use class, but was necessary to reduce the large quantities of surface runoff produced during heavy precipitation events. The fact that areas with high water holding capacities such as colluvial plains could not be modeled legitimates this approach.

Lateral flow initially caused a very nervous reaction of the system, since the majority of lateral flow reached the channel instantly and produced steep peaks. With a slope length of 15 m and the time lag results improved significant.

AET calculations with the Priestley-Taylor method in the first few model runs achieved insufficient results. The calculation with Penman-Monteith is with a mean of 1340 mm/y for PET and 321 mm/y for AET within the expected range.

Groundwater recharge rate is with a mean of 216 mm/y higher than the results of the GREM project with 69 mm/y, ZAGANA et al. calculated 70mm/y. The separate calculation of the recharge rate for the Limnatis catchment exceeds with 269 mm/y as well the previous estimation during the GRC project with 224 mm/y.

SWAT calculates baseflow in the range of 16 – 76 mm/y with a mean of 42 mm/y for the 10 subbasins were baseflow occurs and 17 mm/y for the whole Kouris catchment. This seems plausible since, due to the distribution of precipitation and snowfall/snowmelt, recharge rates are high in the northern half and a connection of groundwater and surface water is obvious.

During the GRC project Transmission losses are determined for several rivers by volume balancing, for instance, for the Chapotami river 86588 m^3/a km, for the

Diarizos 560550 m³/a km. in the essence, transmission losses are considered to be “a major source of recharge for the circum-Troodos sedimentary aquifers”(UDLUFT et al., 2003). *SWAT*, however, did not calculate transmission losses, although the hydraulic conductivity of the channel alluvium is set to 30 mm/h.

With the applied parameter set, *SWAT* produces good results for the simulated discharge. The Nash&Sutcliffe efficiency is for the first simulations in the range of -20 to -30 (Figure 4.16). It improved to 0.78 for the Kouris, 0.63 for the Limnatis.

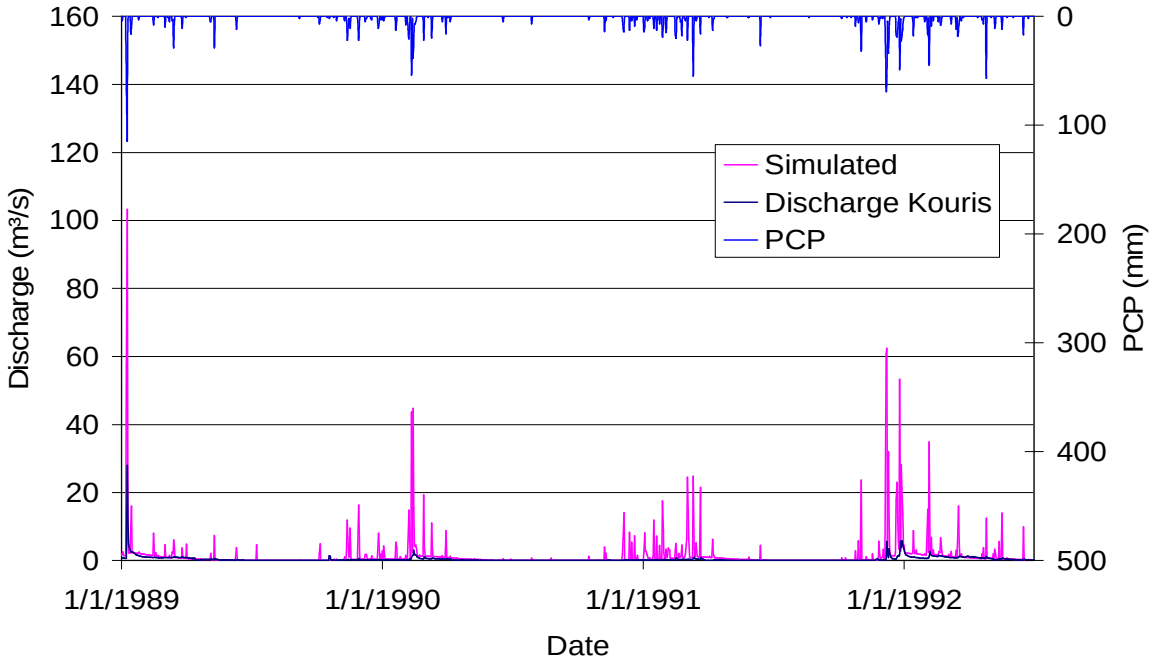

Figure 4.16 Discharge of the uncalibrated model

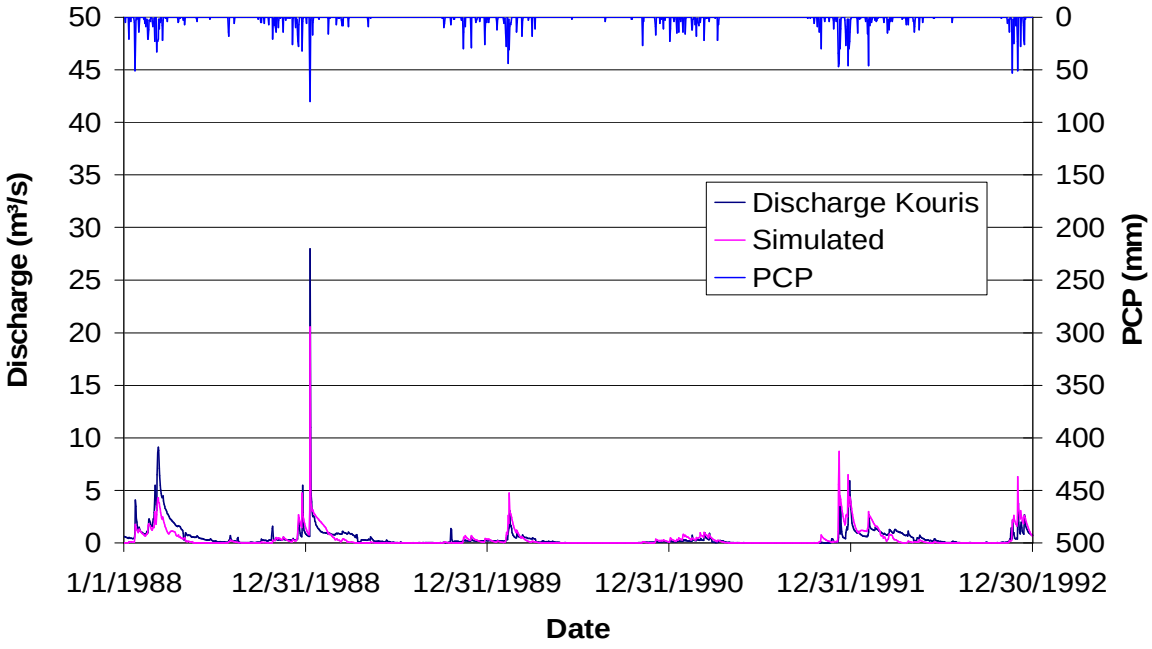

Figure 4.17 Hydrographs of measured and simulated discharge for the Kouris

The simulated hydrographs of both the Kouris and the Limnatis corresponds well with the measured.

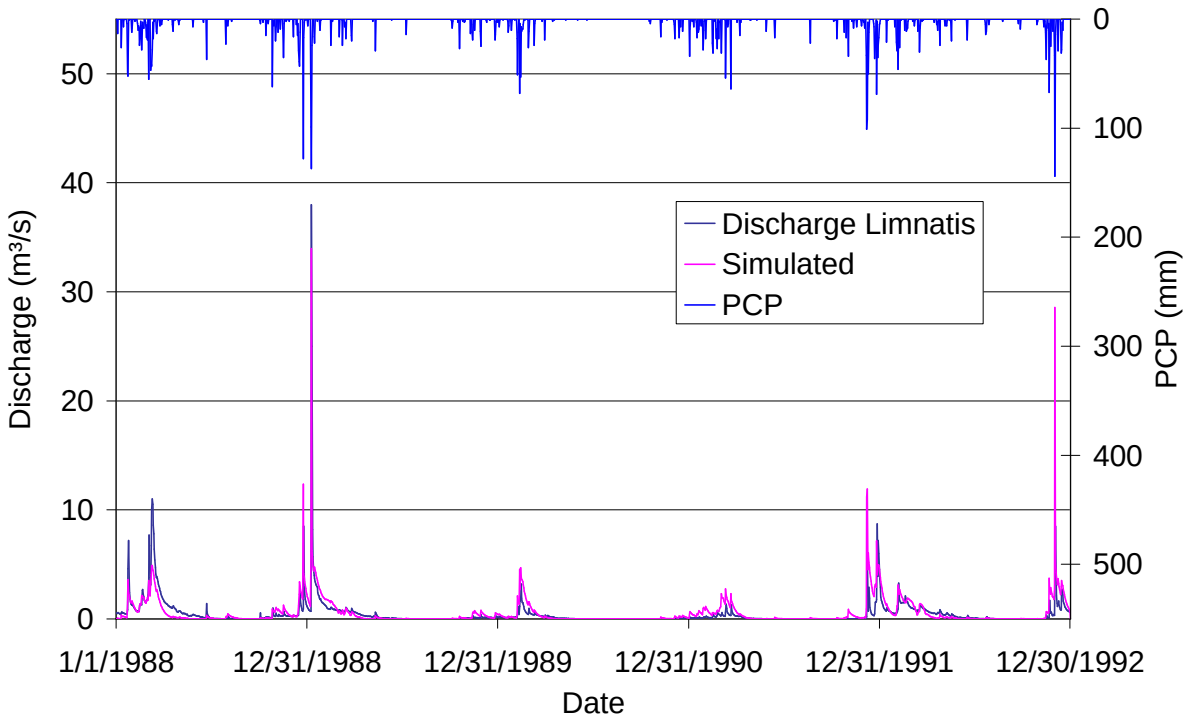

Figure 4.18 Hydrographs of measured and simulated discharge for the Limnatis

4.3 Validation

Nine years of both discharge and climatic data, from 1988 to 1996, are available for this paper. Consequently, the dataset is split in two half's. The first period from 1988 to 1992 is used to calibrate *SWAT*, the second period from 1992 to 1996 is used to validate the results. For calculations of averages for particular compounds, the first year is not taken into account in order to balance out the storages.

Table 4.6 compares the simulated water cycle components of the validation and the calibration periods.

Table 4.6 Comparison of the means of water cycle compounds between calibration and validation

Component	Calibration (1989-1992)	Validation (1993-1996)
Precipitation (mm/y)	726	654
Snowmelt (mm/y)	10	7
PET (mm/y)	1320	1307
AET (mm/y)	339	363
GW Recharge (mm/y)	249	185
Surface Runoff (mm/y)	10	8
Baseflow (mm/y)	14	9
Lateral Flow (mm/y)	124	84

Within the validation period precipitation is 10% less than during the calibration period. Therefore, the amounts of other components are less as well. The results for the Kouris improved the Nash-Sutcliffe efficiency raises from 0.78 to 0.84.

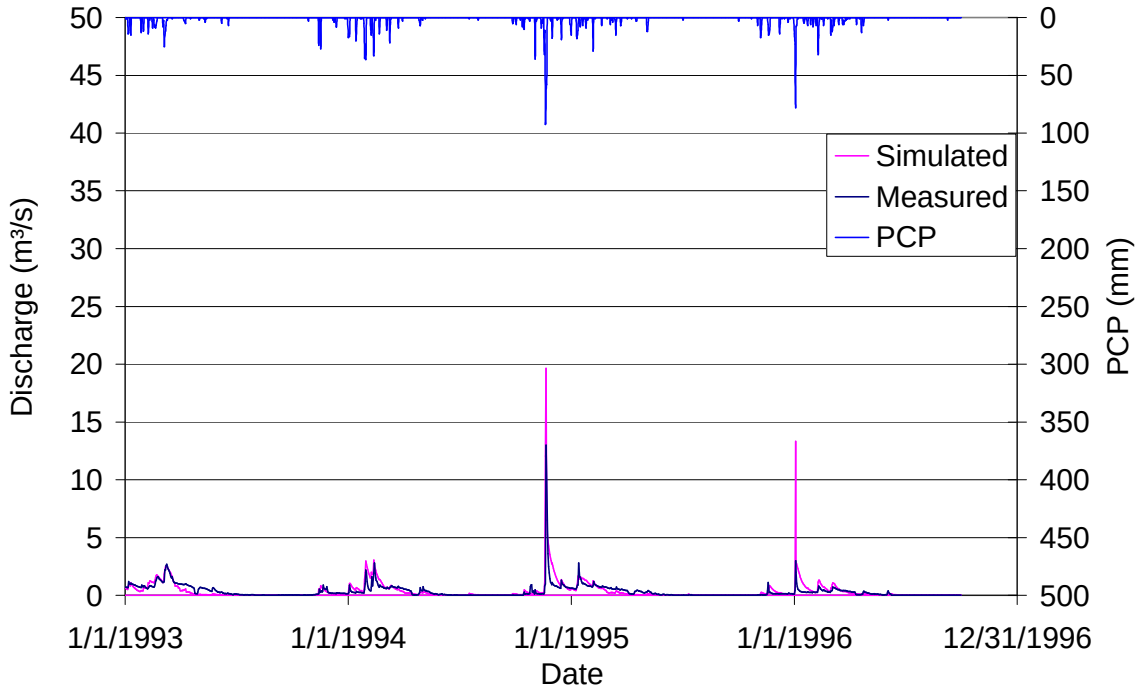

Figure 4.19 Hydrograph for the Kouris during validation period (1993-1996)

For the Kouris, in 1993 and 1995 simulated annual sums of discharge amount 40% less than the measured annual sums of discharge. In 1994 and 1996, however, simulated values are about 35% higher then measured ones. At low watermarks *SWAT* seems to underestimate discharge, while at high watermarks discharge is overestimated by the model.

For the Limnatis the results declined, the Nash-Sutcliffe efficiency is 0.46. As Figure 4.20 displays, the decline of the efficiency is due to different response times in simulation and reality.

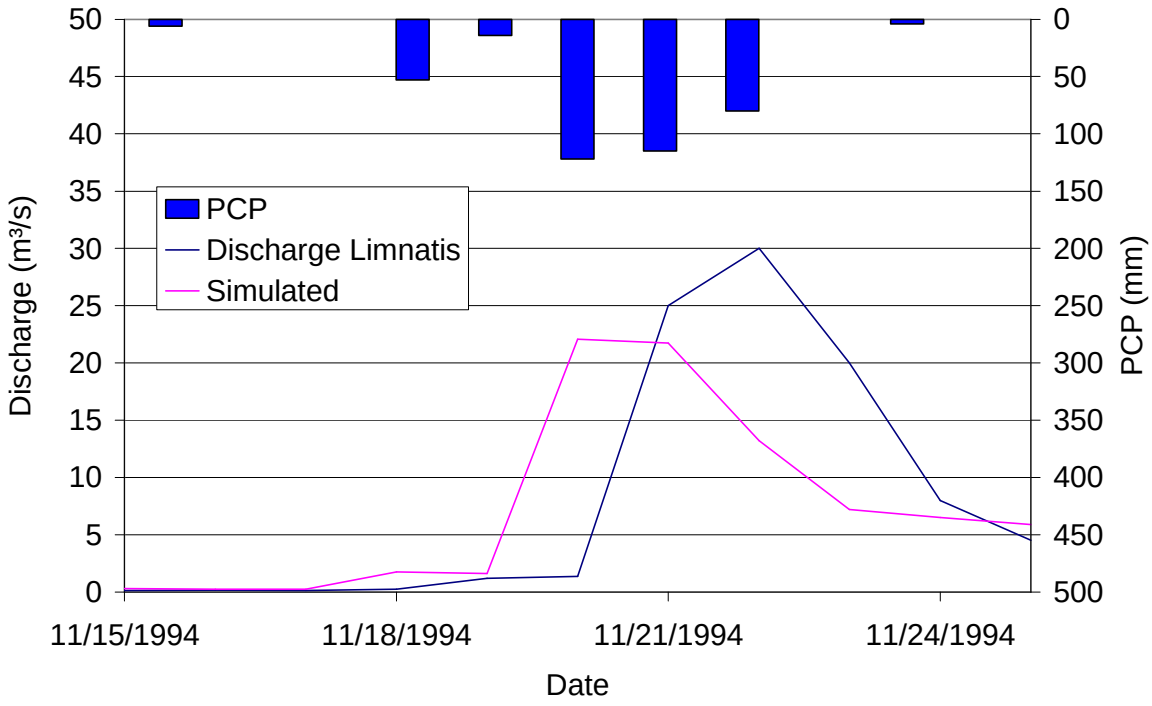

Figure 4.20 Hydrograph for the Limnatis 11/15/1994-11/25/1994.

While the simulated system produces an instant response on the event, the real system shows an offset of one day. In parts this is the case for the calibration period, too, but apparently the influence is smaller.

Nevertheless, the results for the Limnatis are thoroughly acceptable. Figure 4.21 displays the simulated and measured discharge of the Limnatis for the validation period.

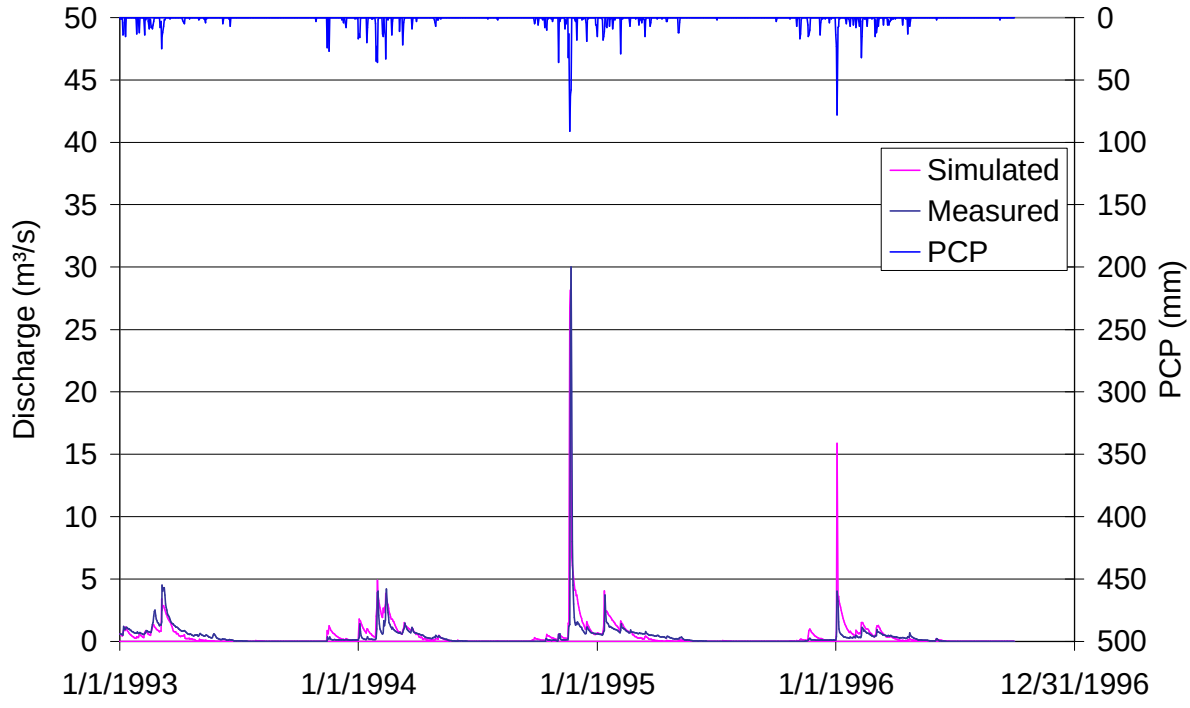

Figure 4.21 Hydrograph for the Limnatis during validation period (1993-1996)

4.3.1 Conclusions

The modeled system proves a good image of reality. By simulating the dominant processes, the hydrograph can be reproduced. Nevertheless, there are processes *SWAT* does not reproduce. For the Limnatis for instance, the events during 1/1/1996 and 1/5/1996, which received a total rainfall volume of 202 mm, produced a measured discharge volume of $0.8*10^6$ m³. The simulated discharge volume, however, amounts $1.96*10^6$ m³. This is an overestimation of measured flow volume by the factor 2.5. Therefore, the question is not whether *SWAT* calculates too much discharge, but why the measured discharge is that small.

5 Climate Change Scenarios

Future atmosphere changes depend on the level of greenhouse gases (GHGs) and aerosol emissions over time. The major sources for the increase these emissions are human activities. These have increased in the past and, although the emissions decrease substantially from present levels, GHG-concentrations in the atmosphere will increase during the century (URL 6).
According to IPCC (2001b), a “continued GHG emission at or above current rates” will not only “cause further warming”, but lead to “changes in the global climate system during 21st century that would very likely be larger than those observed during 20th century”.

As reference for future projections of climate change, IPCC report “Climate Change 2001: Impacts, Adaptation and Vulnerability” is used. It provides a general view of the vulnerabilities and adaptation possibilities grouped by major regions of the world (Africa, Asia, Australia/New Zealand, Europe, Latin America, North America, Polar Regions, and Small Island States). The small island states include the Mediterranean.

For predicting climate change, several AOGCMs (atmosphere-ocean general circulation models) have been compared and validated. “Coupled AOGCMs offer the most credible tools for estimating the future response of climate to anthropogenic radiative forcings”.

Changes of surface air temperature and precipitation have been modeled for two time periods centered on the 2050s (2040-2069) and 2080s (2070-2099).
Two types of scenarios have been performed: scenarios that base on GHG-induced positive radiative forcing only, and scenarios that additionally “take into account the negative radiative forcing of sulfate aerosols”.

The results for the mediterranean are summed in Table 5.1

Table 5.1 Changes of temperature and precipitation of annual mean climate change scenarios for the Mediterranean as inferred from AOGCMs (numbers in brackets show standard deviation between model projections) (IPCC, 2001b)

Temperature Change(℃) 2050s				**Precipitation Change (%) 2050s**			
December-February		*June-August*		*December-February*		*June-August*	
GHG	GHG+A	GHG	GHG+A	GHG	GHG+A	GHG	GHG+A
2.64	2.27	2.93	2.27	8.1	2.6	-4.8	-8.9
(±0.72)	(±0.44)	(±0.53)	(±0.17)	(±14.7)	(±15.7)	(±10.3)	(±6.0)

Annual Mean Temperature Change (℃) 2080s				**Annual Mean Precipitation Change (%)2080s**			
December-February		*June-August*		*December-February*		*June-August*	
GHG	GHG+A	GHG	GHG+A	GHG	GHG+A	GHG	GHG+A
3.94	3.31	4.52	3.70	1.61	9.9	-7.4	-11.6
(±1.34)	(±1.01)	(±1.16)	(±0.72)	(±21.1)	(±21.6)	(±16.2)	(±10.7)

ROSSEL (2001) analyzed records of precipitation for Cyprus from 1916/17 to 1999/00. For the period 1916/17 to 1969/70, the records do not show any trend, while there is a slight decrease for the period 1979/71 to 1999/00. But, this trend “is not significant compared to the variations from year to year”.

For the Troodos, the mean shift in annual precipitation is larger than in the coastal and inland plains. Nevertheless, the IPCC future projections for climate change are chosen for the simulations.

The applied scenarios for the 2050s and 2080s include the negative radiative forcings of aerosols, which “perturb the Earth-atmosphere radiation balance by modulation of cloud albedo and cloud amount” (IPCC, 2001a). Furthermore, to implement the effect of increasing CO_2 concentration on plant transpiration, the scenarios are enhanced by adjusting the CO_2 concentration. The increase of CO_2 is 1.9 ppm/y for time period 1995 to 2005 (IPCC, 2007). With a concentration of 379 ppm CO_2 for 2005, this results in a concentration of 465 ppm for 2050 and 522 ppm for 2080.

The change in mean precipitation is stated for intervals December to February and June to August. For the remaining months, a sinus function is fitted to the values of Table 5.1 . The sinus function for precipitation adjustment for the 2080s is shown in

Figure 5.1. The red bars display the change in precipitation stated by the IPCC (2001b) for December to February and June to August. The data for the remaining months is then calculated by the sinus function.

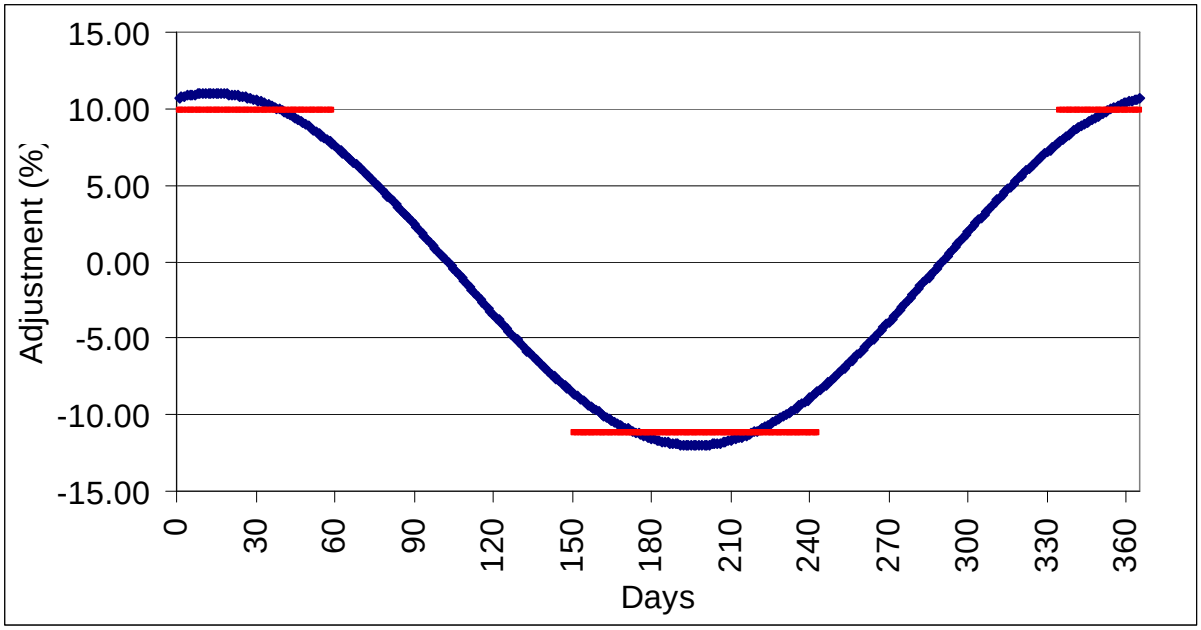

Figure 5.1 Change in precipitation stated by the IPCC (red bars) and the fitted sinus function

The scenarios are calculated for the time period 1988 to 1992. All results of the climate change scenarios are compared to the results of the calibration as a reference. All graphs, hydrographs excluded, contain the data for the subbasins with highest and the lowest means of the particular water cycle compound. Scenario type A is without the CO_2 adjustment, type B is with CO_2 adjustment.

5.1 Scenario 2050A

According to the IPCC future projections of climate change, the mean air temperature is adjusted by a surplus of 2.27 ℃ throughout the whole year. The adjustments of precipitation for the particular months are listed in Table 5.2.

Table 5.2 Changes in precipitation (%) by the IPCC (italic) and fitted sinus function for the 2050s

Jan	Feb	Mar	Apr	May	Jun	Jul	Aug	Sep	Oct	Nov	Dec
2.6	*2.6*	0.20	-2.93	-6.14	*-8.9*	*-8.9*	*-8.9*	-6.51	-3.36	-0.17	*2.6*

As expected, the means of PET and AET increased due to the raise in air temperature by 6 % for PET and 3.3% for AET. In the mean, AET increased during the winter months and decreased during the summer months.

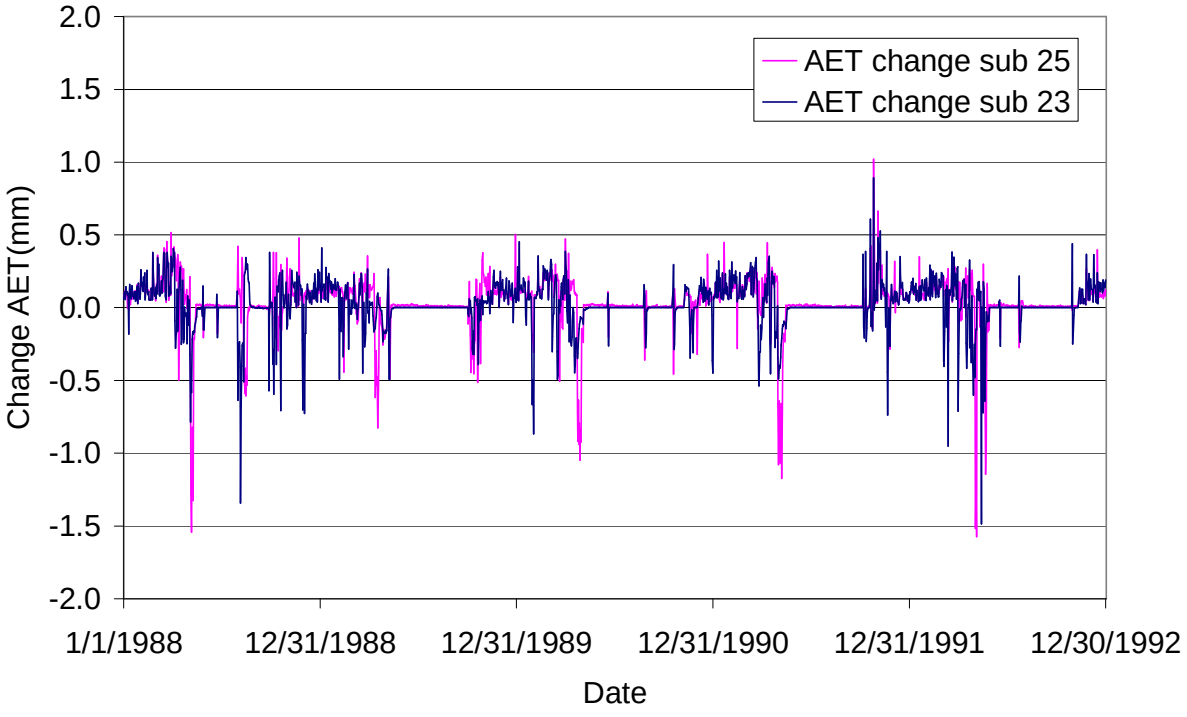

Figure 5.2 Change in daily AET (mm) for scenario 2050A

This results in a decrease of all other compounds, mainly snowmelt and surface runoff.

Table 5.3 summarizes the mean changes of the water cycle compounds (1988-1992) for the 2050s without.

Table 5.3 Mean changes in water cycle compounds for scenario 2050A

Water Cycle Compound	Change (mm)	Change (%)
Precipitation	5.5	0.8
Snowmelt	-9.5	-94.0
PET	83.7	6.3
AET	11.6	3.4
Recharge	-5.1	-2.4
Surface Runoff	-1.5	-14.9
Baseflow	-1.1	-10.3
Lateral Flow	-0.8	-0.9

The mean recharge decreased by 2.4%. The changes in recharge base on differences in the soilwater content. For 1/23/1988 (subbasin 1), the recharge increased by 27 mm due to an increase of 23 mm in the soilwater content for, as an example of an increase in daily recharge.

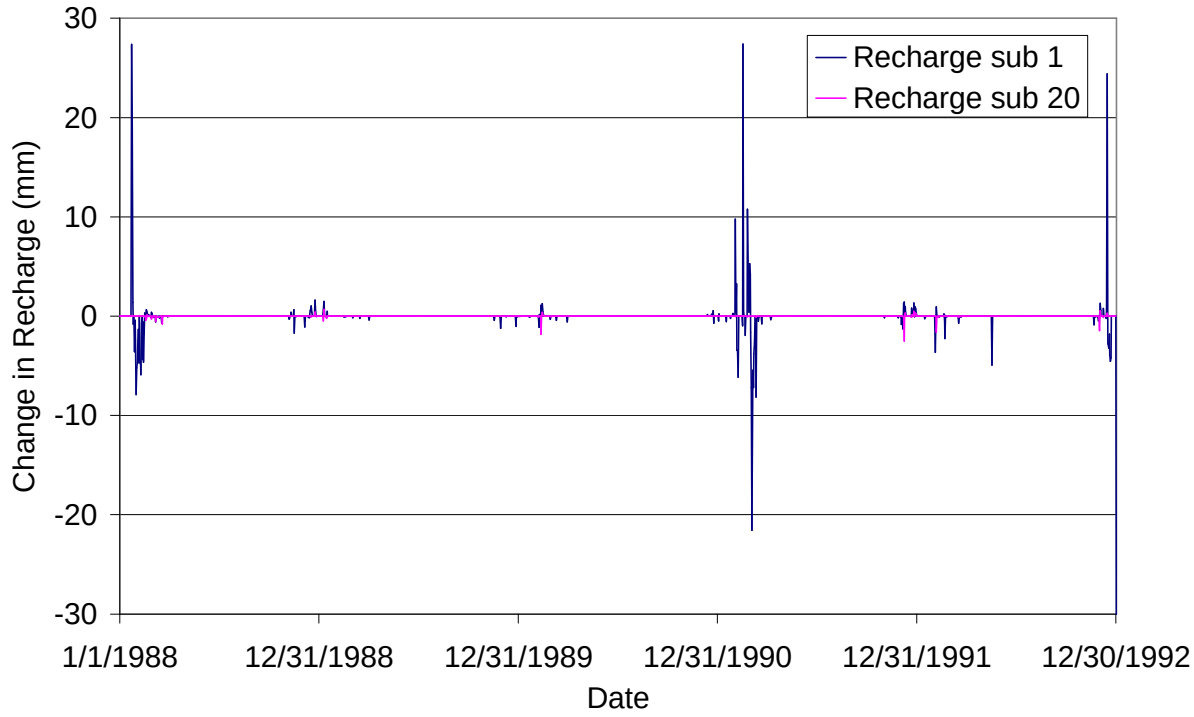

Figure 5.3 Change in daily recharge (mm) for scenario 2050A

Figure 5.4 displays the changes in average soilwater content.

For the whole period, the mean soilwater content is about 7% lower than the reference.

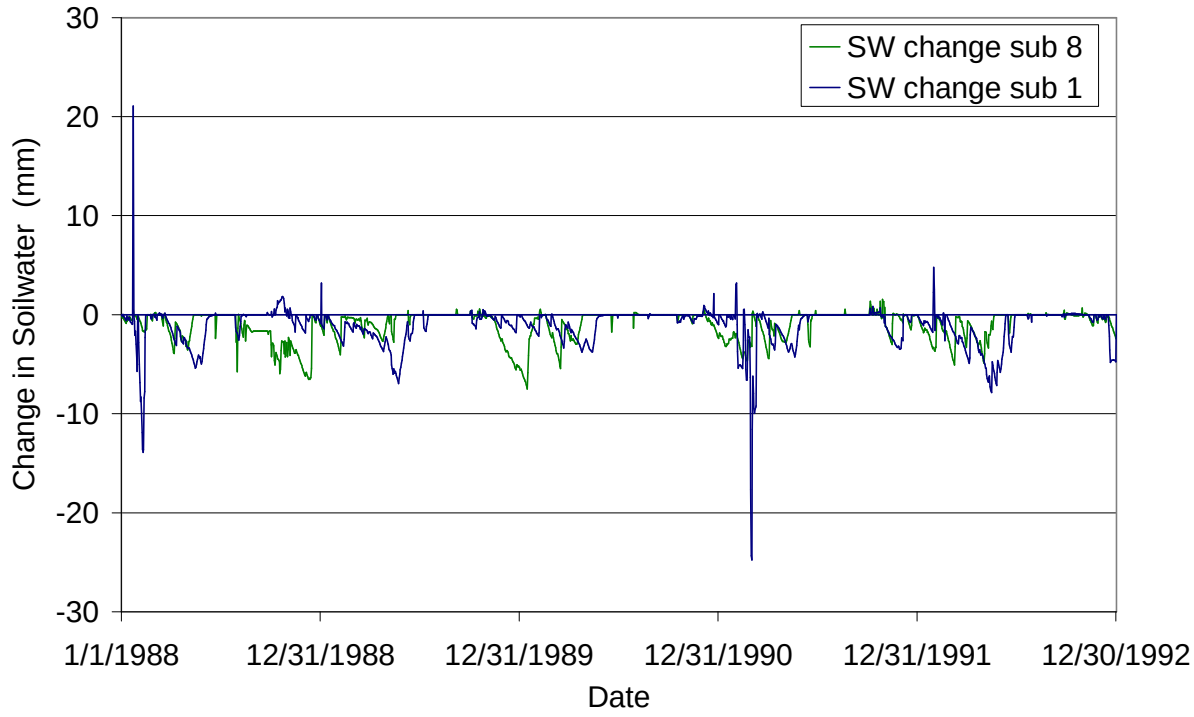

Figure 5.4 Change in daily soilwater content (mm) for scenario 2050A

The discharge for the Kouris decreased as well. The discharge for the Kouris runoff station (No 1964 646 90) decreased by $1.71*10^6$ m³ or 2.6 % with a total volume of $65.4 * 10^6$ m³ for period 1988 to 1992.

The change in soilwater content causes a decrease for low water levels, due to decrease in baseflow. The peak discharges decrease as well, although the heavy precipitation events causing them increase. This has two reasons: On one hand the surface runoff is reduced due to the lower soilwater contents, affecting the soil moisture dependent curve numbers. On the other hand, the lag factor for surface runoff (*SURLAG*), which should prevent an instant discharge surge, causes a portion to be held in storage and. The lagged surface runoff seems in parts to be evaporated, resulting in lower peak discharges.

Figure 5.5 depicts the changes in daily discharge. The days with an increased discharge only occur at low water levels <2.5 m³/s.

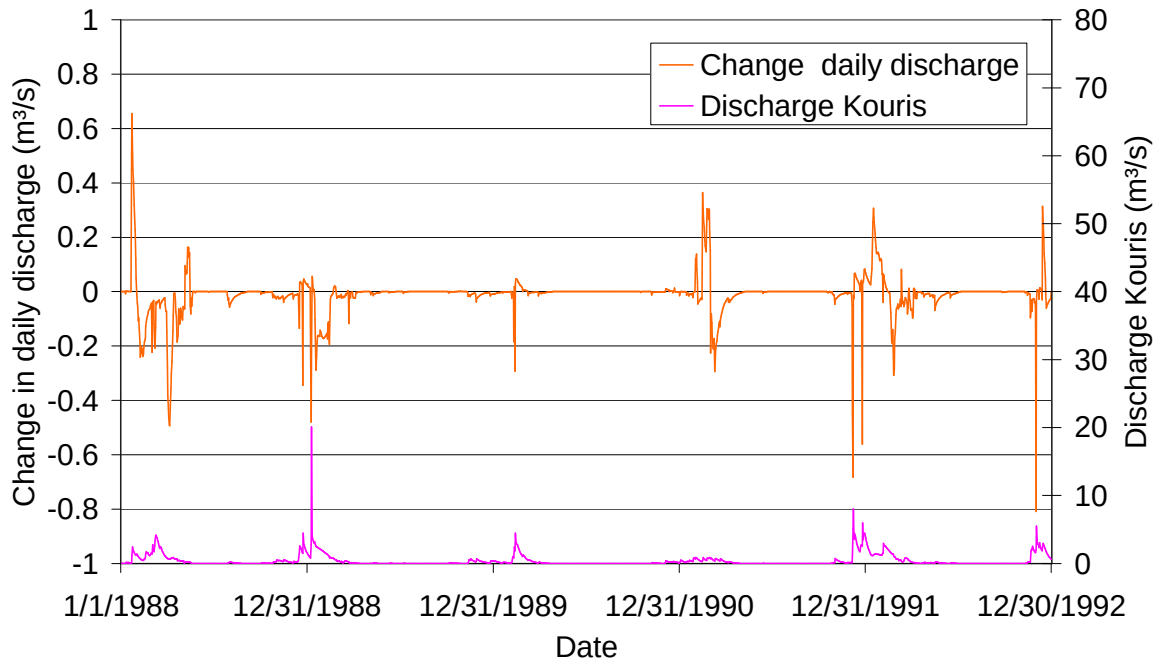

Figure 5.5 Change in daily discharge and total discharge (m³/s) for scenario 2050A

5.2 Scenario 2050B

The changes in daily mean air temperature and daily mean precipitation remain. Additionally, the CO2 concentration is raised to 464 ppm. Among others, this should have two effects. First, it affects the C availability, resulting in an accelerated growth. Very important is weather it is a C3 or a C4 species, response to CO2 is usually lower in C4 than in C3 species. Second, the stomatal conductance decreases, which reduces transpiration rates. This reflects Table 5.4.

The amounts of PET and AET still exceed the reference, but reduced from 6.3% to 3.6% for PET, and from 3.4 to 1.7% for AET.

Table 5.4 Mean changes in water cycle compounds for scenario 2050B

Water Cycle Compound	Change (mm)	Change(%)
Precipitation	5.5	0.8
Snowmelt	-9.5	-94.0
PET	48.1	3.6
AET	5.6	1.7
Recharge	-0.6	-0.3
Surface Runoff	-1.4	-14.2
Baseflow	0.2	1.4
Lateral Flow	0.4	0.3

As a result, more soilwater is available; the mean soilwater content is now about 3.2% lower than the reference compared to 7 % without CO_2 adjustment.

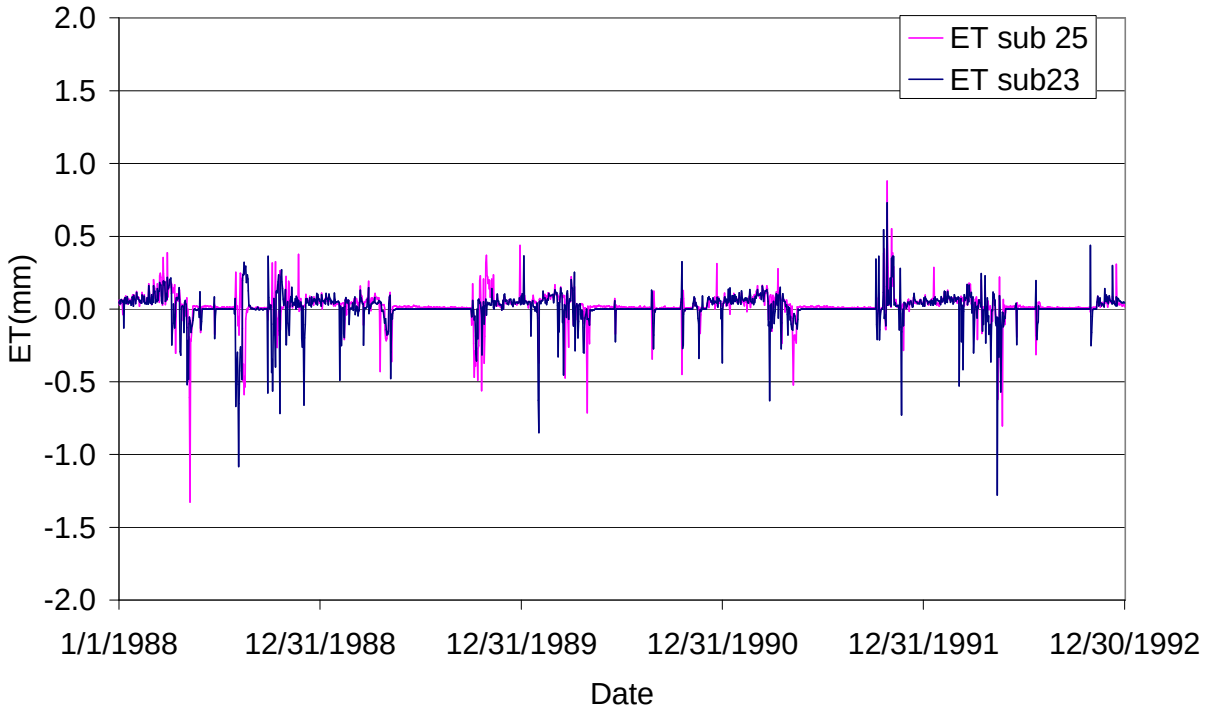

Figure 5.6 Change in daily AET (mm) for scenario 2050B

This leads to an increase in baseflow and lateral flow, which now exceed the reference, although in small amounts.

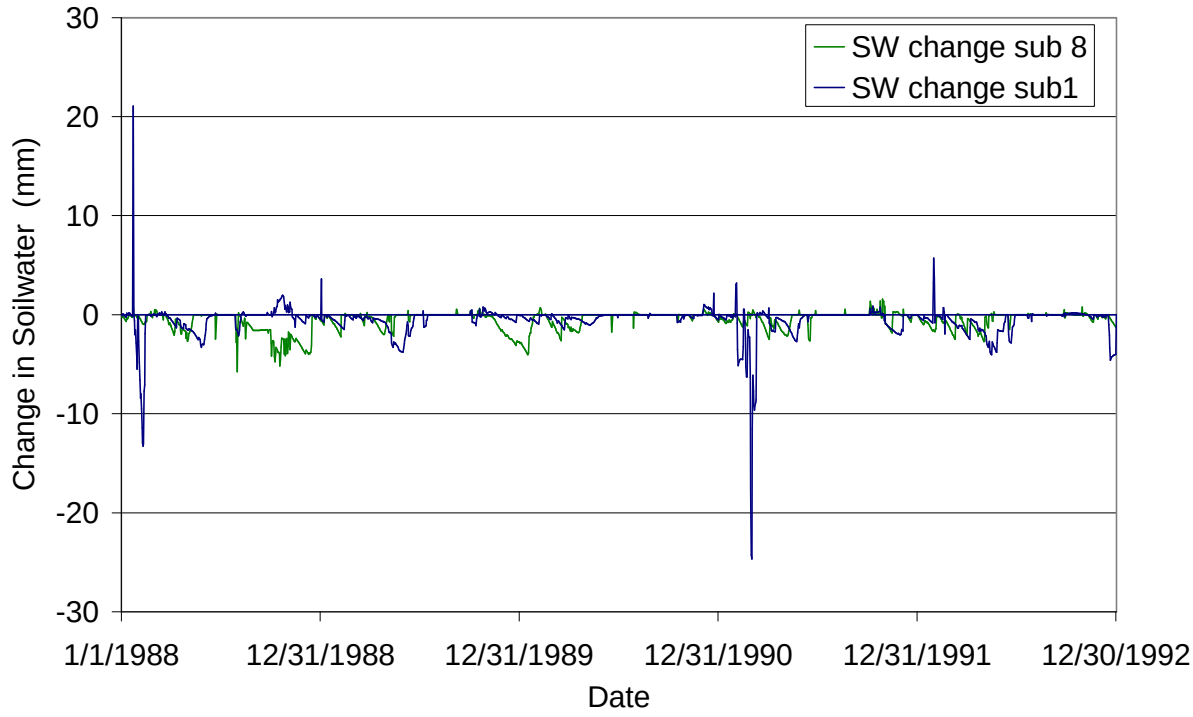

Figure 5.7 Change in daily soilwater content (mm) for scenario 2050B

The recharge is still lesser than the reference, but increased from -2.4% to -0.3%.

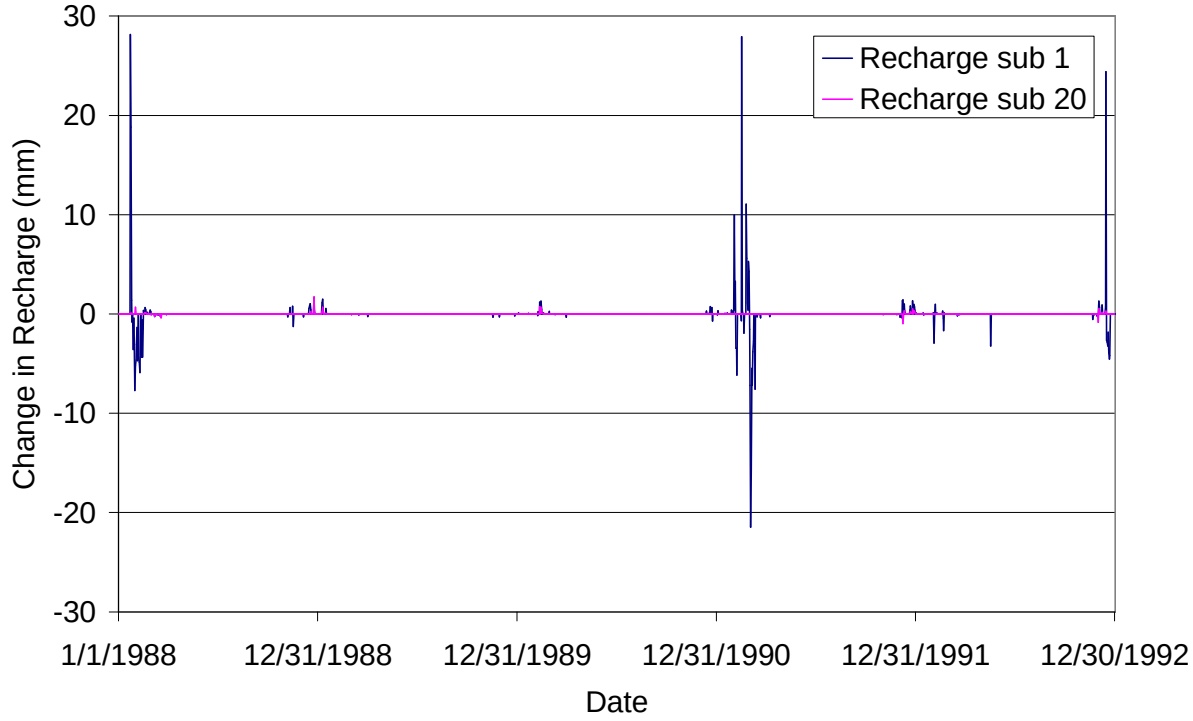

Figure 5.8 Change in daily recharge (mm) for scenario 2050B

The discharge is with a total volume of 66.7 *10^6 m³ about 0.48*10^6 m³ or 0.7% lesser than the reference, compared to 2.6% without taking CO_2 into account.

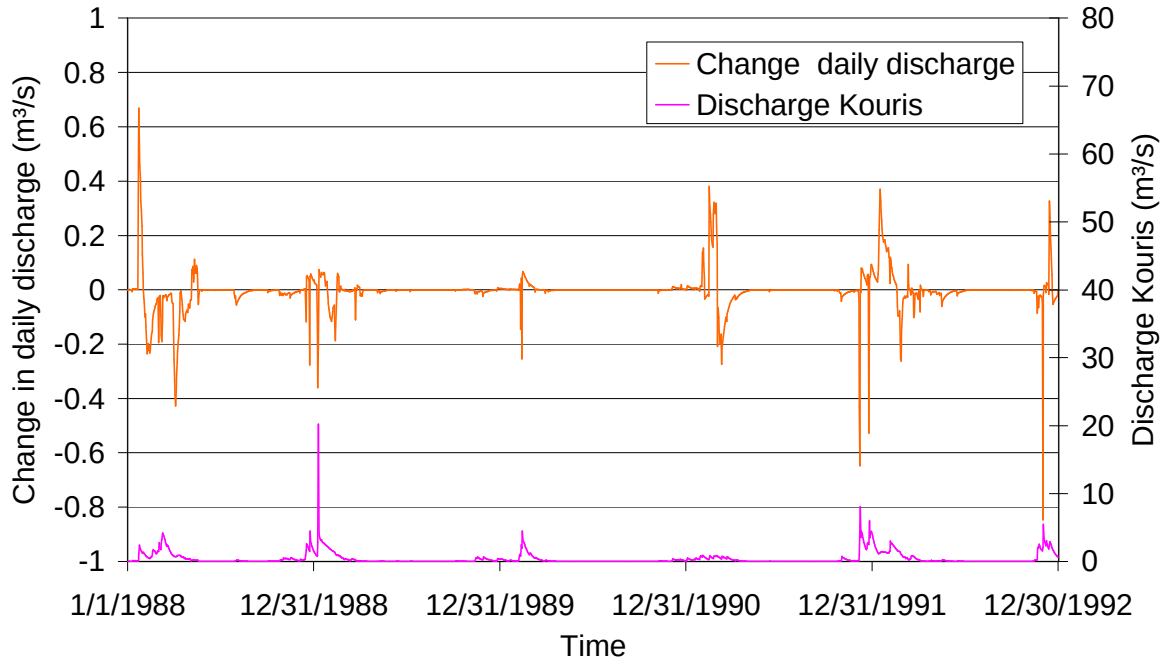

Figure 5.9 Change in daily discharge and total discharge (m³/s) for scenario 2050B

5.3 Scenario 2080B

For the 2080s, the IPCC projects for the mean air temperature a surplus of 3.31 ℃ for December to February and 3.7 ℃ for June to August. Data for the remaining months are calculated similar to precipitation. Table 5.5 lists the adjustments of precipitation for the particular months.

Table 5.5 Changes in precipitation (%) by the IPCC (italic) and fitted sinus function for the 2080s

Jan	Feb	Mar	Apr	May	Jun	Jul	Aug	Sep	Oct	Nov	Dec
9.9	*9.9*	5.57	-0.21	-6.11	*-11.2*	*-11.2*	*-11.2*	-6.80	-0.99	4.89	*9.9*

With the adjustments in precipitation and air temperature, snowmelt is the only decreasing component. All other components increase (Table 5.6).

Table 5.6 Mean changes in water cycle compounds for scenario 2080A

	Difference (mm)	Difference (%)
Precipitation	48.1	6.6
Snowmelt	-9.9	-98.5
PET	126.8	9.6
AET	21.3	6.3
Recharge	16.5	6.6
Surface Runoff	0.6	6.0
Baseflow	3.1	21.9
Lateral Flow	8.4	6.7

Evapotranspiration is 6.3% more than the reference. As Figure 5.10 displays, in the mean there is an increase during the winter months caused by the higher air temperature. During the summer months AET decreases due to lack of water available for ET.

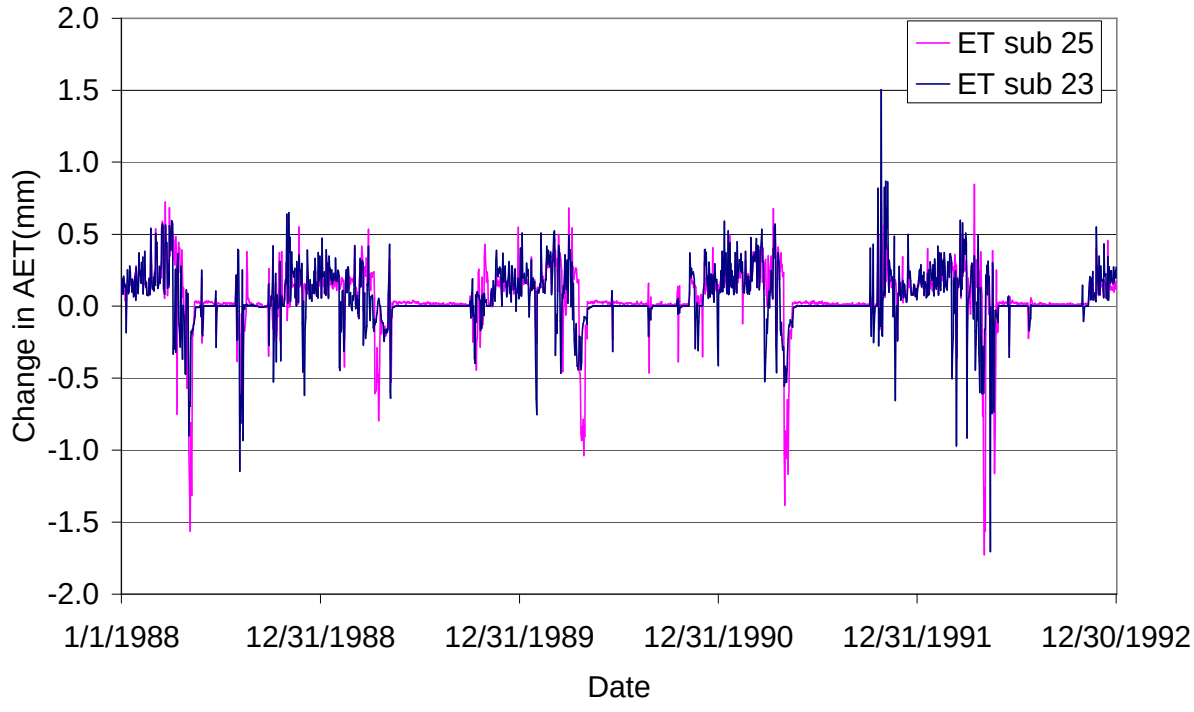

Figure 5.10 Change in daily AET (mm) for scenario 2080A

Evapotranspiration is linked to the soilwater content. Although precipitation increased, it is evident that with few exceptions soilwater content is less, primarily during the winter months, in the mean by 6.6% of the reference.

The surplus in precipitation causes surplus in recharge, lateral flow and surface runoff, even with reduced soilwater content. The recharge increased by 6.6 %.

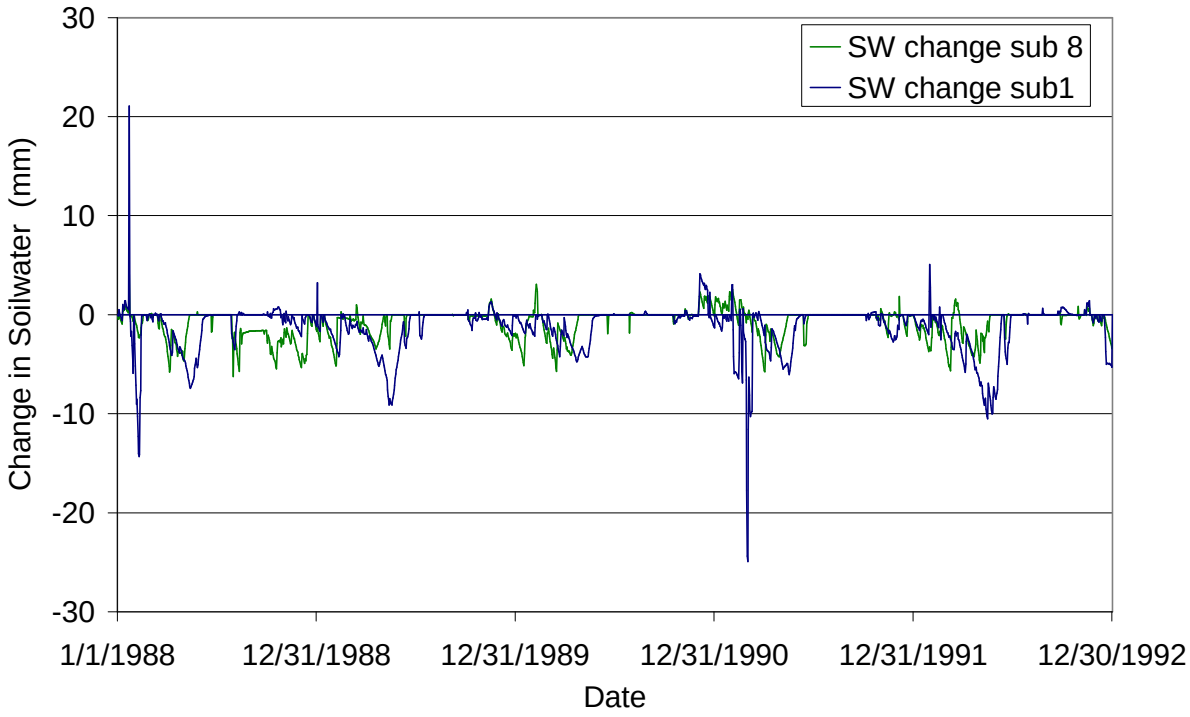

Figure 5.11 Change in daily soilwater content (mm) for scenario 2080A

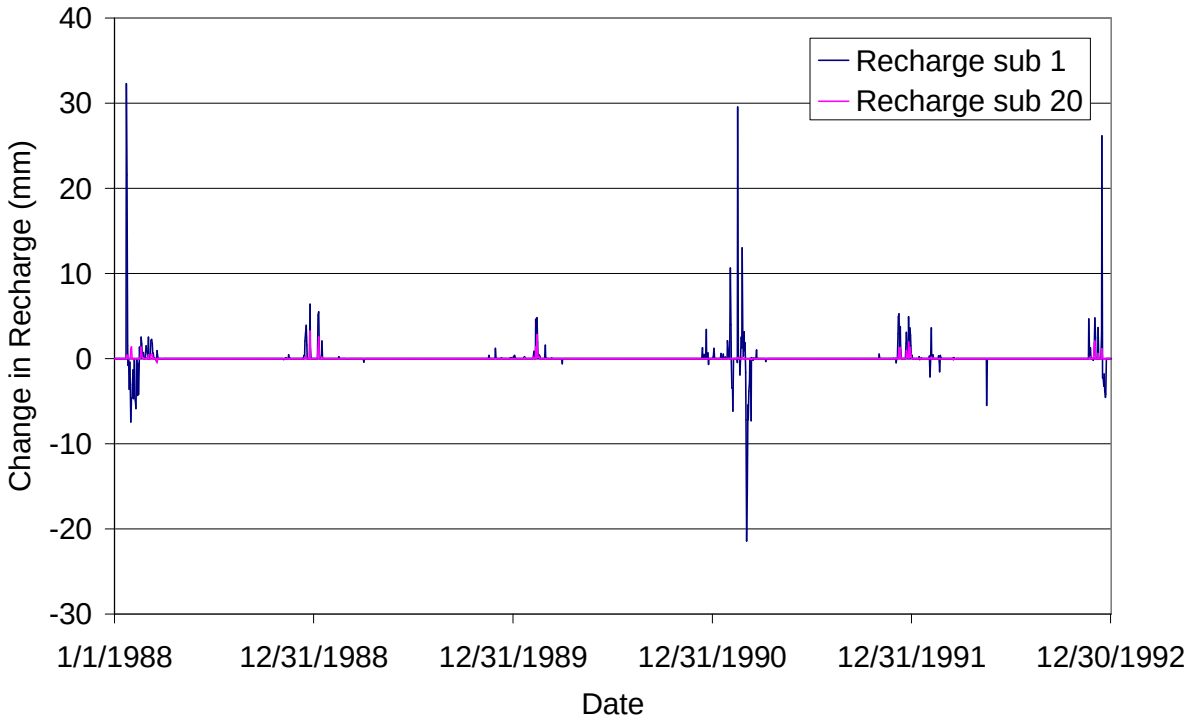

Figure 5.12 Change in daily recharge (mm) for scenario 2080A

With a total volume of $72.5*10^6$ m³ the discharge volume now exceeds the reference volume by 8.1% or $5.4*10^6$ m³. The increased baseflow results in an increase at low water levels, while the increased lateral flow and surface runoff affect the peak discharges.

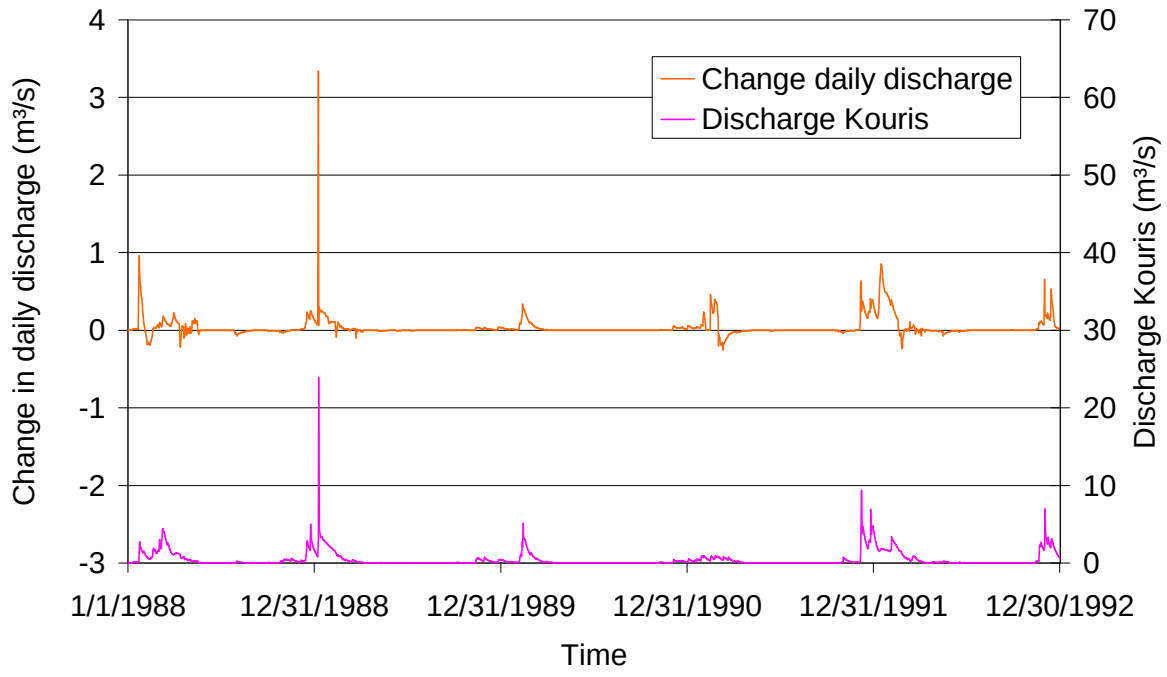

Figure 5.13 Change in daily discharge and total discharge (m³/s) for scenario 2080A

5.4 Scenario 2080B

Again, the adjustments in precipitation and air temperature remain, while the CO_2 content is additionally raised to 522 ppm. The results are similar to the scenario without CO_2 adjustment. Table 5.7 lists the changes for all water cycle compounds.

Table 5.7 Mean changes in water cycle compounds for scenario 2080B

	Difference (mm)	Difference (%)
Precipitation	48.1	6.6
Snowmelt	-9.9	-98.5
PET	72.3	5.5
AET	11.8	3.5
Recharge	23.5	9.4
Surface Runoff	0.7	6.7
Baseflow	4.9	34.9
Lateral Flow	10.3	8.2

Snowmelt is still the only compound that decreased. As expected, both PET and AET reduced, but still exceed the reference by 5.5% for PET and 3.5% for AET. The surplus in AET is less than the surplus in precipitation. This results in an increase of recharge, surface runoff, baseflow and lateral flow.

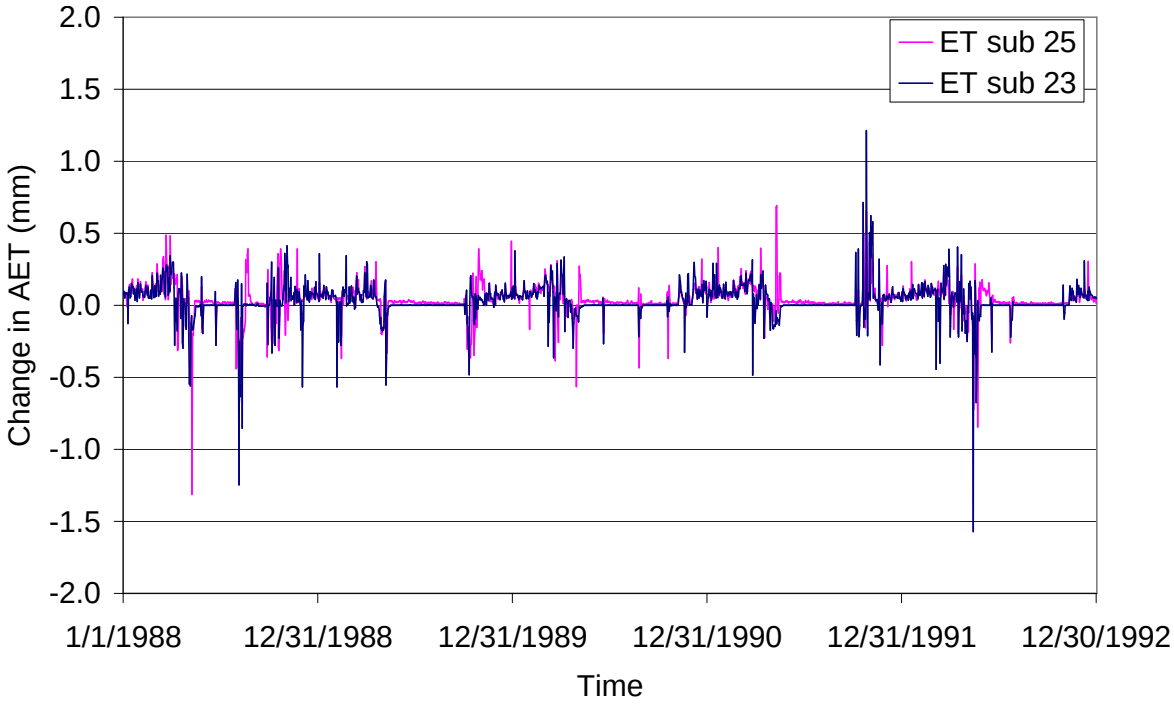

Figure 5.14 Change in daily AET (mm) for scenario 2080B

Because AET decreased, the mean soilwater content is only 1.4 % lesser than the reference, compared to 7% without CO_2 adjustment.

Figure 5.15 contains the changes in daily soilwater content (mm).

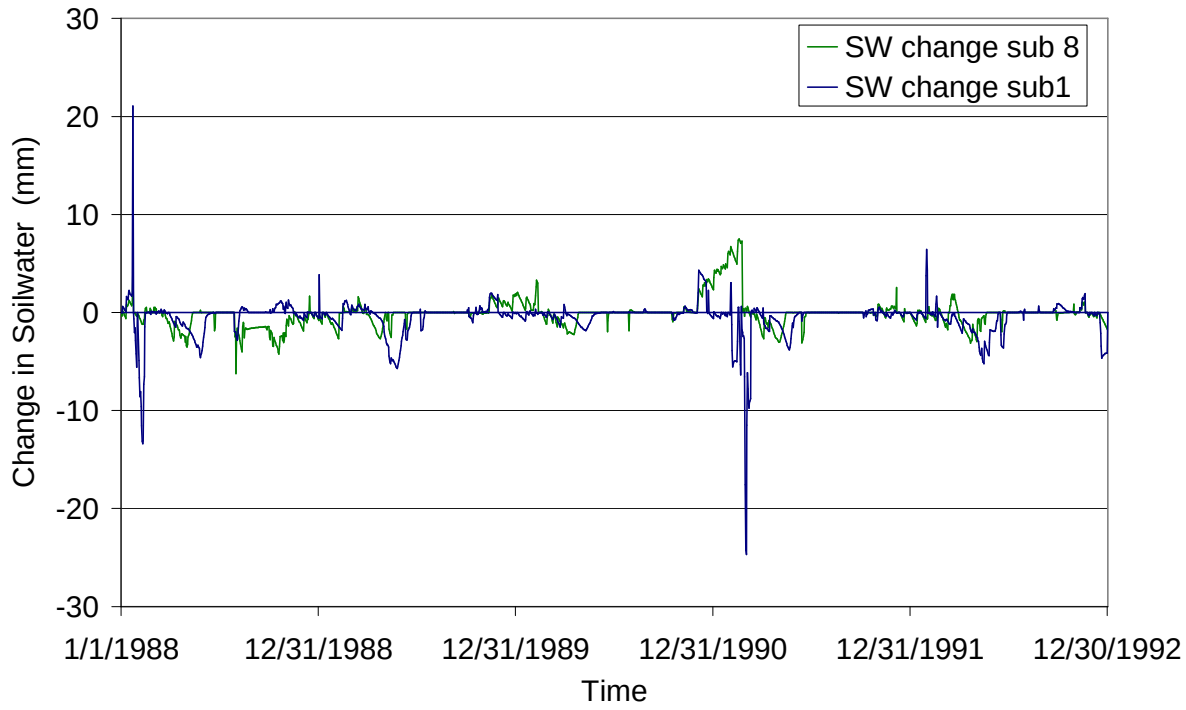

Figure 5.15 Change in daily soilwater content (mm) for scenario 2080B

With the increase in precipitation the recharge increased by 9.4% of the reference, limited to the winter months.

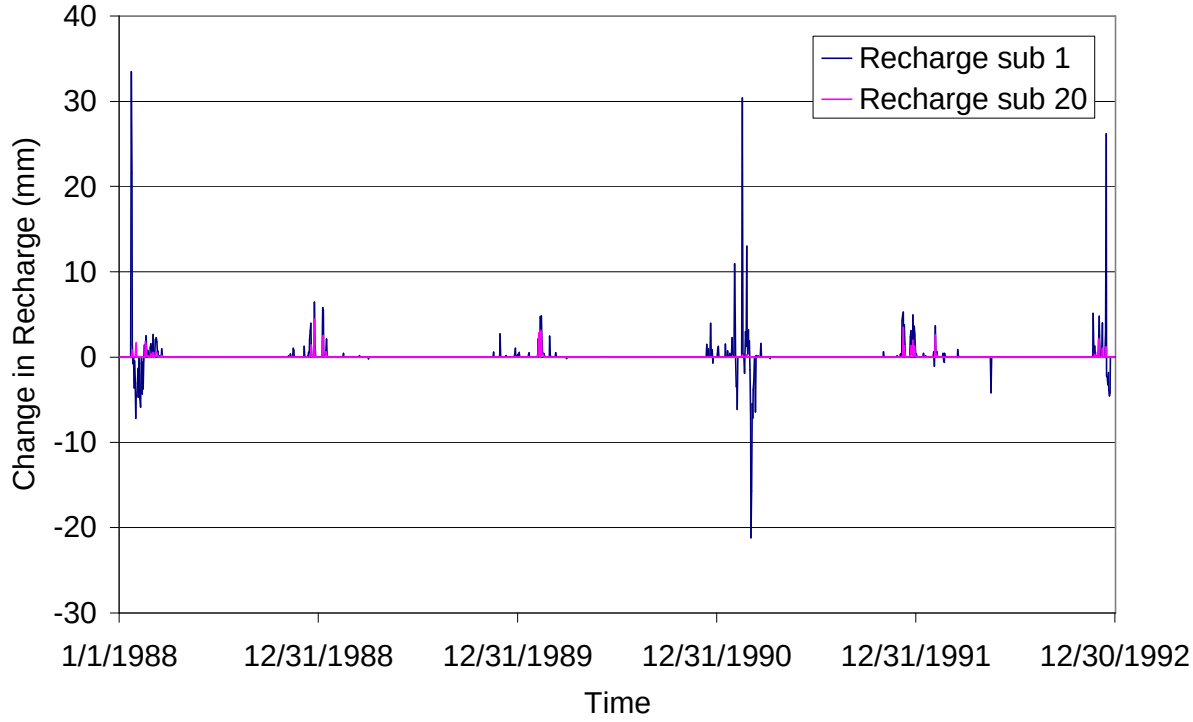

Figure 5.16 Change in daily recharge (mm) for scenario 2080B

With a total volume of $74.3*10^6$ m³ the discharge exceeds the reference by 10.7% or $7.2*10^6$ m³. With a growth of 34.9% the baseflow is the compound most altered, the shallow aquifer threshold level for baseflow to occur is exceeded more often, although the mean soilwater content decreased. The surplus in results in 6.7% more surface runoff and 8.3% more lateral flow. Altogether, this leads to the remarkable increase of 10.7% in the simulated discharge.

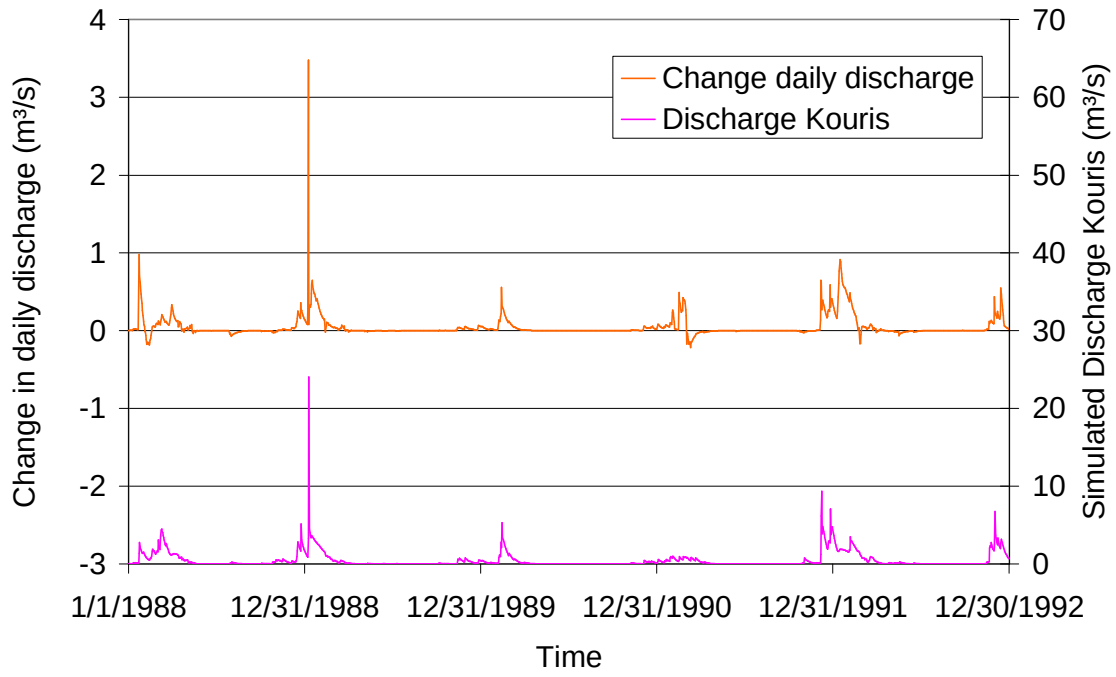

Figure 5.17 Change in daily discharge and total discharge (m³/s) for scenario 2080B

5.5 Conclusions

The IPCC states for the future climate of the Mediterranean an increase in mean daily air temperature and mean annual precipitation.

For all scenarios, the raise in air temperature causes an increase in evapotranspiration and a dramatic decrease in snowfall. Table 5.8 summarizes the changes for all water cycle compounds.

For the 2050s, the increased evapotranspiration weights more than the increased precipitation. As a result, the recharge decreases. While surface runoff is lesser than

the reference for both GHG+A and GHG+A+CO_2 scenarios, the influence of CO_2 on transpiration is obvious when concerning lateral flow and baseflow. Although ET increases and the mean soilwater content decreases, the surplus in precipitation causes an increase in lateral flow and baseflow.

Table 5.8 Percentage changes of all compounds for all scenarios

	2050A	2050B	2080A	2080B
Precipitation	0.8	0.8	6.6	6.6
Snowmelt	-94.0	-94.0	-98.5	-98.5
PET	6.3	3.6	9.6	5.5
AET	3.4	1.7	6.3	3.5
Recharge	-2.4	-0.3	6.6	9.4
Surface Runoff	-14.9	-14.2	6.0	6.7
Baseflow	-10.3	1.4	21.9	34.9
Lateral Flow	-0.9	0.3	6.7	8.2

For the 2080s, the increased precipitation weights more than the increased evapotranspiration and as a result, the recharge increases. Except snowfall, all compounds increase, above all the baseflow. Together with lateral flow and surface runoff, the increase in contributions to the streamflow result in 8.1% resp. 10.7% more discharge than the reference. Table 5.9 sums the changes in discharge.

Table 5.9 Absolute and percentage changes in discharge for all scenarios

	2050A	2050B	2080A	2080B
Absolute ($10^6 m^3$)	-1.71	-0.48	5.41	7.19
Percentage	-2.6	-0.7	8.1	10.7

Figure 5.18 compares the changes is discharge from the reference mean (0.43m^3/s) in daily discharge (%) for the four scenarios. Figure 5.19 depicts the changes in absolute amounts.

For the 2050s, the discharge is in the mean below the reference discharge for both scenarios. Discharge decreased mainly during the winter months. The minus size variation in soilwater content affects the lateral flow and surface runoff contributions to the streamflow. The effect of CO_2 is evident: evapotranspiration decreases, more soilwater is available and the contributions to streamflow increase. The raise in mean daily precipitation weighs in January more than the raise in mean air temperature, the discharge exceeds the reference. For February to December it is vice versa.

For the 2080s, the situation is different. While, for the months May to October, there seems hardly to be a change, the winter months show an obvious increase. The mean discharge for January is 44% resp. 55%, or 0.18 m³/s resp. 0.24 m³/s, above the reference mean.

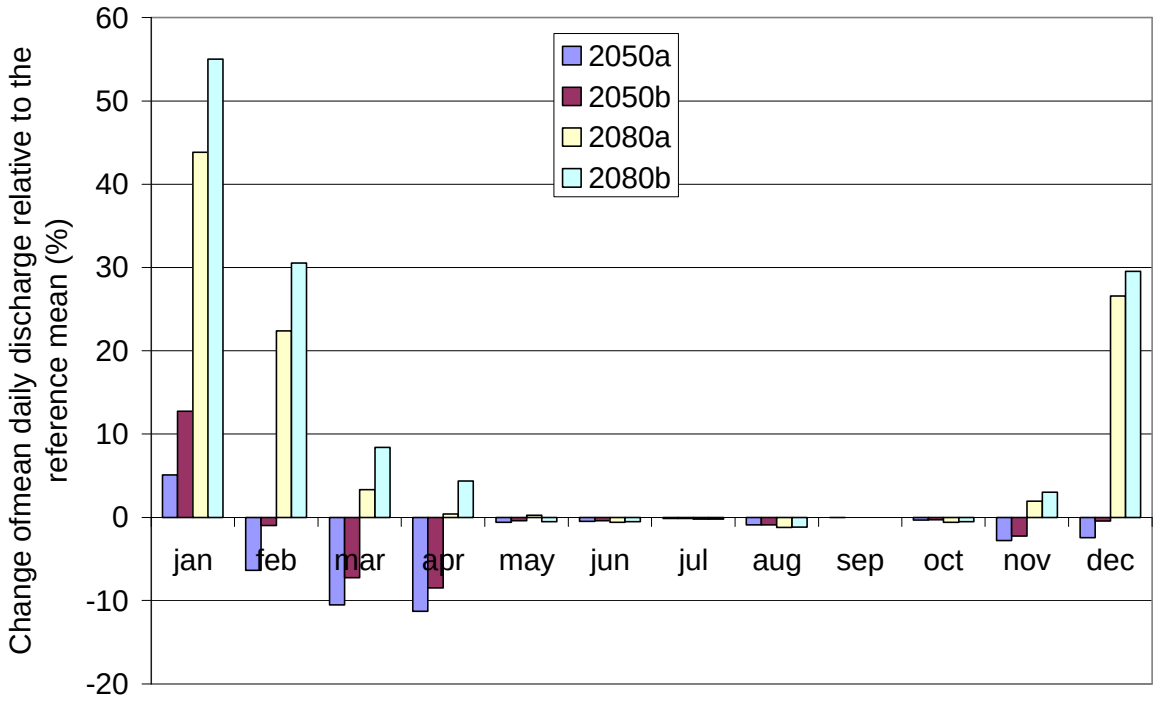

Figure 5.18 Changes in discharge related to the 5-year mean for all scenarios (m³/s)

Although the decreases in discharge during May to October, both in relation to the 5-year mean discharge and as absolute values, seem negligibly small, there is, when displayed in relation to the monthly means of discharge during the 5 years (Figure 5.20), a decrease in the range of 20 to 40%.

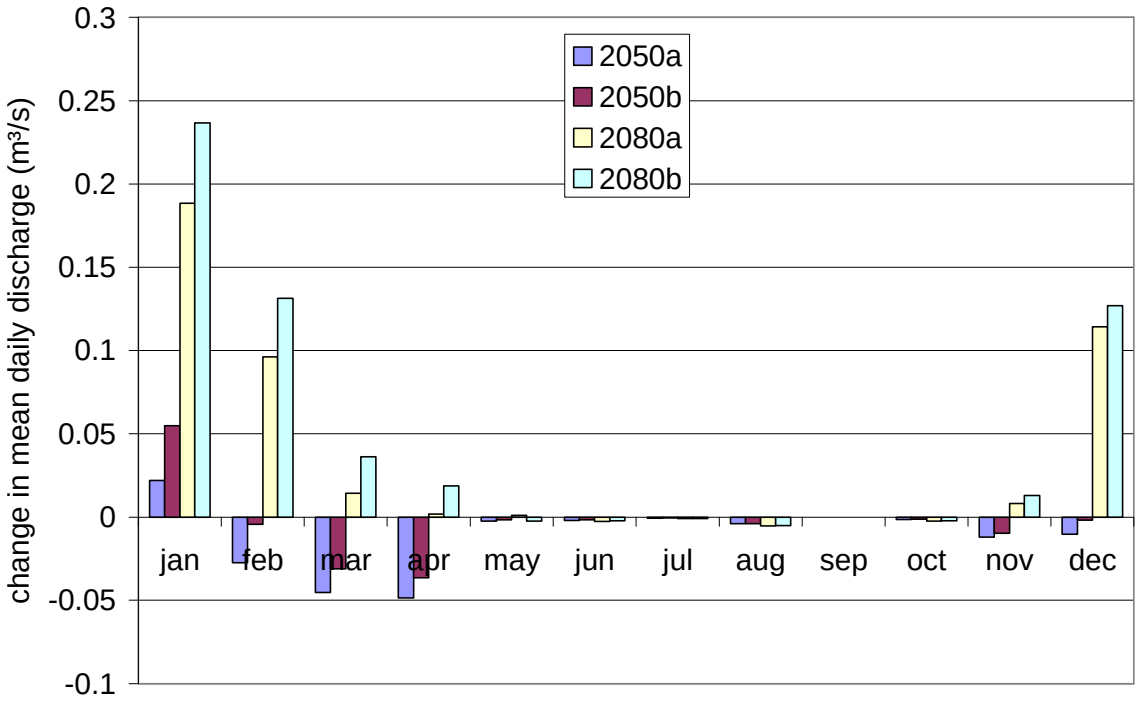

Figure 5.19 Absolute changes in monthly discharge for all scenarios (m³/s)

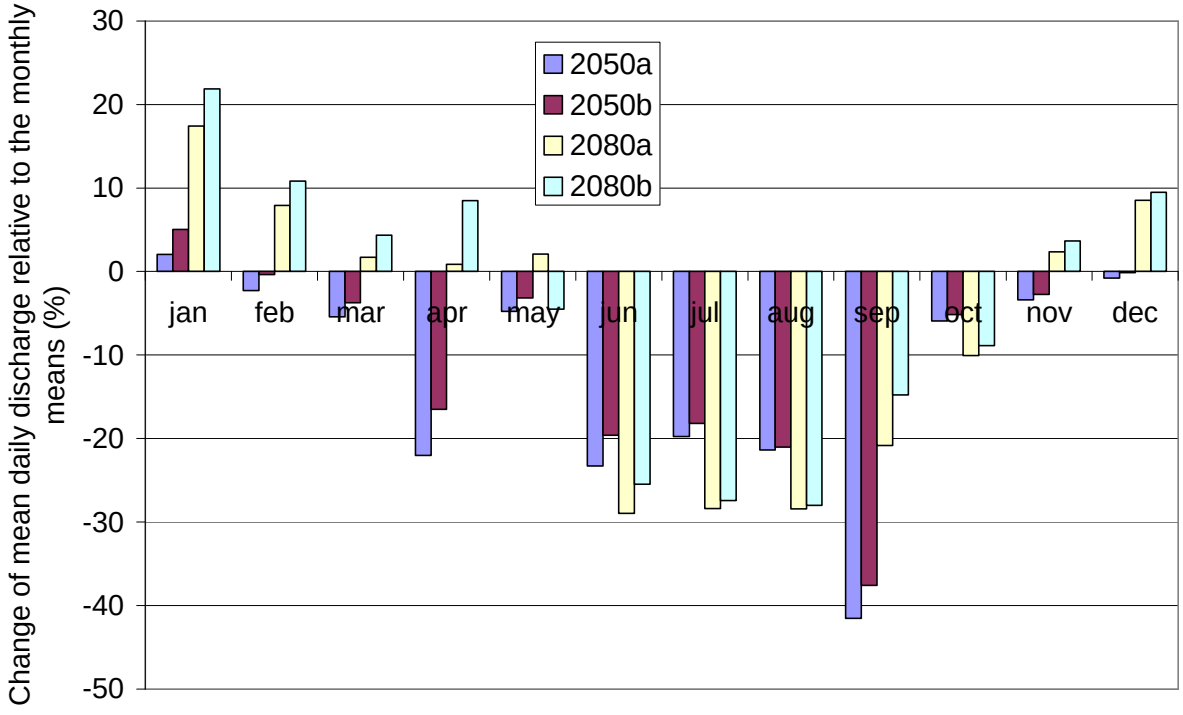

Figure 5.20 Changes in discharge related to the monthly means for all scenarios (m³/s)

6 Conclusions and Recommendations

The simulation of the water balance for the Kouris catchment is the primary objective of this work. Further, scenarios of climate change have been applied referring on the calculations of the IPCC.

The Kouris catchment is located at the southern flank of the Troodos massive. The region is mountainous with slope angles up to 47°. The climate is mediterranean with mild winters, long hot and dry summers and short spring and autumn seasons. About 85% of the annual precipitation distributes from November to March with heavy precipitation events at regular intervals.

From a geological point of view, the Kouris catchment can be subdivided into 3 different regions: the Troodos terrane, the circum Troodos sedimentary succession and the Arakapas sequence. Due to the high permeabilities of the fractured layers, the Arakapas fault zone is of vital importance for the water balance of the Kouris catchment, although the area is rather small compared to the Troodos terrane and the circum-Troodos sedimentary succession.

The shallow Leptosols and Regosols are the dominating soils with more than 50% of the area in the percentage composition.

The land use is dominated by deciduous trees, scrubland and pine forest, extending to around 80% of the area.

Distribution of lithologies and soils, and the climatic influence reflect in the distribution of land use, especially the wetlands, which only occur in the northern half.

For the simulation of the water balance, climatic data of 9 weather gages are statistically analyzed and implemented into the *SWAT* weather generator. In order to improve the spatial calculations of precipitation, a virtual station is created for the southern part of the catchment using inverse distance weighting. Precipitation then ranges from 580 mm/y (virtual station) to 900 mm/y.

The determination of the soil properties is a delicate subject due to the importance for many calculations of the water balance. The GRC Project provides K_f values for the different lithologies. The rock content is for the particular soiltype is determined by the means of the soil name attributes, such as skeletic or rendzic. With the “Soil Water Characteristics” tool by SAXTON, the fractions of clay, sand and silt as well as the bulk density are determined by the means of the provided k_f values. This approach is

a potential error source, where uncertainty can not be specified. Good results and efficiency coefficients could indirectly prove their quality.

A Landsat 5 scene is used within the GRC project to determine the land use classes for Cyprus. For the specified land use scrubland and bareland, SWAT provides no land use classes. A land use class in *SWAT* needs 29 parameters to be specified, which characterize growth, nutrient uptake, transpiration and the potential harvest. Therefore, the predefined land use classes Honey mesquite and Little Bluestem have been selected for scrubland and bareland. The setup of the land use classes in *SWAT* is another error source where uncertainty again can not be specified.

EXCEL spreadsheets are used for the analysis of the model output, providing graphs of all water cycle compounds. The simulated discharge is compared to the measured discharge; the Nash&Sutcliffe efficiency coefficient and the comparison of the volumes of measured and simulated discharge are taken into account for efficiency analysis.

A sensitivity analysis is carried out to distinguish the sensitive parameters. These are mainly parameters adjusting lateral flow and groundwater. Together with the results of the first model runs, lateral flow, surface runoff and snowmelt are identified as most important processes for the streamflow discharge.

The important processes are analyzed stepwise within *SWAT* according to the theoretical documentation. The

The calibration refers to the period 1988-1992. For water balance analysis, the first year is not taken into account in order to balance out the storages.

Lateral flow and surface runoff are the dominant processes for runoff generation within the Kouris catchment. Most peak discharges issue from surface runoff.

Lateral flow initially caused a very nervous reaction of the system, since the majority of lateral flow reached the channel instantly and produced steep peaks. The adjustments in slope length and lateral flow lag time improved the results. About 17% of the mean annual precipitation is contributed to the streamflow by lateral flow.

With the default curve numbers, SWAT produced too much surface runoff. The adjustment of the curve numbers may not reflect the natural behavior of the particular land use class, but is necessary to reduce the large quantities of surface runoff produced during heavy precipitation events. This approach is legitimated by the fact that areas with high water holding capacities such as colluvial plains could not be modeled.

Snowmelt occurs in the northern third of the catchment. The parameters affecting snowfall and snowmelt had to be adjusted in order to reduce the amount of snowmelt. The spatial distribution of snowmelt reflects in the distribution of recharge.

The calculated groundwater recharge is with a mean of 216 mm/y more than calculations of the previous projects. The distribution shows a gradient from north to south with a maximum in the north-east.

As snowmelt, baseflow only occurs in the northern third. The baseflow reduces to zero during the summer months and with it the simulated streamflow. Although, this hardly affects the efficiency coefficient, it is not a satisfying result. Therefore, the baseflow and the relevant parameters should be scrutinized further.

Actual evapotranspiration is at first less than expected. The increase in windspeed to 1.5 m/s resulted in a mean of 321 mm/y, which seems plausible.

The occurrence of transmission losses in the Kouris catchment is obvious. *SWAT*, however, did not calculate transmission losses.

Altogether, with applied parameter set *SWAT* produces good results for the simulated discharge. The Nash-Sutcliffe efficiency is 0.78 for the Kouris, 0.63 for the Limnatis.

By simulating the period 1992-1996, the model is validated. While the results for the Limnatis declined, the results for the Kouris improved. *SWAT* both under- and overestimated the annual volumes discharge, depending on the observed year. But, the quality of the calibrated parameters is proven.

The last to mention about the calibration is the issue of equifinality. As over-parameterization is a possible reason for equifinality, one might consider modeling with *SWAT* as delicate. However, the determination of the dominant hydrologic processes and the stepwise calibration are an approach to counteract this issue.

With the calibrated model, climate change scenarios are applied according the future projection of the IPCC. Several AOGCMs have been compared predicting the changes in air temperature and precipitation caused by GHGs solely and GHGs with aerosols. The changes have been modeled for the period 2040-2069 and 2070-2099. Altohether four scenarios have been modeled; all include the effects of aerosols, for each time period one additionally takes the effect of CO_2 into account.

The scenarios predict an increase in mean annual precipitation for both the 2050s (0.8%) and the 2080s (6.6%). In both cases, there is an increase during the winter months and a decrease during the summer months. ROSSEL (2001) analyzed

climatic data from 1916/17 to 1999/00. He stated a slight decrease in precipitation for the period 1969/70 to 1999/00, but it is not significant.

For all scenarios, the raise in air temperature causes an increase in evapotranspiration and a dramatic decrease in snowfall.

For the 2050s, the increased evapotranspiration weights more than the increased precipitation. While surface runoff is lesser than the reference for both GHG+A and GHG+A+CO_2 scenarios, the influence of CO_2 on transpiration is obvious when concerning lateral flow and baseflow. Although ET increases and the mean soilwater content decreases, the surplus in precipitation causes an increase in lateral flow and baseflow. Groundwater recharge decreases in both cases.

Although the decrease in discharge is small in absolute amounts, the discharge for months June to September decreases in relation to the monthly means in the range of 18-42%, depending on the scenario. Except for January, the discharge decreases for all months. In the mean, the discharge decreases by 2.6% for the scenario without CO_2 adjustment, and by 0.7% for the scenario with CO_2 adjustment.

For the 2080s, the increased precipitation weights more than the increased evapotranspiration. With the exception of snowfall, all compounds increase, above all the baseflow. Together with lateral flow and surface runoff, the streamflow exceeds the reference by 8.1% resp. 10.7%. The recharge now exceeds the reference.

To sum up, the effects of climate change on the annual water balance depends on the combined influence of a raise in air temperature and precipitation. Whether water cycle compounds increase or decrease depends on the weighting. Thus, the increase in air temperature can be balanced by the increase in precipitation.

In either case, there is a decrease during the summer months and an increase during the winter months. This means one has to manage with less water available when mostly needed. Therefore, further efforts to improve water and demand management as well as the use of storage and recharge enhancement techniques is recommended.

7 References

BODENKUNDLICHE KARTIERANLEITUNG (1994): Ad hoc „Arbeitsgruppe Boden“ der Geologischen Landesämter und der Bundesanstalt für Geowissenschaften und Rohstoffe der Bundesrepublik Deutschland. 4. verbesserte und erweiterte Auflage,392 p., Hannover

BORONINA AGOLUBEV S., BALDERER W. (2005): Estimation of actual evapotranspiration from an alluvial aquifer of the Kouris catchment (Cyprus) using continuous streamflow records, Hydrological Processes Volume 19, Issue 20, P. 4055 - 4068

DI LUZIO M., SRINIVASAN R., ARNOLD J.G., NEITSCH S.L. (2002): ArcView Interface for Swat2000, User’s Guide

DRIESSEN P., DECKERS J., SPAARGAREN O., NACHTERGAELE F. (Ed.) (2001): Lecture Notes On The Major Soils Of The World, World Soil Resources Report 94; Food And Agriculture Organization Of The United Nations, Rome

GASSMAN P., REYES M., GREEN C., ARNOLD J. (2007): The Soil and Water assessment Tool: Historical Development, Applications, and Future Research Directions, Transactions of the ASABE Vol. 50(4): p. 1211-1250, American Society of Agricultural and Biological Engineers

HÄCKEL H., (1999): Meteorologie, 4th Edition, Verlag Eugen Ulmer, Stuttgart, Germany, 448 p.

IPCC (2001a): Climate Change 2001: The Scientific Basis. Contribution of Working Group I to the Third Assessment Report of the Intergovernmental Panel on Climate Change. Cambridge University Press, Cambridge, United Kingdom and New York, USA, 881pp.

IPCC (2001b): Climate Change 2001: Impacts, Adaptation, and Vulnerability. Contribution of Working Group II to the Third Assessment Report of the Intergovernmental Panel on Climate Change. Cambridge University Press, Cambridge, United Kingdom and New York, USA

IPCC (2007): Global Climate Projections. In: Climate Change 2007: The Physical Science Basis. Contribution of Working Group I to the Fourth Assessment Report of the Intergovernmental Panel on Climate Change Cambridge University Press, Cambridge, United Kingdom and New York, USA.

MAIDMENT D.R. (Ed.), (1993): Handbook of Hydrology, McGraw-Hill Inc., New York, USA

NEITSCH S.L., ARNOLD J.G., KINIRY J.R., WILLIAMS J.R. (2005): Soil and Water Assessment Tool, Theoretical Documentation Version 2005**,** 494p.

NEITSCH S.L., ARNOLD J.G., KINIRY J.R., SRINIVASAN R., WILLIAMS J.R. (2005): Soil and Water Assessment Tool Input/Output File Documentation, Version 2005 541 p.

SCHEFFER F., SCHACHTSCHABEL P., BLUME H.P., (2002): Lehrbuch der Bodenkunde, 15. Ed., Spektrum Akademischer Verlag, Heidelberg, Berlin, Germany, 593 p.

SOIL SURVEY STAFF (1999): Soil Taxonomy: A basic system of soil classification for making and interpreting soil surveys, 2nd edition. Agricultural Handbook 436, Natural Resources Conservation Service, USDA, Washington DC, USA, pp. 869

ROSSEL F., (2001): Hydrometeorological study examining changes in recorded precipitation, Final Report, Ministry of Agriculture, Natural Resources and Environment of the Republic of Cyprus, Water Development Department; Food and Agriculture Organization of the United Nations Land and Water

Development Division, TCP/CYP/8921, REASSESSMENT OF THE ISLAND'S WATER RESOURCES AND DEMAND

UDLUFT P., (2001): GRC Project Task 1: Review of existing data, reports and publications, Re-evaluation of Groundwater Resources of Cyprus for the Republic of Cyprus for Ministry of Agriculture, Natural Resources and Environment Geological Survey Department Nicosia 59 p.

UDLUFT P., DÜNKELOH A., MEDERER J., KÜLLS C., SCHALLER J. (2003): GRC Project Task 6/7: Water balances for catchments and for the whole island, Re-evaluation of Groundwater Resources of Cyprus for the Republic of Cyprus for Ministry of Agriculture, Natural Resources and Environment Geological Survey Department Nicosia, 223 p.

USDA (2002): Plant Fact Sheet, Honea Mesquite, Prepared By: Hurteau M.D. Formerly SDA, NRCS, National Plant Data Center, c/o Environmental Horticulture Department, University of California, Davis, USA, 3 p.

USDA (2002): Plant Fact Sheet, Little Bluestem; USDA NRCS National Plant Materials Center Beltsville, Maryland, USA, 2 p.

WIEGAND, G. (2002): Modifikation des inverse-distance-Algorithmus zum Vermeiden der Übergewichtung von Messstellen-Clustern, DeCluster, 5. Teilbericht; für Umweltbundesamt II 6.4

ZAGANA E., KÜLLS Ch., UDLUFT P., CONSTANTINOU C., (2006): Methods of groundwater recharge estimation in eastern Mediterranean - a water balance model application in Greece, Cyprus and Jordan, Hydrological Processes, Volume 21, Issue 18 , p. 2405 - 2414

URL1:http://www.issg.org/database/species/ecology.asp?si=137&fr=1&sts=, global invasive species database (9/28/07)

URL2:http://www.eeob.iastate.edu/research/iowagrasses/ornamental/SchizScopaOr.html (9/28/07)

URL3:http://www.tarleton.edu/~range/Cook%20Pictures/Photo%20Slides_4/177%20western%20honey%20mes.jpg (9/28/07)

URL4:http://www1.agric.gov.ab.ca/$department/deptdocs.nsf/all/aesa1861 (9/28/07)

URL5:http://www.brc.tamus.edu/swat/soft_links.htm (9/28/07)

URL6:http://epa.gov/climatechange/science/futurecc.html (9/28/07)

URL7:http://wwwalt.uni-wuerzburg.de/hydrogeologie/inco/ (9/28/07)

Ehrenwörtliche Erklärung

Hiermit erkläre ich, dass die Arbeit selbständig und nur unter Verwendung der angegebenen Hilfsmittel angefertigt wurde.

Ort, Datum Unterschrift